Crystallographic and microstructural study of as-cast and heat-treated Srmodified Al-12.7Si alloys

Xiaorui Liu

UNIVERSITÉ DE LORRAINE NORTHEASTERN UNIVERSITY

DISSERTATION

Presented at
Université de Lorraine and Northeastern University

Xiaorui LIU 刘晓蕊

To obtain the doctor's degree of
University of Lorraine and Northeastern University

SPECIAL FIELD: Engineering Sciences
OPTION: Materials Science

Crystallographic and microstructural study of as-cast and heat-treated Sr-modified Al-12.7Si alloys

To be defended on the 29th July, 2016 in front of the jury:

Werner SKROTZKI	Professor	Technical University Dresden, Germany	Reviewer & Jury member
Zheng LIU	Professor	Shenyang University of Technology, China	Reviewer & Jury member
Tadao WATANABE	Professor	Tohoku University, Japan	Jury member
Zhidong ZHANG	Professor	Institute of Metal Research Chinese Academy of Sciences, China	Jury member
Liang ZUO	Professor	Northeastern University, China	Supervisor
Yudong ZHANG	Doctor HDR	Université de Lorraine, France	Supervisor
Benoît BEAUSIR	Doctor	Université de Lorraine, France	Co-Supervisor
Fuxiao YU	Professor	Northeastern University, China	Co-Supervisor
Claude ESLING	Professor	Université de Lorraine, France	Invited member

Laboratoire d'Étude des Microstructures et de Mécanique des Matériaux, LEM3
Ile du Saulcy 57045 Metz Cedex 1

Acknowledgements

This work is supported by the China Scholarship Council (Grant No. 201306080056), 111 Program of China (Grant No. B07015) and the Program for Liaoning Innovative Research Team in University (Grant No. LT2013007). The work presented in this dissertation is accomplished between October 2013 to August 2016 at LEM3 (University of Lorraine, France) and the Key Laboratory for Anisotropy and Texture of Materials (ATM, Northeastern University, China). I had the honor to work with numerous colleagues in two laboratories and I would like to give my hearted thanks for their kind help.

First of all, I sincerely extend my deepest gratitude to my supervisors, Dr. Yudong Zhang and Dr. Benoît Beausir at University of Lorraine, Professor Liang Zuo and Professor Fuxiao Yu at Northeastern University, for their guidance and support to my PhD work. I have benefited tremendously from their knowledge and experiences, their persistence and strive for excellence. I would like to express special appreciation to Dr. Yudong Zhang for her patient guidance during the entire span of my thesis work, and for her selfless help in my academic study as well as for her encouragement in my daily life. I am very lucky to have Dr. Benoît Beausir as my co-supervisor, an inspiring and extraordinary person to work with, who helps me a lot during the last three years. Sincere appreciation is extended to Professor Claude Esling for his kind support and critical suggestions on my experiments. Many thanks go in particular to Professor Fuxiao Yu, for introducing and guiding me to the amazing world of aluminum-silicon alloys. Lastly, I would like to express my most sincere gratitude to Professor Liang Zuo for providing me such a chance to learn from those excellences.

I would like to sincerely appreciate all the jury members for taking time out of their busy schedules to achieve the defense of my dissertation.

A sincere thank goes to Professor Xiang Zhao in ATM laboratory, Northeastern University in China, for his carefully revision and constructive suggestions on my final thesis writing.

I would like to express my gratefulness to Dr. Weimin Gan for his technical assistance and helpful discussions on texture and strain measurements by neutron diffraction at FRM Π Garching, Germany. I would like to express my appreciation to Dr. Jean-Jacques Fundenberger and Dr. Perroud Olivier at LEM3, France, for their helpful and inspiring discussions on texture and strain analysis, and technical support (strain measurement by X-ray). I would like to express my appreciation to Dr. Hui Yuan for his technical support for TEM sample preparation by FIB cutting. I am deeply indebted to Professor Tamas Ungár from Budapest, Hungary, for valuable suggestions on the post analysis of neutron diffraction data. I would like to express my appreciation to Professor Anthony Rollett from Carnegie Mellon University, for having offered a critical reading to improve the English wording of my paper.

I am grateful to all the staffs and students who shared their experiences with me and offered help to my study, including Dr. Zongbin Li, Dr. Fang Liu, Dr. Dazhi Zhao, Dr. Bo Yang, Dr. Nan Xu, Dr. Shiying Wang, Dr. Zhangzhi Shi, Dr. Yajun Zhao, Dr. Cai Chen, Mr. Haile Yan, Mr. Jiangkun Fan, Mr. Chunyang Zhang, Ms Jing Wen, Ms Chunqing Lin, Mr. Shun Xu, Mr. Naifu Zou, Mr. Ke Hu and Mr. Ke Hua.

Last but not least, I would like to express my deep love and gratitude to my family, to thank my parents who have loved, supported and trusted me throughout my life. Without their encouragement and support, I would never have made it this far.

Abstract

Al-Si alloys have attracted considerable attention due to their importance to industrial applications. In the present work, both crucible slowly solidified and slowly directionally solidified (DS) high-purity Al-12.7 wt. % Si alloys with and without 400 ppm Sr addition have been prepared and heat treated. The influence of Sr addition and post heat treatments on the microstructural and crystallographic features of the eutectic phases has been systematically studied.

The growth characteristics of eutectic Si in the unmodified and the Sr-modified Al-12.7Si alloys were investigated. For the non-modification case, the formation of repeated single-orientation twin variants enables rapid growth of eutectic Si according to the twin plane re-entrant (TPRE) mechanism. Microscopically, Si crystals are plate-like elongated in one <1 1 0> direction that is not in accordance with the <1 1 2> growth assumed by the TPRE model. The <1 1 0> extension is realized by paired <1 1 2> zigzag growth on parallel twinning planes, leading to alternative disappearance and creation of 141° re-entrants. This growth manner ensures Si crystals to expose only their low-energy {1 1 1} planes to the melt. For the Sr-modification case, substantial changes appear in eutectic Si morphology, attributable to the restricted TPRE growth and the impurity induced twinning (IIT) growth. The first enhances lateral growth by forming new twins with parallel twinning planes, while the second leads to isotropic growth by forming differently oriented twins.

Heat treatment brings about refinement of both eutectic phases. The refinement of the α-Al occurs concomitantly with the fragmentation and spheroidization of Si and is mainly related to the fracture of the Si crystals due to their limited capacity to accommodate the giant thermal expansion of the α-Al and the diffusion of Al atoms to the cracks during the heat treatment. The Si fracture generates “capillarity” force that activates the diffusion of Al atoms to the gap of the crack. Due to the substitutional feature of Al diffusion, the migration of vacancies toward the interior of the α-Al is induced when Al moves to the gaps, thus the voids of the Si fracture are transferred to the α-Al. In this way, the crystals of α-Al are distorted and

defected. The produced crystal defects, in turn, initiate recovery and even recrystallization of the α-Al, resulting in grain refinement.

The α-Al phase in the directionally solidified Al-12.7Si-0.04Sr alloy, displays a strong <1 0 0> fiber texture in the solidification direction. Giant <1 0 0> α-Al grains are mainly formed in the outer circle region of the cylindrical specimen due to the favorable heat evacuation directions available for the three <1 0 0> directions. After heat treatment, the texture intensity of the α-Al phase decreases due to the recovery and recrystallization, but the texture type does not change. For the eutectic Si phase in the as-cast alloy, there are two main fiber texture components, <1 0 0> and <1 1 0> in the DS direction, accompanied by two weak components, <2 2 1> and <1 1 3> in the same direction. The <1 0 0> and <1 1 0> components are from Si crystals located in the outer circle and center regions of the cylindrical specimen. The <2 2 1> and the <1 1 3> components are from multiple twins of the <1 1 0> and <1 0 0> oriented crystals. The weak intensities of these two components are related to their minor volume fraction. Once heat treated, the twinned parts with minor volume fractions enlarge at the expense of their twin related matrix, thus the <1 1 0> component is weakened and accompanied by the intensification of the components from the twins. The disappearance of the <1 1 3> component and the appearance of the <1 1 5> component are due to crystallographic rotation of Si crystals during their fragmentation.

Keywords: Al-Si alloys; Sr modification; Heat treatment; EBSD; Growth twin; Recrystallization; Neutron diffraction; Texture.

Résumé

Les alliages aluminium-silicium (Al-Si) ont attiré une attention considérable en raison de leur importance pour les applications industrielles. Dans le présent travail, des alliages à haute pureté (Al-12.7 wt. % Si) avec et sans ajout de strontium (400 ppm), solidifiés lentement en creuset ou de façon dirigée (DS), ont été préparés et traités thermiquement. L'influence de l'ajout de strontium et des post-traitements thermiques sur les caractéristiques microstructuraux et cristallographiques des phases eutectiques a été étudiée de façon systématique.

Les caractéristiques de croissance du silicium eutectique (Si) dans l'alliage non modifié ainsi que dans l'Al-12.7Si Sr-modifié ont été étudiés. Pour le cas du non-modifié, la formation répétée de variantes de mâcles mono-orientatées permet une croissance rapide du silicium eutectique selon le mécanisme twin plane re-entrant (TPRE). Microscopiquement, les cristaux de silicium ont une forme de plaque allongée dans la direction <1 1 0> non conforme à la croissance selon <1 1 2> présumée par le modèle TPRE. L'élongation selon <1 1 0> est réalisée par des paires en zigzag <1 1 2> sur des plans de maclage parallèles, conduisant à une disparition alternative et à la création de mâcles rentrantes à 141°. Ce mécanisme de croissance permet aux cristaux de silicium de n'exposer que les plans {1 1 1} à faible consommation d'énergie à la consolidation. Pour les alliages modifiés au strontium, des changements importants de morphologie apparaissent dans le silicium eutectique, attribuable à la croissance de TPRE restreinte et au maclage induit par les impuretés (IIT). Ce dernier améliore la croissance latérale en formant de nouvelles mâcles avec des plans de mâcles parallèles, tandis que le second conduit à une croissance isotrope en formant des mâcles orientées différemment.

Le traitement thermique provoque l'affinement des grains des deux phases eutectiques. L'affinement de l'α-Al se produit en même temps que la fragmentation et la sphéroïdisation du silicium et est principalement lié à la fracture des grains de silicium en raison de leur capacité limitée à accommoder la très grande dilatation thermique l'α-Al, ainsi qu'à la diffusion des

atomes d'aluminium au cours du traitement thermique. La rupture du silicium génère une force de "capillarité" qui active la diffusion d'atomes d'aluminium dans la fissure. En raison du caractère de substitution de la diffusion de l'aluminium, la migration des lacunes vers l'intérieur de l'α-Al est induite lorsque l'aluminium se déplace dans les fissures, ainsi les vides de la fracture du silicium sont transférés à l'α-Al. De cette façon, les cristaux d'α-Al sont altérés et déformés. Les défauts cristallins produits, à leur tour, initient la restauration et même la recristallisation du α-Al, ce qui entraîne une diminution de taille de grain.

La phase α-Al dans l'alliage de Al-12.7Si-0.04Sr solidifiée directionnellement, affiche une forte texture de fibre <1 0 0> parallèle à la direction de solidification. De très gros grains <1 0 0> α-Al sont principalement formés à la périphérie de l'échantillon cylindrique en raison des directions d'évacuation de chaleur favorables disponibles pour les trois directions [1 0 0]. Après traitement thermique, l'intensité de la texture de la phase α-Al diminue en raison de la restauration et de la recristallisation, mais le type de texture ne change pas. Pour la phase de silicium eutectique dans l'alliage de coulée, il y a deux fibres principales de texture, <1 0 0> et <1 1 0> parallèles à la direction de solidification, accompagnées de deux composantes faibles, <2 2 1> et <1 1 3> dans la même direction. Les fibres <1 0 0> et <1 1 0> correspondent à des grains de silicium situés sur la périphérie et dans le centre de l'échantillon. Les composantes <2 2 1> et <1 1 3> proviennent de plusieurs mâcles de grains orientés <1 1 0> et <1 0 0>. Les faibles intensités de ces deux composantes sont liées à leur fraction volumique mineure. Une fois traité thermiquement, les parties mâclées avec des fractions de volume mineures s'agrandissent au détriment de leur matrice, ainsi la composante <1 1 0> est affaiblie et s'accompagne par l'intensification des composantes de mâcle. La disparition de la composante <1 1 3> et l'apparition de la composante <1 1 5> est due à la rotation cristallographique des cristaux de silicium au cours de leur fragmentation.

Mots clés: Alliages Al-Si; Modification au Strontium; Traitement thermique; EBSD; Croissance de macle; Recristallisation; Diffraction des neutrons; Textures.

摘 要

铝硅合金对于工业应用具有重要的作用，已经引起了研究者广泛的关注。本论文通过坩埚缓冷和慢速定向凝固技术制备出未变质和锶变质（400 ppm）共晶铝硅合金铸锭，并对铸锭进行了热处理，系统地研究了锶添加和热处理对铝硅合金中共晶相的微观组织和晶体学特征的影响。

本工作调查了共晶 Si 在未变质和锶变质铝硅合金中的生长特点。在未变质合金中，单取向 Si 孪晶变体的形成使得共晶硅能够按照孪晶面凹角边缘（TPRE）机理快速生长。在微观尺度上，未变质共晶 Si 呈层片状并沿着 <1 1 0> 方向伸长，这与 TPRE 模型中的 <1 1 2> 择优生长方向不符。通过平行孪晶面上成对出现的 <1 1 2> 锯齿型生长，从而导致 141° 凹角交替的消失和产生，进而实现了 Si-<1 1 0> 的择优快速生长。这种生长方式保证了 Si 晶体能够将其低能 {1 1 1} 面与熔体接触。在锶变质合金中，共晶硅的形貌发生了很大的变化，这主要是由于限制 TPRE 生长和杂质诱导孪晶（IIT）生长。

热处理进一步细化了共晶组织。共晶铝相细化的同时伴随着共晶硅的碎化和圆整化。在热处理过程中，由于两相间具有很大的热膨胀不相容性，共晶硅不能随着铝相一起热膨胀，进而导致了硅的破碎。硅的破碎产生了“毛细管”力，从而激发 Al 原子向裂纹间隙处扩散。 由于 Al 原子具有置换扩散的特点，当 Al 原子向裂纹间隙处扩散的同时，空位迁移到铝基体的内部，这样硅破碎产生的空位被转移到铝基体内部。通过这种方式，共晶铝相产生了畸变和缺陷。这样产生的晶体学缺陷引发了铝基体的回复和再结晶，进而导致了铝晶粒的细化。

在铸态定向凝固 Al-12.7Si-0.04Sr 合金中，α-Al 相表现出很强的沿着凝固方向的 < 1 0 0 > 丝织构。铸锭边部比中心更容易产生粗大的 <1 0 0> 取向的大晶粒， 这是由于边部的传热条件能够满足三个 <1 0 0> 方向的传热。热处理后，由于发生了回复和再结晶，α-Al 的织构强度降低，但是织构类型没有改变。铸态共晶硅相沿着定向凝固方向，主要具有 <1 0 0> 和 <1 1 0> 两个丝织构组分，同时伴随出现了其他两个弱织构组分：<2 2 1> 和 <1 1 3> 丝织构。<1 0 0> 和 <1 1 0> 两个丝织构分别来自于铸锭边部和中心位置的 Si 晶体。<2 2 1> 和 <1 1 3> 组分是来自于 <1 0 0> 和 <1 1 0> 丝织构组分的多变体孪晶。另外 <2 2 1> 和 <1 1 3> 织构强度较弱，这是由它们所占的小体积分数决定的。一旦热处理，具有小体积分数的孪晶部分通过消耗对应的基体进行长大，因此 <1 1 0>

织构强度降低。另外， <1 1 3> 组分消失而 <1 1 5> 组分出现并增强，这是因为热处理过程中 Si 晶体破碎时发生了 Si 的晶体学旋转。

关键词：铝硅合金；锶变质；热处理；电子背散射衍射（EBSD）；生长孪晶；再结晶；中子衍射；织构。

Content

Chapter 1 Literature review

1.1 General introduction

With the increasing environmental pressure, energy efficiency has been a primary consideration for researches and developments worldwide. Thus materials with light-weight and environmental friendly have attracted attention. Aluminum alloys, with low density (2.7 g cm^{-3} as compared to 7.927 g cm^{-3} for steel), high specific strength, resistance to corrosion, high electrical and thermal conductivities, are accounted as one of such promising materials. They are ranked the third among the commercially used engineering materials [1, 2], and have been widely applied in automobiles, rail transportation and aerospace industries. For example, in automobile applications, full engine block can be made with aluminum alloys [3], which allows significantly reducing the weight of the vehicle, and thus greatly saving fuel consumption.

According to the processing techniques, aluminum alloys can be classified into two groups, wrought and cast. The wrought aluminum alloys have excellent extending workability, and are widely used in sheets, foils, pipes, rods, wires, rivets bars and profiles. The cast aluminum alloys possess excellent castability (*e.g.* high fluidity and low thermal contraction), and are used for sand casting, shell mold casting, metal mold casting, die casting and so on.

Among commercial aluminum foundry alloys, Al-Si-based alloys constitute ~ 90 % of the shape castings [4], due to their superior castability (*e.g.* high fluidity), low thermal expansion coefficient, excellent thermal conductivity, low cost, good wear resistance and corrosion resistance [5-7]. This is because Si addition increases the fluidity of the melt, reduces the melting temperature and decreases the contraction associated with solidification. Si has a low density (2.3 g cm^{-3}), showing an advantage of reducing the overall weight of the cast components. Besides, Si has a very low solubility in aluminum and precipitates as pure Si, which is hard and hence improves the anti-abrasion property of the alloys [8]. Due to the these advantages, Al-Si alloys have long been used as casting components in the fields of electronic packaging, aerospace, machinery/heavy industry, automotive industry and petroleum industry, especially for complex shaped aerospace and automotive components, such as engine/cylinder blocks [3], brake rotors, pistons and connecting rods [9]. General Motors firstly introduced die-cast Al-Si alloy (16-18 % Si and 4-5 % Cu) cylinder blocks

without cast iron cylinder liners in their Vega engines [10]. Some applications of Al-Si components in automotive components are shown in Fig. 1.1.

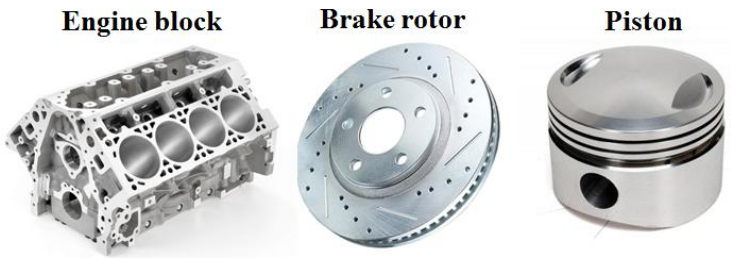

Fig. 1.1 As-cast Al-Si alloys for automobile components.

1.2 Binary Al-Si eutectic system

1.2.1 Phase equilibrium

The equilibrium phase diagram of Al-Si binary alloy is displayed in Fig. 1.2. Al-Si alloy is a simple eutectic system with two solid solution phases, face-centered cubic (FCC) α-Al and diamond cubic Si, with almost no solubility of Al in Si and limited Si in Al [11]. The solubility of Si in Al reaches a maximum 1.5 at. % at eutectic temperature (577 ℃), and decreases to 0.05 at. % at 300 ℃, denoted as α-Al.

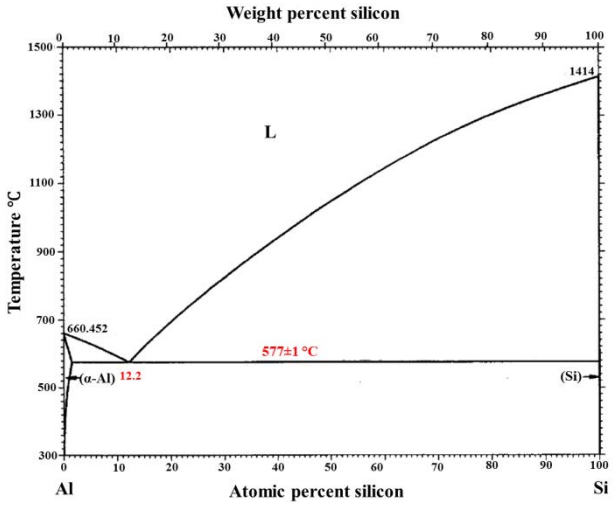

Fig. 1.2 The equilibrium phase diagram of Al-Si binary alloy [11].

Binary Al-Si alloys are classified into three groups: hypoeutectic, eutectic and hypereutectic alloys, depending on silicon content [11]. By conventional ingot metallurgy, the characteristic microstructures of three groups are as follows: eutectic structure comprising of

coarse plate-like silicon phases embedded and split in the continuous α-Al matrix; hypoeutectic structure composed of primary α-Al dendrites that solidifies first and the eutectic structure; hypereutectic structure containing coarse angular primary Si and eutectic structure [1].

1.2.2 Unmodified microstructural feature

1.2.2.1 Microstructure

The Al-Si eutectic alloys consist of two eutectic phases: the ductile globular α-Al phase and the coarse, brittle and hard Si plates embedded in the globular α-Al matrix. The typical microstructure of conventionally solidified Al-12.7Si alloy is illustrated in Fig. 1.3. The Si phase is in black and the α-Al matrix is in grey. Large Si plates are detrimental to the mechanical properties. With such a microstructure, it is difficult to perform deformation on these alloys, due to the presence of the brittle and hard Si phase. Therefore, to render Al-Si alloys deformable, the microstructures should be refined, especially the coarse eutectic Si plates (The refinement will be detailed later).

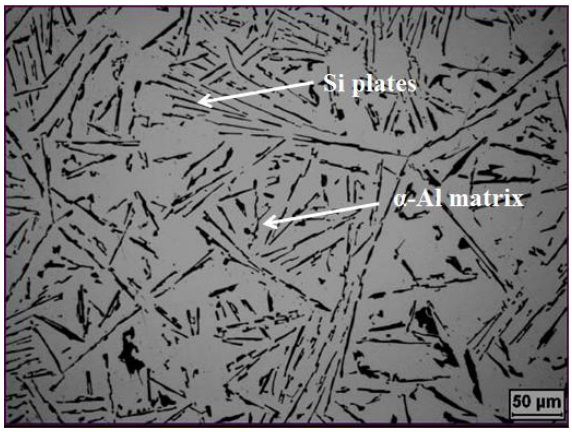

Fig. 1.3 The typical eutectic microstructure in crucible slowly solidified Al-12.7Si alloys (Black: Si and grey: α-Al).

1.2.2.2 Si twin

Most microstructural observations revealed that eutectic Si crystals contain twins, suggesting that Si crystals have an intrinsic tendency to form twins from Al-Si melt [12] during the eutectic nucleation and growth. The twin formation mechanisms and twin-matrix atomic correspondences have been studied experimentally and theoretically. It is found that

eutectic Si twins with the diamond face-centered cubic (FCC) structure are solely of the {1 1 1} <1 1 $\bar{2}$> reflection type. They could be regarded as either deformation twins that initiate under internal stresses induced by the thermal expansion difference between α-Al and Si eutectics during solidification [13], or growth twins generated owing to the intrinsic low stacking fault energy (SFE) of Si during nucleation [14] or subsequent growth [15]. Dayeh et al. [15] adopts molecular dynamics (MD) simulations to investigate the growth kinetics of Si-Ge nano wires, and proposed that four-atom Si clusters may deposit at faulty locations at the {1 1 1} facets leading to the nucleation of stacking faults thus the formation of another twin. As the Si crystals growing along [1 1 1] direction layer-by-layer, this process repeats and then multiple parallel twins formed. The formation probability of stacking fault is closely related to the stacking fault energy of the metal: the higher the fault energy the lower probability.

Moreover, there is a great interest in characterizing the eutectic Si twinning characters. Shamsuzzoha et al. [14, 16] reported that twinning showed different characters in unmodified and Sr-modified alloys, co-zonal (parallel twins) in unmodified Si and non-co-zonal (multiple twins) in Sr-modified Si (for twins in chemically modified alloys, it will be described later in [17]). It is proposed that twins appeared on the unmodified eutectic Si crystals are not produced due to the irregularity of the deposition of the Si atoms from the melt to the growth tip; rather a random stacking fault which occurred during the nucleation stage of the silicon plates at the point of origin of eutectic growth [14]. According to the high-resolution transmission electron microscope (HRTEM) observations on eutectic Si twins [14], the {1 1 1} atomic stacking sequence …ABCABC… of the cubic structure is changed across the twinning plane to be …AB<u>C</u>BAC…, where <u>C</u> atomic layer acts as the twinning plane. Considering that the diamond FCC structure deals with two nonequivalent sites for Si atoms, the {1 1 1} atomic stacking sequences in two twinned crystals should be ...AABBCC… and …CCBBAA…, respectively. It is well known that during solidification, two types of stacking fault can be easily produced in normal FCC crystals, *i.e.* …ABCA<u>BA</u>BC… by missing one C atomic layer or …ABCAB<u>A</u>CABC… by inserting one A atomic layer. To form a twin, only local stacking faults over several atomic layers are needed, while the entire crystal keeps the same stacking sequence. Obviously, it differs from the situation of the twin formation in diamond FCC structure by reversed stacking sequence. For the latter, crystal twins with reversed stacking sequence may be unstable.

1.2.3 Solidification behavior of eutectic Si

1.2.3.1 Nucleation of eutectic Si

Nucleation studies have shown that the growth of the Al-Si eutectics starts with the nucleation of eutectic Si phase [18]. For eutectic Si nucleation, several mechanisms have been proposed. These mechanisms state that there are three possible heterogeneous nucleation sites for the unmodified Si phase: the AlP phase [19-27], β-(Al, Si, Fe) phase [28-31] and the oxide bi-films inherently present ahead of the α-Al dendrites [21].

Usually, P appeared in commercial Al-Si alloys as impurity. It is well accepted that the P reacts with Al in the melt to form a fine dispersion of aluminum phosphide (AlP) particles. The AlP phase is believed to be the major nucleation site for eutectic Si phase as the crystal structure and lattice parameter of AlP has an excellent match with that of Si [32]. The lattice constants for AlP and Si are 0.55 nm and 0.54309 nm, and the corresponding space group are $^{-}$ and $^{-}$, respectively [33]. As early as in 1966, Crosley and Mondolfo [27] first proposed the AlP particles might act as the potent nucleation sites for the eutectic Si. Later Ho [25] reported that the Si morphology depended on the level of P element: the more the P content is, the coarser the Si particles are.

Besides, commercial Al-Si alloys invariably contain trace amounts of iron [30]. Shankar et al. [30] proposed a nucleation theory (see Fig. 1.4) based on the iron impurities in commercial hypoeutectic Al-Si alloys. As illustrated in Fig. 1.4, during the solidification process, primary α-Al dendrites nucleated at the liquidus temperature, and β-(Al, Si, Fe) particles nucleated in the solute field ahead of the growing primary α-Al dendrites. Eutectic Si particles nucleated at these β-(Al, Si, Fe) particles; then eutectic α-Al phase nucleated on the eutectic Si phase. Consequently, when the eutectic α-Al phase and primary α-Al phase impinged together, the growth of primary α-Al dendrites was arrested.

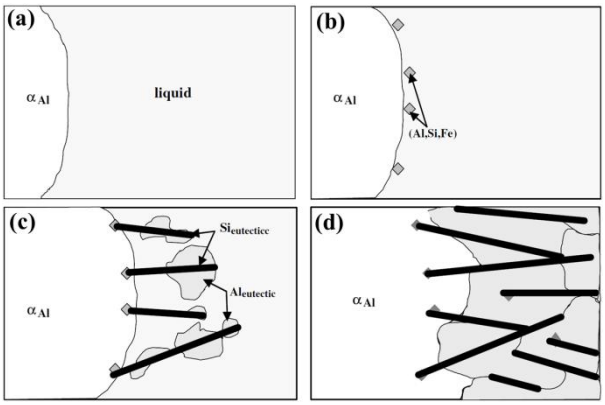

Fig. 1.4 Nucleation sequence of eutectic phases in hypoeutectic Al-Si alloys. (a) primary α-Al phase, (b) nucleation of β-(Al, Si, Fe) phase, (c) nucleation of eutectic Si on the β-(Al, Si, Fe) phase, nucleation and growth of eutectic α-Al phase on the eutectic Si phase, (d) impingement of the primary and eutectic α-Al grains resulting in the arrest of the primary dendrites and further nucleation and growth of the eutectic α-Al phase [30].

1.2.3.2 Growth of eutectic Si

Long studies have been devoted to understanding Si growth mechanisms, which is a prerequisite for its refinement. Al-Si eutectic alloy has a typical irregular eutectic microstructure, with non-facet α-Al phase growing isotropically and Si being a facet phase with anisotropic growth along specific crystallographic directions.

For Si crystals, the twin plane re-entrant edge (TPRE) growth mechanism has been well recognized. It was first proposed in explaining the unlimited propagation along <1 1 2> directions in germanium dendrites, and it concluded that at least two parallel twin planes are a prerequisite for continued rapid propagation of Ge dendrite [34], as shown in Fig. 1.5. This model was later applied to explain the growth of eutectic Si crystals, where the presence of twins forms re-entrant edges that acted as favorable growth sites and facilitate a rapid growth of eutectic Si crystals in <1 1 2> directions [12].

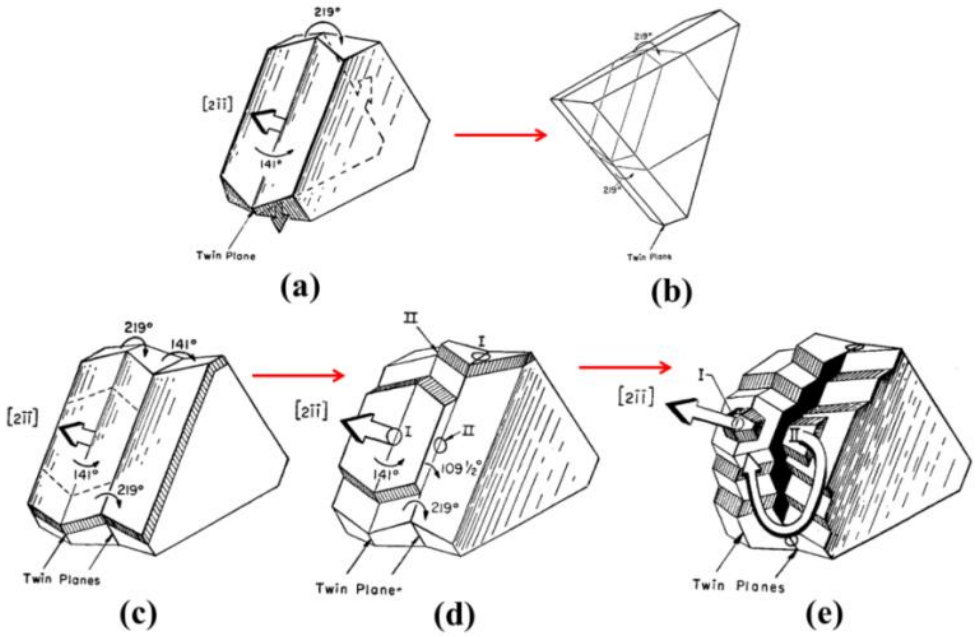

Fig. 1.5 Schematic illustrating of the TPRE model accounting for the rapid propagation of Ge dendrite along the <1 1 2> directions. (a) A twinned crystal of one twin plane with three 141° re-entrants; (b) The final crystal morphology from (a) with no re-entrants; (c) A twinned crystal of two twin planes with six 141° re-entrants; (d) <1 1 2> preferred growth at two of the 141° re-entrants, creating new corners of 109°; (e) all the re-entrants growing forward at once.

In 1985, Kobayashi and Hogan [12] found that eutectic Si crystals grew as thin flat plates by growing straight for some distance and then branching or changing direction at a large angle. Besides, they observed that plate shaped Si has a rapid growth along <1 1 2> directions. Thus, they proposed the growth model of unmodified Si crystals, as illustrated in Fig. 1.6.

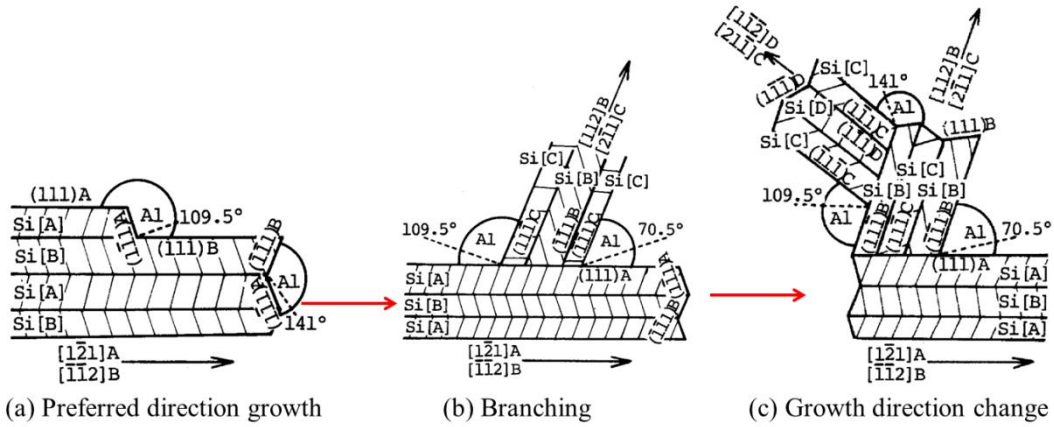

Fig. 1.6 Schematic illustration of growth mechanisms of eutectic Si [12] based on the TPRE model.

However, Lu and Hellawell [13, 35] observed in TEM that the inter-spacing between twins in Si crystals were relatively wide. Hence they proposed that Si flakes grew predominantly by the layer growth mechanism instead of the TPRE mechanism. The layer growth mechanism depicted that there are flat terraces and partial-layer steps on a crystal surface which contains kinks. The atoms attached themselves to the kink sites preferentially than to the terraces. Growth rate at different facets of the crystal was different [36], hence resulting in an anisotropic growth of Si particles.

In both layer growth mechanism and TPRE growth models based on {1 1 1} twinning, Si phase is required to have a <1 1 2> preferred growth along the solidification direction [12, 37-39]. Kobayashi and Hogan [12] found unmodified eutectic Si flakes grow in <1 1 2> directions. Li et al. [40] observed Si twins showed a <1 1 2> preferred growth direction on {1 1 1} growth planes under TEM in high-purity melt-span Al-5Si alloys. However, other preferred growth directions of unmodified Si crystals have been reported, *i.e.* <1 1 0> [17, 41], in addition to the <1 1 2> [12, 40] preferred growth direction. Day and Hellawell [42] observed a Si-<1 0 0> fiber texture in high-purity directionally solidified unmodified Al-Si alloys (containing 12-16 wt. % Si) at low freezing rate by SEM and X-ray techniques. In this sense, both layer growth and TPRE growth models seem not operate in unmodified Si growth.

Although both layer growth mechanism and TPRE growth mechanism are widely accepted, the growth process of Si from the atomic scale to microscopic scale has not been clearly addressed. It can be seen that the former investigations of the preferred orientation (texture) of eutectic Si phase were mainly performed in the directionally solidified Al-Si alloys at nano or atomic scale by TEM technique. At such a limited nano or atomic scale, the statistical information about the texture of Si phase could not be obtained due to the fact that eutectic Si phase possess a large size out of the level what a TEM technique could attain.

1.2.4 Orientation relationship between eutectic α-Al and Si phases

Crystallographic orientation relationship (OR) can be a valuable indicator in differentiating the sequence of precipitation events during a liquid-to-solid transformation, *i.e.* eutectic reaction. Normally for eutectic reaction, as the two eutectic phases form almost at the same time, specific ORs between them may be required to lower down the interface energy.

Day and Hellawell [42] reported a random crystallographic orientation relationship between α-Al and Si eutectic phases in unmodified Al-Si alloys using X-ray diffraction.

Kobayashi et al. [38] investigated the crystallographic orientation relationships of eutectic α-Al and Si in unmodified Al-Si alloys under TEM, and the most frequent one was $[0\ 0\ 1]_{Al}$ // $[1\ 1\ 0]_{Si}$ - $(1\ 0\ 0)_{Al}$ // $(\bar{1}\ 1\ \bar{1})_{Si}$. Shamsuzzoha and Hogan [43] adopted bulk specimen and determined the orientation relationships between eutectic α-Al and Si in unmodified Al-Si alloys. They observed the ORs at lower growth velocities (about 100 μm s^{-1}): $[\bar{1}\ 1\ 0]_{Si}$ // $[2\ 1\ 1]_{Al}$ - $(1\ 1\ 1)_{Si}$ // $(1\ 0\ \bar{2})_{Al}$ // twinning plane, $[\bar{1}\ 1\ 0]_{Si}$ // $[1\ 0\ 0]_{Al}$ - $(1\ 1\ 1)_{Si}$ // $(0\ 1\ 2)_{Al}$ // twin plane. Ho and Cantor [25] found a range of ORs existing between coarse facet Si and surrounding α-Al matrix in Al-3Si and Al-3Si-P alloys by using TEM. Dahle [44] predicted that there is no crystallographic ORs between α-Al and Si. Al-Si eutectic alloys are irregular eutectics. Branching and termination of growth occurred so that there is not a unique lamellar spacing in these eutectics. Si could change its growth direction by twinning, thus there might not necessarily be a specific OR between α-Al and Si eutectic phases.

As mentioned above, it can be seen that the results are quite divergent. Occasionally, controversial claims have even appeared on whether or not there exists a specific OR in eutectic α-Al and Si mixtures [44].

1.3 Refinement of eutectic Si

1.3.1 Modification techniques

To realize eutectic Si refinement, there are two well accepted techniques applied to the solidification process. One is quenching during rapid cooling state and the other is chemical addition during melting state through which the eutectic Si phase can change from the plate-like to a finer fibrous morphology. This plate-to-fiber transition of the eutectic Si morphology in Al-Si alloy is commonly known as eutectic modification. For quenching modification, some advanced processing technologies based on rapid solidification techniques such as powder metallurgy [45-47] and spray deposition [48-55] have proven to be effective in producing deformable Al-Si alloys with microstructure significantly refined [52, 56]. In Northeastern University, a process based on traditional technologies, direct chill (DC) semi-continuous casting followed by hot deformation and heat treatment, has been developed for potential mass production of wrought Al-Si alloys. Superior mechanical properties in view of their strength and ductility have been obtained. Yu et al. [57-60] reported that the DC casting process could be employed to refine both primary and eutectic Si phase in hypereutectic Al-Si

alloys without introducing chemical modification and other means such as electromagnetic stirring [61].

Based on the conventional ingot metallurgy, another way to realize the modification of eutectic Si crystals is to add chemical modifier [62]. Usually, trace additions of chemical modifiers, *i.e.* Sr or Na, can realize the morphological change of the eutectic Si phase from coarse plates to fine fibrous crystals.

The modification of eutectic Si morphology either by quenching or by chemical modification has important industrial interests, because it brings about beneficial effect on strength, bendability and ductility [5, 13, 63, 64]. Therefore, many researchers have devoted themselves to the investigation of the modification phenomenon and modification mechanisms of both quecnhing modification and chemical modification [12]. Despite the long research over 90 years since the discovery of chemical modification, theories that rigorously explain the formation of the eutectic Si phase and the modification of the Si morphology by specific chemical additives or with a high cooling rate remain inconclusive. In present PhD work, we only focus on the study of the chemical modfication mechanism.

1.3.2 Chemical modification

1.3.2.1 Chemical modifiers

The addition of chemical modifiers into Al-Si alloys which can transform the eutectic Si morphology from the plate to the finer fibers was reported 95 years ago. In 1921, Pacz [65] firstly introduced sodium chloride and calcium fluoride to Al-Si alloys, and achieved significant microstructural refinement and excellent mechanical property improvement. Since then, an explosion of ideas has been conceived based on this technologically morphological transition. Later, Jeffries [66] (in 1922), Edwards [67] (in 1924), Archer and Kempf [68] (in 1926), Gwyer and Phillips [69] (in 1926) found similar effects of alkali metals, alkali earth metals and their oxides and hydroxides on Si refinement.

Until 1970s, Na was uniquely accepted as chemical modifier for Al-Si eutectic alloys because of its low cost and its uniform and fast dissolution in Al-Si melt. However, it possesses an important drawback: volatilization, especially at elevated temperatures. Due to this feature, excessive fuming is produced during melting and its concentration in the melt is difficult to be controlled. As reported by Makhlouf [70], this was first revealed by Curran and

his co-workers in 1922. They observed a "fading" effect: when Al-Si melt was held for a long period of time under convection, the modification phenomenon disappeared. Thus he proposed that this fading effect was caused by the vaporization of Na from the melt. Later Jenkinson and Hogan [71] found that it was difficult to control the chemical composition when Na was added during directional solidification (DS), due to its volatilization and diffusion through crucible. In view of these shortcomings, efforts have long been made in searching for its replacements.

Moreover, the chemical modification effect by the addition of other chemical elements, such as Ba [72], Ca [72], Y [72, 73], Yb [40, 72, 74], B [75], Sb [19, 76], Eu [77-79], and rare earth metals (La, Ce, Pr, Nd, Sm, Eu, Gd, Tb, Dy, Ho, Er, Tm, Yb and Lu) [77] has been investigated. Among them, the Ba [72], Ca [72], and Eu [77-79] can be used as modifiers which have the same modification effect of plate-to-fiber transition; the addition of Y, Yb, Sb and rare earth metals (La, Ce, Pr, Nd, Sm, Eu, Gd, Tb, Dy, Ho, Er, Tm, Yb and Lu) brought about a refined plate-like Si; the addition of B has almost no effect on the microstructure, namely no modification effect or refinement.

Although the Ba, Ca, and Eu have been verified to possess the plate-to-fiber modification effect, the widely industrial used modifiers are Na and Sr chemical modifiers. From 1975 to 1983, Al-Sr master alloys were designed [71, 80, 81]. Later Sr modifier became especially attractive due to its numerous advantages: such as durability, easy addition, good recovery and low fuming [71, 80].

To date, the most widely applied modifier is Sr. In view of its numerous advantages, Sr was selected as the chemical modifier for the present PhD work.

1.3.2.2 Microstructural features after chemical modification

Correct recognition of morphology of Si is a prerequisite to understand the role that the chemical additives play in influencing its morphology for interpreting the modification mechanisms.

1.3.2.2.1 Eutectic Si phase

Before 1965, most of the work assumed that the silicon particles in both unmodified and modified alloys were isolated crystals. In 1963, Kim and Heine [82] conducted quench experiments and thermal analysis of hypoeutectic, eutectic and hypereutectic alloys and found

that flake silicon that is the characteristic morphology of the unmodified eutectic was obtained at high temperature, whereas fibrous Si obtained in the modified eutectic at relatively lower temperature associated with substantial undercooling. They proposed that the Si morphology depended on the temperature at which Si crystals grow (the so called "growth temperature/phase-shape" hypothesis), and was not affected by the presence or absence of modifiers in the melt. However, this hypothesis was later disproved by Gigliotti and Colligan [83] who reported that the eutectic Si morphology do not change with growth temperature. In 1966, Crosley and Mondolfo [27] suggested that unmodified needle-like Si should be in flake or sheet shape.

In 1965, Bell and Winegard [84] adopted the method of etching out the α-Al phase and leaving the Si phase untouched, and found that the Si phase in both rapidly cooled high-purity Al-Si eutectic alloys and Na-modified alloys was interconnected in the α-Al matrix, even when the eutectic colonies are 2 mm in diameter. Later, Kobayshi and Hogan [12] observed the three dimensionally (3D) interconnected fibrous Si phase in Al-14Si-0.18Sr alloys by adopting the similar etching method. Moreover, they found that unmodified eutectic Si crystals grew as thin flat plates that grew straight for some distance and then might branch or change direction by a large angle. With the availability of electron microscope, it was confirmed that unmodified Si has a plate-like morphology [70].

Now it has been well accepted the typical morphology for slowly solidified unmodified eutectic Si crystals is coarse plate-like and that for modified Si (either by chemical modification or by quenching modification) is fine fibrous. The eutectic Si phase is 3D interconnected.

Moreover, to clarify the fibrous Si growth mechanism, a statistical examinations have been made to confirm the preferred growth direction of modified eutectic Si crystals [12, 13, 41, 71, 85]. And other preferred growth directions of modified Si crystals have been reported, *i.e.* <1 0 0> [13, 42, 71] and <1 1 0> [17, 41], in addition to the <1 1 2> [12, 40] preferred growth direction. Since the <1 1 2> growth direction is the featured growth direction contributing to the IIT and restricted TPRE growth mechanisms, both models seem not operate in the fibrous Si growth.

Steen and Hellawell [41] found that Si fibers in the quenching modified Al-Si alloys showed a <1 1 0> preferred growth direction along the solidification direction observed in TEM. Jenkinson and Hogan [71] observed a Si-<1 0 0> fiber texture along the directional

solidification direction under TEM in both quenching and Sr-modified Al-Si alloys (containing 9-17 wt. % Si) alloys. Kobayashi and Hogan [12] found in both quenching and chemical modified eutectics, the Si fibers showed the preferred growth directions of probably <1 0 0>, or <1 1 0>, but <1 1 2> is rarely observed under TEM. Lu and Hellawell [13] reported that in Na-modified fibers, the preferred growth axis was in the <1 0 0> direction with symmetrical branching in <1 1 2> directions. Heiberg and Arnberg [86] found Si-<1 1 0> texture in high-purity Sr-modified Al-7Si alloys by SEM/EBSD technique. Li et al. [40] observed Si twins showed a <1 1 2> preferred growth direction on {1 1 1} growth planes under TEM in high-purity melt-span Al-5Si alloys with and without 200 ppm Sr addition.

In conclusion, it can be seen that the former investigations of the preferred orientation (texture) of eutectic Si phase were mainly performed in the directionally solidified Al-Si alloys. There has not been a representative preferred growth/extension direction of eutectic Si phases. Such dispersion may arise from that fact that most of the investigations were performed at nano or atomic scale by TEM technique.

1.3.2.2.2 Eutectic α-Al phase

In addition to the significant effect of refinement on eutectic Si crystals, the effect of chemical modifiers on eutectic α-Al matrix also received attention. Most researchers had the opinion that the chemical modifiers can cause a coarsening of eutectic α-Al grains [12, 19, 71, 87, 88], while few concluded there is no effect on the eutectic α-Al grains [13]. The size and morphology of eutectic α-Al are still not well clarified, because it requires complex characterization techniques, such as the addition of segregating elements [86, 89], chemical or thermal etching [71, 90], and most commonly interrupting solidification by quenching [19, 87, 88].

Meussner [90] adopted special etchants and a chemical extraction technique and found that α-Al matrix in unmodified Al-Si alloy consists of many grains of special orientations rather than large grains extending over wide regions. Later, Jenkinson and Hogan [71] observed the grain morphology of α-Al phase by examining anodized surfaces of unmodified and modified Al-Si specimens under polarized light. They showed that unmodified α-Al grains were much finer than their modified counterparts. The α-Al grains in the unmodified alloy were equiaxed in both longitudinal and transverse sections, while in the modified one they were not equiaxed but are elongated in the growth direction. Kobayashi and Hogan [12]

found that α-Al phase was polycrystalline within a single eutectic colony in the unmodified eutectic, but mono-crystalline in the modified eutectic. Shamsuzzoha and Hogan [39] indicated that the α-Al grains in the as-cast DS Al-14Si-0.18Sr alloy extended along the entire length of adjacent silicon fibers, which is in consistence with the former observation [71], with a typical length in sub-millimeter range. Moreover, TEM examination showed that aluminum phase displays a <1 1 0> fiber texture.

It was until in 2001 that systematic investigations on the effect of chemical modifiers on the eutectic α-Al phase initiated by McDonald and his colleagues [18, 19, 87, 88, 91] have been widely developed to account for the eutectic modification mechanisms. They [18, 19, 87, 88, 91] observed that chemical modification significantly increases the grain size by means of interrupted solidification technique. McDonald et al. [88] concluded that Na and Sr additions resulted in large eutectic grains; and Na additions brought about coarser eutectic grains. Moreover, the size of eutectic grains decreases with the increased cooling rate. Dahle et al. [19] found that in hypoeutectic Al-10Si alloys, Sb and Sr additions increases the grain size by an order of 10. The eutectic grain sizes were the largest in Sr-modified Al-Si alloys, intermediate in Sb-modified alloys, and the smallest in unmodified alloy. Based on these, they proposed a coarsening mechanism of eutectic grains by chemical additions. The addition of modifiers poisoned the P-containing nucleus, *i.e.* AlP, thus reducing the nucleation sites. With less eutectic grains formed, the final α-Al grains are coarsened.

In summary, there is amounts of evidence to elucidate that the chemical addition increases the α-Al eutectic grains to millimeter scale [18, 92]. However, structures in α-Al interiors have not been well addressed. Although local disorientations of ~ 2^{o}, were observed in both unmodified and Na-modified alloys [13], the formation of subgrains and their further development is not clear yet.

1.3.3 Chemical modification mechanisms

1.3.3.1 Overview

Since the discovery of the modification effect with Na addition by Pacz [65], great efforts have been made to understand the underlying mechanisms. Several theories have been proposed to explain the modification mechanism, and these theories have been well reviewed [8, 70].

The former reported modification mechanisms include fluxing effect on oxide compounds [70], formation of the Al-Si-Na ternary alloy [70], dispersed colloidal phase theory [67, 93], surface energy based theory [27, 94-97] (as illustrated in Fig. 1.7), reduced Si diffusion [98], growth temperature based theory [82], reduced Si growth [83], AlP poisoning theory [27], restricted twin plane re-entrant edge (TPRE) growth [39, 43] and impurity induced twinning (IIT) growth mechanisms [13, 35]. And among them, restricted TPRE and IIT growth mechanisms are widely accepted.

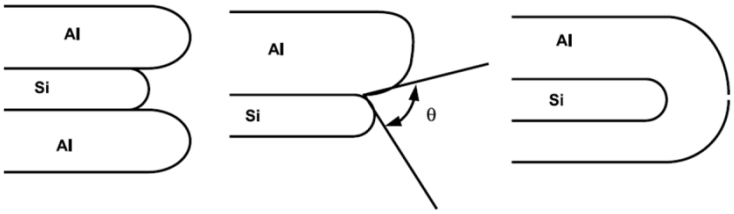

Fig. 1.7 Eutectic solidification theory based on the surface energy at the α-Al/Si solid interface in Na-modified alloys [94].

In 1985, Kobayashi and Hogan [12] studied a hypereutectic Al-Si alloy over-modified by Na addition using X-rays. They observed that Na-rich distributed at the boundaries of twins on the primary Si crystals. Thus they proposed that Na concentrated at the twin plane re-entrant edges at the Si growth tips and reduced or eliminated the growth rate advantage of the TPRE mechanism. Moreover, they found that the modified Si fibers with rounded shape grew along the <1 0 0> or <1 1 0> but rarely <1 1 2> directions. Based on these observations, they concluded that the TPRE mechanism does not operate on the fibrous Si growth [12]. The modified Si fibers grew in an isotropic manner covering a larger set of directions ranging from <1 0 0> to <1 1 0>, Shamsuzzoha and Hogan [39, 43] proposed that the growth of fibrous eutectic Si crystals were compatible with the TPRE growth mechanism, with internal <1 1 2> branching mechanisms permitting a wide range of crystallographic orientations.

In 1985-1987, Lu and Hellawell [13, 35] found that Na or Sr addition brought about higher density of Si twins. Therefore, they proposed the impurity induced twinning (IIT) theory explaining the chemical modification mechanism based on the layer growth mechanism. The IIT mechanism depicts that the adsorption of impurity atoms at monolayer steps on the solid-liquid interface contributes to the alteration of the Si-{1 1 1} atomic stacking sequence, thus promoting the formation of Si twins.

The former reported modification mechanisms can be classified into two groups: the restricted nucleation (reduction in nucleation frequency) and restricted growth theories (restricted TPRE and IIT), as detailed below.

1.3.3.2 Restricted nucleation theory

Some believe that the nucleation is the dominant factor in influencing the modification process. The AlP phase is believed to be responsible for the Si nucleation [19-27]. McDonald et al. [87, 88] suggested that AlP particles in the unmodified alloys were removed or poisoned by the addition of Sr elements. Dahle et al. [19] further experimentally evidenced that it was the Sr-containing intermetallic (most likely Al_2Si_2Sr) that removed or neutralized the AlP nucleation sites. Cho et al. [21, 26] proposed that AlP was also the nucleus of iron intermetallic in commercial aluminum alloys, even at low levels around 10 to 20 ppm. Besides, they assumed that the AlP – potent nuclei for Al-Si eutectics, was poisoned by the formation of Al_2Si_2Sr phase surrounded the P-rich particles. Thus the nucleation of the eutectic Si became more difficult when it was preceded by the formation of β-Al_5FeSi or the Al_2Si_2Sr phases. Zarif et al. [22] studied the eutectic modification effect in high-purity Al-Si alloys with controlled P and Sr additions. They found that unlike P, the addition of Sr did not promote nucleation, while it decreased the eutectic nucleation temperature. The simulation of Scheil indicated the Al_2Si_2Sr intermetallic was formed before eutectic solidification. Therefore, they proposed that Sr-contained phase (Al_2Si_2Sr intermetallic observed under TEM or Sr_3P_2 compounds which were not evident) could consume or detrimentally affect potent AlP nucleation sites.

1.3.3.3 Restricted growth theory

With respect to the anisotropic growth of the unmodified eutectic Si crystals, two models have been proposed and widely accepted, namely, layer growth [35] and twin plane re-entrant edge (TPRE) growth model [34, 42, 43]. The layer growth model depicts that the Si atoms attach themselves to the kink sites preferentially. Growth rate at different facets of the Si crystal is different [36], hence resulting in an anisotropic growth. Compared with the layer growth model, the TPRE further specifies that the Si atom attaching sites are twinning plane related 141° re-entrants.

On this basis, two representative chemical modification mechanisms focusing on the eutectic Si growth are proposed, namely impurity induced twinning (IIT) [13] and restricted TPRE growth [12] mechanisms. The IIT model is proposed based on the layer growth mechanism [13]. The impurity atoms absorbed at the monolayer steps on the solid-liquid interface contribute to the alteration of the stacking sequence of {1 1 1} planes and thus the formation of twins, thereby locally enabling isotropic growth in many <1 1 2> directions. The restricted TPRE growth model assumes that the modifiers will poison the 141° re-entrant {1 1 1} twin grooves, thereby deactivating the anisotropic TPRE growth and promoting isotropic growth.

To find out possible modification mechanisms either restricted nucleation or restricted growth, long efforts have been paid to mainly two aspects, including the Si twin characters and the distribution of chemical modifiers.

1.3.3.3.1 The Si twin characters

In either IIT or restricted TPRE growth mechanism, the increased twin density is prerequisite condition contributing to the eutectic modification [39, 41, 42]. Thus great attention has been paid to investigate the relationship between the eutectic modification and the Si twin population.

To date, there is still a dispute about the possible Si twin density in both unmodified and modified Al-Si alloys. Some hold the opinion that chill casting with high undercooling brought more twins than slow solidification [41, 42, 99, 100], some others assumed that chemical modifiers brought about higher twin populations [12, 13, 39, 71, 85, 100]. In 1975-1987, Shamsuzzoha, Hogan and his co-worker [12, 43, 71, 100, 101] reported that higher twin density was found in both quenching modified and Sr-modified Si fibers than in unmodified Si flakes. Besides, Si twin density in Sr-modified alloys was higher than that in quenching modified alloys. In the Sr-modified Si fibers, at least two {1 1 1} twin systems operate in each fiber; while in the quenching modified alloy only a single {1 1 1} twinning system was observed in each fiber. In 1985-1987, Lu and Hellawell [13, 35] found increased Si twin density in Na-modified alloys, while this increase was not found in quenching modified alloys. According to these observations of Si twin density, they proposed the famous IIT modification mechanism. In 2003, Nogita et al. [75, 85] disapproved the IIT mechanism through evaluating the relationship between the twin density and the modification effect of Ba,

Ca, Y and Yb in A356 (Al-7Si-Mg) alloys by optical microscope (OM), thermal analysis, X-ray diffractometry and TEM techniques. It showed the sequence of Si twin density from high to low in: chemical-modified, unmodified, chill-modified Al-Si alloys. Especially in chill-modified materials, Si twin frequency was almost zero. Additions of Ba and Ca caused the modified Si fibers, while the addition of Y and Yb resulted in the refined plate-like eutectic structure. After all the modifiers addition, the twin density was higher than the unmodified alloy. There was no significant difference of the Si twin density between the modified fibrous Si (Ba and Ca) and the refined plate-like Si (Y and Yb). They concluded that the twin density induced by the modifier addition was too low to explain modification using the IIT model. In 2005, Dahle et al. [19] found there were twins in both Sb-modified and Sr-modified Si fibers, with the twins lying parallel to the apparent growth direction of the fibers. However, there was no twin existing inside unmodified Si crystals. In 2015, Li et al. [40] observed a higher Si twin density in the Al-5Si alloys with 50 ppm Na addition than that without or with 200 ppm Sr addition. Besides, the addition of Yb didn't have significant effect on Si twinning, when compared to the addition of Sr or Na.

1.3.3.3.2 The distribution of modifiers

As shown in former reports [13, 35], the trace addition of chemical modifiers in Al-Si alloys, *i.e.* Sr, only modified the eutectic Si morphology, while no significant impact on that of α-Al phase. Thus, the hypothesis that the Sr is preferentially adsorbed inside the eutectic Si phase has been proposed in both IIT and restricted TPRE growth models. In these models, the modifier atoms would preferably be segregated either at the re-entrant 141° grooves (for restricted TPRE growth) or at the intersection of Si twins (for IIT). The main difference between them is the absorption location. Therefore, to determine the distribution and concentration of the modifiers within the eutectic microstructure is of interest. However, it is difficult to detect the Sr elements due to the fact that their concentrations are below the sensitivity limit of most analytical techniques [102], *i.e.,* Sr concentration used is often ranged from 20 ppm to 600 ppm.

Thus, extensive investigations [5, 79, 102-111] of the distribution of the modifier elements has been performed with high resolution characterization techniques [102, 104], *i.e.* 3D APT (atom probe tomography) and HRTEM [5, 109, 110]. Kobayashi and Hogan [12] adopted X-ray technique to examine hypereutectic Al-Si alloys over-modified by Na, and found Na-rich distributed at the boundaries of twins on the primary Si. Clapham and Smith

[102] studied the Sr distribution through individual phase analysis by selectively dissolving Al and Si eutectic phases using an atomic adsorption spectroscopy (AAS) technique. They found that Sr modifier segregated preferentially to the eutectic Si phase during slowly solidification and to the eutectic α-Al phase during rapid solidification. Thus, it was proposed that the Sr was rejected from aluminum phase during solidification of modified Al-Si alloys and was incorporated into Si phase. Nogita et al. [104] examined the Sr elements distribution in Al-10 wt. % Si-1 wt. % Cu alloy with 250 ppm Sr addition, utilizing a μ-XRF (X-ray fluorescence) technique with a spatial resolution below 100 nm at the SPring-8 synchrotron radiation facility X-ray source. The result indicated that the Sr elements segregated exclusively and homogeneously to the eutectic Si phase. They proposed that the strong segregation of Sr into eutectic Si was the cause of larger eutectic growth undercooling that occurred in modified alloys. Simensen et al. [105] adopted NanoSIMS analysis to quantify the micro-scale spatial distribution of trace elements in the as-cast industrial A356 alloy. It was observed that both Sr and Na segregated preferentially to the Si particles rather than to the α-Al matrix, but Ca segregates preferentially to the α-Al matrix and was not found in Si. In contrast to Sr, Na was inhomogeneously distributed in the Si particles and tended to accumulate at parts of their surfaces. They proposed that the IIT mechanism was not responsible for the flake-fiber transition in the Ca-modified Al-Si alloys. Faraji and Katgerman [106] quantitatively investigated Sr distribution in the commercial hypoeutectic A356 foundry alloy using electron probe microanalysis technique (EPMA). The results showed that Sr resided mostly inside the silicon phase. At the same year, Nogita et al. [79] studied the Eu and Yb segregation in hypoeutectic Al-Si alloy, utilizing a μ-XRF (X-ray fluorescence) technique. It showed that Eu strongly segregated to the Si phase and was of negligible concentration in the primary and eutectic α-Al phases. Eu was distributed relatively homogeneously in the Si fibers. On the contrary, the Yb precipitated and was not present either in α-Al or in Si phases. These observations highlighted that the geometrical ratio to predict IIT behavior was not sufficient when considered in isolation. Together with their former report using μ-XRF [104], it showed that all structures under the fibrous modification effect had the modification element distributed homogeneously inside the eutectic Si phase. Timpel et al. [5] studied the Sr element distribution in Al-10 wt. % Si-0.1 wt. % Fe with 200 ppm Sr addition by means of atom probe tomography (APT) in atomic and TEM in nanometer resolution. The combined investigation indicated that Sr co-segregated with Al and Si within the Si phase in two types, as shown in Fig. 1.8. For Type I, nanometer-thin rod-like

co-segregation is responsible for the formation of multiple twins in a Si crystal and enabled its growth in different crystallographic directions. For Type II, segregations come as more extended structures, restricted the growth of a Si crystal and control its branching. The two types Sr-Al-Si co-segregations contribute to the former reported mechanisms, respectively, namely, the IIT (via type 1) and restricted TPRE (via type II).

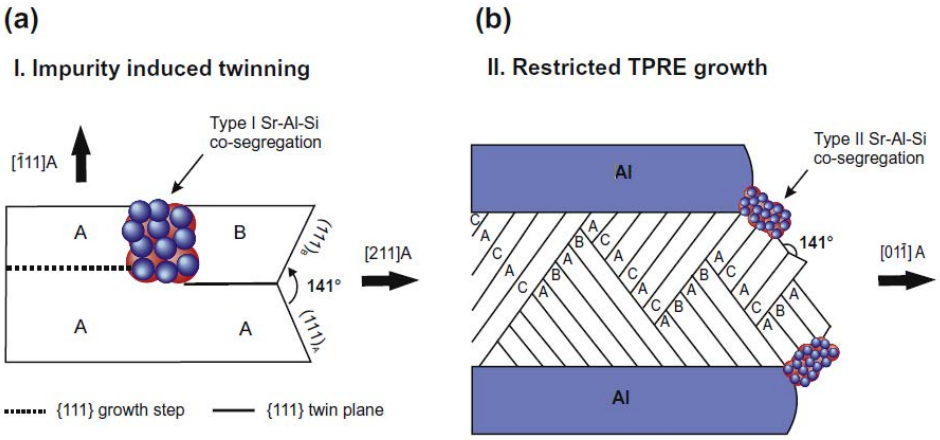

Fig. 1.8 Schematic representation of (0 1 1) plane projection of eutectic Si phase: (a) type I Sr-Al-Si co-segregation that promotes twinning by changing the stacking sequence; (b) locations of type II Sr-Al-Si co-segregations within the eutectic Si phase at the re-entrant edges or growing surfaces [5].

With the accumulating evidence, the hypothesis that Sr elements tend to segregate onto the Si crystals homogeneously, in the form of Al_2Si_2Sr compound instead of single Sr atoms has been confirmed.

And many researchers hold the opinion that it is the Al_2Si_2Sr compound instead of single Sr atoms that contributes to the chemical modification. Manickaraj et al. [110] studied the distribution of Al_2Si_2Sr by nano-diffraction experiments using X-ray high energy synchrotron beam source and by X-ray fluorescence elemental mapping. They found that Al_2Si_2Sr exist at the boundary between the eutectic Si and Al grains. Barrirero et al. [109] compared the segregations formed in unmodified and Sr-modified Al-Si alloys by APT and TEM. The compositional analysis of eutectic Si phase show that there are 430 ± 160 at-ppm Al and 40 ± 10 at-ppm Sr in Si and the total amount of Al trapped in the Si phase is 4 times higher in the Sr-modified alloys than in the unmodified, confirming that a large fraction of Al together with Sr was incorporated into the Si phase. Srirangam et al. [111] probed the local atomic structure of Sr-modified Al-Si alloys by extended X-ray adsorption fine structure (EXAFS)

spectroscopy and atom probe tomography (APT) measurements and found that Sr prefers bonding to Si atoms to form Al_2Si_2Sr clusters in Al-3Si and Al-12.5Si alloys and Al_4Sr intermetallic compound in Al-10Sr master alloy. They proposed that such clusters could play an important role in poisoning of the nucleation sites, delaying the nucleation of eutectic phase and causing the morphological changes.

However, Li et al. [40] firstly proposed that it is the Al_2Si_2X (X, Sr or Yb) phase or X-rich clusters formed within Si to be an "artefact" caused by the solute entrapment during Si growth, rather than active factor affecting the modification. They adopted high-resolution transmission electron microscope (HRTEM) and atomic-resolution scanning transmission electron microscope (STEM) to investigate the segregation of Sr, Na and Yb atoms during eutectic Si growth in high-purity Al-5Si alloys. It was found the Sr and Na atoms distributed along the $<1\ 1\ 2>_{Si}$ growth direction of Si and at the intersection of multiple Si twins, which can be used to interpret the restricted TPRE and IIT modification mechanisms, respectively. Besides, no significant Yb-rich cluster was observed at the intersection of Si twins, while considerable Yb-rich segregation lines were observed along the $<1\ 1\ 2>_{Si}$ direction. Restricted TPRE and IIT modification mechanisms were not observed due to the absence of Yb within Si, in particular at the twin re-entrant edges or at the intersection of Si twins.

1.3.4 Influence of chemical modification on OR between α-Al/Si eutectics

There is an interesting but not better understood phenomenon that unmodified eutectic silicon phase leads over the eutectic α-aluminum phase by a large margin at the growth interface of eutectic colony and such obvious lead disappears in the modified Al-Si alloy [12]. However, this leading over disappears when chemical modified. Explanation to this phenomenon is likely to be sought with more information on the crystallographic orientation relationship (OR) between eutectic α-Al and eutectic Si phases.

Shamsuzzoha and Hogan [43] compared the ORs of eutectics in both unmodified and chill modified Al-Si alloys. And they observed the following relations at lower growth velocities (about 100 μm s^{-1}): $[\bar{1}\ 1\ 0]_{Si}$ // $[2\ 1\ 1]_{Al}$ - $(1\ 1\ 1)_{Si}$ // $(1\ 0\ \bar{2})_{Al}$ // twinning plane, $[\bar{1}\ 1\ 0]_{Si}$ // $[1\ 0\ 0]_{Al}$ - $(1\ 1\ 1)_{Si}$ // $(0\ 1\ 2)_{Al}$ // twin plane. At higher growth velocities (750 μm s^{-1}), the most frequently observed relationship was $[0\ 0\ 1]_{Al}$ // $[1\ 1\ 0]_{Si}$ - $(1\ 0\ 0)_{Al}$ // $(\bar{1}\ 1\ \bar{1})_{Si}$, which was the same as that reported by Kobayashi [38]. The common feature of these relationships was that $\{1\ 0\ 2\}_{Al}$ lies parallel to the $\{1\ 1\ 1\}_{Si}$ twinning plane. This OR minimized the

difference of inter-planar spacing at the Al/Si interface. Later, Shamsuzzoha and Hogan [100] observed the same OR: $[1\ 0\ 0]_{Al}$ // $[\bar{1}\ 1\ 0]_{Si}$ - $(0\ 1\ 0)_{Al}$ // $(1\ 1\ \bar{1})_{Si}$ when studying the twinned growth of Si in chill modified Al-Si eutectic alloys. This result indicated that eutectic Al grew by repeated re-nucleation on Si surface, the same as that in unmodified Al-Si alloys. They concluded that growth crystallography of chill modified Si fibers and that of unmodified Si flakes were similar; whereas impurity modified fiber Si had a different growth mechanism. Heiberg and Arnberg [86] found that frequently the α-Al has a <1 0 0> or <1 1 0> axis parallel to the <1 1 0> direction of the Si fibers in high-purity Sr-modified Al-7Si alloys.

So far numerous orientation relationships between the α-Al/Si eutectics in both unmodified and modified Al-Si alloys have been reported in literature, as summarized and listed in table 1.1. It should be noted that most of the studies were conducted in TEM. The investigations were very local and individual. The ORs identified in such ways may not be representative or statistical.

Table 1.1 Identified ORs between eutectic α-Al and eutectic Si in Al-Si alloys.

Time	Composition (wt. %)	Characterization technique	Cast condition	OR between Al_{eut} and Si_{eut}		Ref.
1979	Al-12.7Si thin films	TEM	Chill modification	$(1\ 0\ 0)_{Al}$ // $(\bar{1}\ 1\ \bar{1})_{Si}$	$[0\ 0\ 1]_{Al}$ // $[1\ 1\ 0]_{Si}$	[38]
1986	Al-12.7Si bulk specimen	TEM	Chill modification (DS)	$(1\ 0\ 0)_{Al}$ // $(\bar{1}\ 1\ \bar{1})_{Si}$	$[0\ 0\ 1]_{Al}$ // $[1\ 1\ 0]_{Si}$	[43]
			Un-modification (DS)	$(1\ 0\ \bar{2})_{Al}$ // $(1\ 1\ 1)_{Si}$	$[2\ 1\ 1]_{Al}$ // $[\bar{1}\ 1\ 0]_{Si}$	[43]
				$(0\ 1\ 2)_{Al}$ // $(1\ 1\ 1)_{Si}$	$[1\ 0\ 0]_{Al}$ // $[\bar{1}\ 1\ 0]_{Si}$	
1986	Al-Si-Sr	TEM	Sr-modification (DS)	No consistent OR, $<1\ 1\ 0>_{Al}$ texture		[39]
1987	Al-14Si	TEM	Chill modification (DS)	$(0\ 1\ 0)_{Al}$ // $(1\ 1\ \bar{1})_{Si}$	$[1\ 0\ 0]_{Al}$ // $[\bar{1}\ 1\ 0]_{Si}$	[100]
1995	Al-3Si	TEM	Un-modification	$(1\ \bar{1}\ 1)_{Al}$ // $(1\ \bar{1}\ 1)_{Si}$	$[1\ 1\ 0]_{Al}$ // $[1\ 1\ 0]_{Si}$	[25]
	Al-3Si-P		Un-modification	$(1\ 1\ 0)_{Al}$ // $(1\ 1\ 0)_{Si}$	$[0\ 0\ 1]_{Al}$ // $[0\ 0\ 1]_{Si}$	
2001	Al-7Si-0.015Sr	EBSD	Sr modification (DS)	–	$<1\ 0\ 0>_{Al}$ // $<1\ 1\ 0>_{Si}$	[86]
					$<1\ 1\ 0>_{Al}$ // $<1\ 1\ 0>_{Si}$	
2004	Al-7Si	TEM	Directional solidification	–	$[1\ 1\ 2]_{Al}$ // $[1\ 1\ 0]_{Si}$	[30]
				–	$[1\ 1\ 0]_{Al}$ // $[1\ 0\ 3]_{Si}$	
				–	$[1\ 1\ 2]_{Al}$ // $[1\ 1\ 2]_{Si}$	

	–	$[1\ 1\ 1]_{Al}$ // $[1\ 1\ 0]_{Si}$
Air cooling	–	$[1\ 1\ 2]_{Al}$ // $[1\ 1\ 2]_{Si}$
Furnace cooling	–	$[1\ 1\ 2]_{Al}$ // $[1\ 1\ 2]_{Si}$

Despite much effort has been made to the investigation of the chemical modification mechanisms of the eutectic Si phase during the past 95 years [5, 13, 19-27, 43, 65, 70], there are still some open questions for the understanding of this mechanism. Firstly, the Si morphology modification by chemical modification happens at which stage, nucleation or growth or both, should be specified. Moreover, for the widely accepted TPRE growth model of the unmodified eutectic Si phase, the directional growth along <1 1 2> direction and the exposure of closed-packed {1 1 1} planes to the melt to reduce interfacial energy, cannot be simultaneously satisfied. Besides, there are many ambiguities about the preferred growth direction (texture) of eutectic Si phase and the representative ORs between eutectic Si and eutectic α-Al.

Such a situation arises from the lack of thorough investigation into the eutectic growth by correlated microstructural and crystallographic analyses at microscopic scale. In this regard, the SEM-based electron backscatter diffraction (EBSD) appears to be a useful tool that bridges the thermodynamic measurements at macroscopic level and the advanced APT and high-resolution TEM examinations at nano and atomic scale. However, conventional EBSD systems suffer from a difficulty in differentiating the face-centered cubic α-Al phase (space group $\bar{}$, No. 225) and the diamond cubic Si phase (space group $\bar{}$, No. 227), as they generate very similar EBSD diffraction patterns. Therefore, special efforts should be made to separate the two eutectic phases without ambiguity.

1.4 Heat treatment on Al-Si alloys

Al-Si alloys are natural metal matrix composite (MMC) materials with Si phase embedded in α-Al matrix. In such a system, the thermal behaviors and mechanical properties of the two phases are very different. Si is hard and brittle (Young's modulus E_{Si} = 170 GPa) with limited thermal expansion ($\alpha_{Si} = 2.6 \times 10^{-6}$ m m^{-1} K^{-1}), whereas α-Al is soft and ductile (Young's modulus E_{Al} = 70 GPa, about 0.4 times of that of Si) with giant thermal expansion capacity ($\alpha_{Al} = 26.1 \times 10^{-6}$ m m^{-1} K^{-1}, almost 10 times of that of Si). Under an ideal microstructural combination of the two phases, *i.e.* fine spherical Si crystals embedded

homogeneously in fine equiaxed α-Al matrix [112], superior thermal and mechanical performances could be achieved.

For Si crystals, former researchers indicated that both chemical modification during solidification and spheroidization during post heat treatment in Al-Si alloys led to a significant improvement in strength and ductility [113, 114]. The chemical modification by adding trace elements to the melt before casting, such as Na or Sr, has been proved to be an effective method to change the morphology of Si crystals. Under chemical modification, Si crystals could change from coarse plate-like into finer coral-like or bar-like [17]. Three-dimensional (3D) studies have shown that at the as-cast state of eutectic Al-Si alloys, Si crystals are 3D interconnected [84, 115]. Such morphology becomes unstable when the alloy is exposed to high temperature (just below the eutectic temperature (577 °C)). The 3D interconnectivity will disappear and be displaced by the elongated particles or spherical particles [115-118]. The morphological change of eutectic Si crystals during heat treatment has been intensively studied [119-127]. Zhu et al. [128] investigated an Al-13Si alloy at 540 °C for 2 h and found two stages of the spheroidization process: the dissolution separation of eutectic Si branches and the spheroidization of these branches. The driving force for the spheroidization was the minimization of the surface energy under the effect of surface tension. Ogris [127] stated that microstructural variation of eutectic Si during high temperature treatment composed of three steps: disintegration, spheroidization and growth. Wang et al. [118] proposed that there were four stages: necking, fragmentation, spheroidization and coarsening of Si grains; the driving force of the spheroidization of eutectic Si comes from the decrease of the surface energy and lattice deformation energy. The disintegration and spheroidization process further aided the refinement of Si phases and improved the ductility and deformability. It has been found that disintegration or fragmentation happens at the joints of the Si branches or at the necks and then spheroidization occurs to the fragmented parts [118, 127, 128]. The spheroidization is mainly driven by capillarity force [122] or surface tension generated by surface curvature variation, the so-called shape instability, and realized by diffusion [119] through either surface self-diffusion [129] or Al-Si inter-diffusion at Si/Al interface [130] at elevated temperature. Hence post heat treatment at relatively high temperature (just below eutectic temperature) is effective for Si spheroidization. Besides, the brittle fracture of Si crystals is reported along the cleavage planes, *i.e.* {1 1 1} and {1 1 0} planes [131-133], but the preferred cleavage system of propagation for Si is still in debate.

To achieve an optimum strength-ductility combination of the Al-Si alloy systems, the refinement of α-Al matrix is also imperative. For a soft metal without allotropic transformation in its solid state, the refinement can only be realized by recovery and recrystallization after the metal has been severely defected. For aluminum, recrystallization is achieved through polygonalization of crystal defects, especially dislocations. To introduce sufficient amount of crystal defects for recovery and recrystallization, deformation is the usual way. Thus for Al-Si alloy systems, hot deformation, especially hot extrusion, is usually applied to achieve the refinement of the two microstructural components. It should be noted that large thermal incompatibility exists between the Si and the α-Al phase when the alloy is subjected to temperature change, thus large thermal stress can be created between the two phases. As Si is brittle with almost zero deformation capacity, the thermal stress may crack it, resulting in fragmentation of Si crystals. The cracks will create a kind of capillarity force acting on the surrounding α-Al matrix. The accumulated thermal constraints and the capillarity forces together with the effect of high temperature could be utilized to generate crystal defects in α-Al for recovery and recrystallization. It has been reported [134] that there was localized recrystallization occurred inside the eutectic α-Al matrix, during the heating stage when the as-cast A356 alloy was heated to the solution temperature. This localized recrystallization area was confined to the elasto-plastic zone surrounding the eutectic Si phases. There was no evidence of recrystallization occurring within the primary α-Al dendrites. Haghdadi et al. [135] studied the microstructural evolution of A356 (Al-7Si-0.4Mg) alloy processed by accumulative back extrusion (ABE). They found that overall recrystallization occurred inside α-Al matrix. Subgrains about 2-3 μm in size with low angle grain boundaries formed within the primary α-Al phase and grains about 0.47 μm in size with high angle grain boundaries in the eutectic α-Al matrix.

1.5 Content of the present work and contributions

Despite the intensive investigations in revealing the formation characteristics of the eutectic Si crystals, the possible modification mechanisms of eutectic Si phase by adding chemical modifiers and the effect of post heat treatment on the eutectic phases in the eutectic Al-Si alloys, many issues remain inconclusive. In view of such a situation, the scientific aim of the present work is set to first study the growth behaviors of unmodified and Sr-modified eutectic Si phase, then to examine the refinement mechanism of α-Al matrix and Si crystals in Sr-modified eutectic Al-Si alloy through post heat treatment and finally to study the

macroscopic and microscopic textures. The aim of the present work is to provide some new insights into the formation mechanisms of Si growth and the microstructural evolution features during post heat treatments. Special efforts were made in assuring statistical reliability of the experimental evidence. The followings are the main content of the present work:

(1) Reveal detailed growth behaviors of unmodified and Sr-modified Si crystals in eutectic Al-Si alloys. To simplify the growth process, the possible influence factors on the eutectic Si morphology from the cooling rates and impurities were excluded. The crucible slowly (close to equilibrium state) solidified high-purity Al-12.7Si alloys with and without 400 ppm Sr additions were used. Microstructural characterizations were performed using SEM/EBSD.

(2) Work out the refinement mechanisms of α-Al matrix and Si crystals during post heat treatment. A series of post heat treatments were performed on the crucible slowly solidified Al-12.7Si-0.04Sr ingots. Microstructural and crystallographic characterizations were performed using TEM, SEM/EBSD and in-situ neutron diffraction.

(3) Examine the global and local texture characteristics of directionally solidified and heat treated Al-12.7Si alloys with and without 400 ppm Sr additions and find out the relations between texture and heat transfer directions. Microstructural and crystallographic characterizations were performed using SEM/EBSD and neutron diffraction.

Chapter 2 Experimental methods

In this chapter, the detailed experimental processes for preparing and characterizing Al-Si samples are summarized. The Al-12.7 wt. % Si alloys with and without Sr addition were cast by two ways: crucible slow solidification and slow directional solidification. The main characterization techniques include SEM/EBSD, TEM, FIB and neutron diffraction.

2.1 Alloy preparations

2.1.1 Crucible slowly cast samples

To investigate the role of sole Sr addition on the modification mechanism of eutectic Si phase, the possible influences from other impurities or cooling rates were excluded. Thus the ideal alloys should be of high-purity and solidified in an almost equilibrium state. Moreover, to obtain only eutectic structure, the nominal chemical composition was controlled to be the eutectic composition.

Binary Al-12.7 wt. % Si alloys with and without 400 ppm Sr modification were prepared by the crucible slow solidification method. The pure Al (99.996 wt. %) and pure monocrystalline Si (99.999 wt. %) were used as raw materials. To obtain the Sr-modified alloy, an Al-10 wt. % Sr master alloy was prepared with Al and Sr elements. Considering the easy loss of Sr element during melting (efficiency of Sr is about 70 %), a nominal composition of Al-13.7 wt. % Sr was designed to ensure the real composition of the master alloy (Al-10 wt. % Sr). Al-Sr master alloy was chill-cast in an iron mold. To avoid involving in Fe-contained impurities, the surface layers of the Al-Sr ingots were removed. For the unmodified Al-Si alloy, bulk pure Al was melt in a 200 mL alumina crucible in an electric resistance furnace, and then pure monocrystalline Si was added to the pure Al melt after the Al melt was held at 850 °C for two hours. To obtain the modified Al-12.7 wt. % Si alloy with 400 ppm Sr, the Al-10 wt. % Sr master alloy was added to the Al-Si melt when the melt was cooled to 705 °C. Prior to casting, all the alumina crucibles and alumina melt-stirring rods were soaked in an 80-90 % hydrochloric acid for about 24 hours to remove the metallic impurities and then cleaned with alcohol. At the same time, the iron mould was brushed with titanium dioxide. Then the crucibles and iron mould were preheated at 200 ℃ for approximately 10 hours in the electric resistance furnace to remove moisture before being

cooled down to room temperature. Both the unmodified and Sr-modified Al-12.7 wt. % Si alloys were slowly solidified in the 30 mL alumina crucibles. The cooling rate is not higher than 0.5 °C/s.

2.1.2 Directional solidification samples

To investigate the crystallographic anisotropic growth of both eutectic α-Al and eutectic Si phases in the Sr-modified eutectic Al-Si alloy, directional solidification samples were prepared.

For the directionally solidified alloys, the Al-12.7 wt. % Si-0.04 wt. % Sr ingots with a size of 10 mm in diameter were prepared by melting high-purity Al (99.996 wt. %), monocrystalline Si (99.999 wt. %) and Al-10 wt. % Sr master alloy. The alloys are directionally cast under a pulling rate of R = 30 μm sec^{-1} and with a thermal gradient of G = 100 °C cm^{-1}.

2.1.3 Alloy heat treatment

The ingots prepared by both crucible slow solidification and directional solidification techniques were then isothermally treated at 520 °C for 1 h, 4 h and 8 h, respectively, in a salt bath. The samples were loaded into the salt bath when the bath temperature reached 520 °C without any preheating and cooled in air after the isothermal holding.

2.2 Sample preparation for characterization

2.2.1 Scanning electron microscope (SEM) based electron back-scatter diffraction (EBSD)

For the crucible slowly solidified unmodified and Sr-modified Al-12.7Si alloys, specimens were cut out from the middle of the ingots by wire-electrode cutting. Microstructural observations were performed at room temperature using a JEOL JSM-6500F field emission gun scanning electron microscope (SEM) and a Zeiss Supra 40 field emission gun SEM. The crystallographic orientation measurements were performed with the JEOL JSM-6500F SEM equipped with the electron back-scattered diffraction (EBSD) facilities and the Aztec acquisition software package (Oxford Instruments).

Samples were prepared using standard metallographic techniques. Each specimen was mechanically ground with emery (SiC) papers up to 4000 # (5 μm) and then polished with diamond suspension (1 μm) to produce a mirror-like sample surface. In order to remove the residual stress induced by the mechanical polishing, further polishing with oxide polishing suspension (OP-S) was conducted using a Struer's Tegramin-25 automatic polishing machine at a rotation speed of 200 ~ 300 rpm for ~ 10 min. The polished specimens were rinsed with tap water for 10 min and cleaned in ethanol in an ultrasonic bath for 30 min.

To detect the three dimensional (3D) morphology of the eutectic Si phase in both unmodified and Sr-modified crucible solidified alloys, the specimens were further electrolytically polished to partially dissolve the α-Al matrix. The electrolytic polishing was performed using a solution of 20 % perchloric acid in methanol at 25 V for 10 s at a temperature lower than 10 °C.

For the directionally solidified (DS) Sr-modified Al-12.7Si alloy, both JEOL JSM-6500F and JEOL JSM-6490 tungsten (W) filament SEMs equipped with an EBSD camera and the Aztec acquisition software package (Oxford Instruments) were utilized for microstructural characterizations. The microstructural characterizations were performed on both the cross and the transverse sections, via the same metallurgical procedures as above.

2.2.2 Transmission electron microscope (TEM) and Focused Ion Beam (FIB) preparation

The substructural features of the eutectic α-Al phase and the eutectic Si particles in the as-cast and the heat treated Sr-modified alloys, such as dislocation configurations, were further examined with a Philips CM200 TEM equipped with a LaB_6 cathode, a Gatan Orius 833 CCD camera and a homemade automatic orientation analysis system, Euclid's Phantasies (EP) [136, 137]. The Kikuchi line pattern based orientation mapping was performed at accelerating voltage of 200 kV in a beam controlled mode with a step size of 20 nm, covering an area of 2×2 μm^2.

The stress-free and contamination-free foil specimen for transmission electron microscope (TEM) observation and orientation mapping were prepared in a Carl ZEISS Auriga 40 Focused Ion Beam (FIB) workstation (Oberkochen, Germany). This FIB workstation was equipped with an Orsay Physics CORBA ion column, a multi-gas injection system and a Klocke sample manipulator by the "lift-out" method [138]. About 2 μm thick

thin foils were first cut out of the bulk sample using Gallium (Ga) ion source. They were further thinned with reduced ion beam currents at 30 keV to about 150 nm and then milled at 5 keV to remove the amorphized surface layers induced by Ga ion bombardment.

2.2.3 Neutron diffraction

In-situ neutron diffraction measurements were utilized during the solidification process of Al-12.7Si-0.04Sr alloy. The measurements were performed at the Stress-Spec at Heinz Maier-Leibnitz Zentrum (MLZ), Garching, Germany. The neutron diffractometer STRESS-SPEC is located at a thermal beam port and comprises a highly flexible monochromator arrangement. High-purity Al-12.7Si-0.04Sr samples with the dimension of ϕ 5 mm × 7 mm was cut for *in-situ* measurements. The layout of the machine is displayed in Fig. 2.1. The cylindrical samples were inserted into an austenite steel crucible using a high temperature furnace from MLZ and immersed in the neutron beam with a gauge volume of 5 × 10 × 5 mm^3. The sample detector distance is 1005 mm and the pixel size is 1.00 mm. Ge (3 1 1) monochromator was selected to produce the neutrons with a wavelength of 1.68 Å. $(1\ 1\ 1)_{Si}$ and $(1\ 1\ 1)_{Al}$ diffraction peaks were acquired with the detector position at $2\theta = 37°$. A thermal couple was inserted from top of the furnace to record the temperature of the sample. Argon (Ar) was used to prevent oxidation of the specimen at high temperature. The specimens were firstly heated to 650 °C and isothermally held for 5 min, to ensure the specimen to be completely melted. Then the ingot was cooled at a rate of 30 °C/min. Neutron diffraction patterns were dynamically acquired from 468 to 46 °C during the cooling with a 10 second acquisition time for each pattern. The software StressTextureCalculator (STeCa) was used to extract the diffraction patterns.

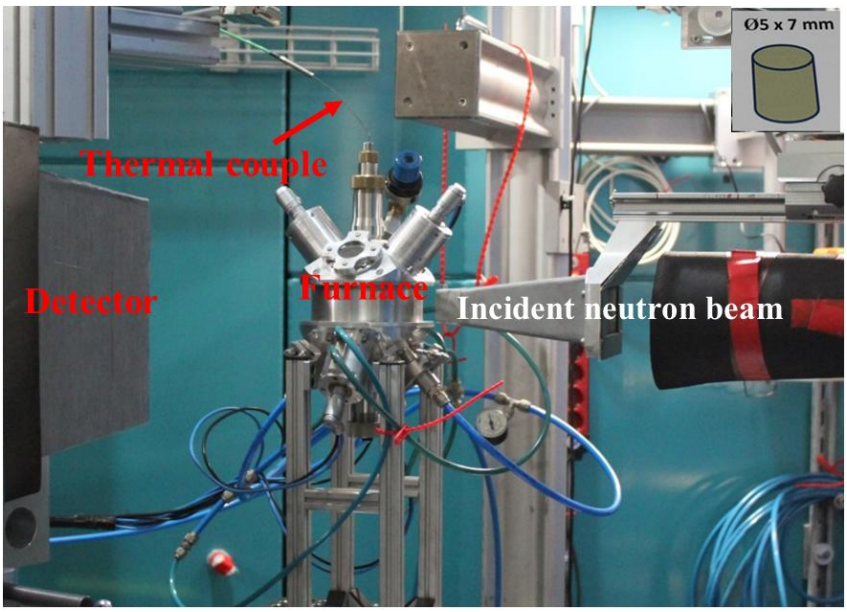

Fig. 2.1 The STRESS-SPEC [139] diffractometer devices for in-situ solidification measurement located in Garching, Germany.

The global texture of the directionally solidified Al-12.7Si-0.04Sr alloy was investigated by neutron diffraction. The through-volume texture measurements were performed at the STRESS-SPEC at Heinz Maier-Leibnitz Zentrum (MLZ), Garching, Germany, using a neutron diffractometer located at a thermal beam port and comprising a highly flexible monochromator arrangement. The device is shown in Fig. 2.2a. A robot system which enables the automatic sample manipulation was used, as displayed in Fig. 2.2b. Cylindrical samples with a diameter of 10 mm and a length of 7 mm were cut. As shown in Fig. 2.2, the pole figure measurements were performed in a transmission manner with a chi tilting from 0 to 90° tilting and combined with a phi rotation from 0 to 360° at each chi angle. Cylindered samples were bathed in the neutron beam with a gauge volume 5 × 5 × 5 mm^3. Ge (3 1 1) monochromater was selected to obtain the wavelength of 1.602 Å. For texture measurement, one needs low indexed reflections. As a small detector is available for the experiment, two 2θ detector positions were necessary to cover 5 reflections: $\{1\ 1\ 1\}_{Al}$, $\{2\ 0\ 0\}_{Al}$,$\{2\ 2\ 0\}_{Al}$, $\{2\ 2\ 0\}_{Si}$ and $\{3\ 1\ 1\}_{Si}$. A continuous scanning routine was used with a step velocity of 0.25 °/s for the first detector $2\theta = 44°$ and the second detector $2\theta = 63°$, and the total counting time needed was 4.8 hours, a sum of 1728 diffraction patterns were collected. The distance between the sample and the detector is 900 mm. Due to the high penetration power of neutrons, complete pole figures were obtained. The software StressTextureCalculator (STeCa)

[140] allowed to extract pole figure (PF) data from the intensity PF (crystallographic texture) [139]. JTEX software [141] was used to recalculate the orientation distribution function (ODF) and to plot the pole figures of $\{1\ 0\ 0\}_{Al}$, $\{1\ 1\ 0\}_{Al}$, $\{1\ 1\ 1\}_{Al}$, $\{1\ 0\ 0\}_{Si}$, $\{1\ 1\ 0\}_{Si}$ and $\{1\ 1\ 1\}_{Si}$.

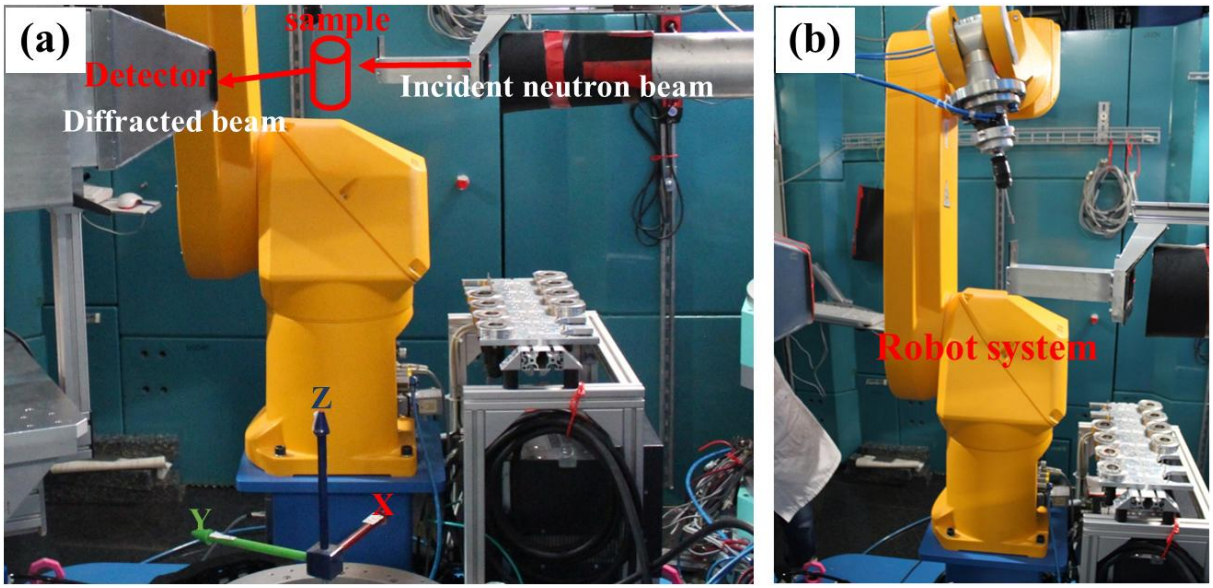

Fig. 2.2 (a) STRESS-SPEC [139] diffractometer layout for texture measurements, with the sample mounted on (b) the robot system, located at Heinz Maier-Leibnitz Zentrum (MLZ), in Garching, Germany.

Chapter 3 Twin controlled growth of eutectic Si crystals in unmodified and Sr-modified eutectic Al-Si alloys

3.1 Introduction

In this chapter, a thorough investigation on both unmodified and Sr-modified crucible slowly cast eutectic Al-Si alloys was conducted. The SEM/EBSD system and a home-made dedicated post-analysis software package were used for the correlated microstructural and crystallographic analyses. The results provide new insights into the growth mechanisms of eutectic Si crystals in the unmodified and Sr-modified Al-Si alloys.

3.2 Experimental procedure

Both high-purity Al-12.7 wt. % Si alloys with and without 400 ppm Sr addition were slowly solidified in the alumina crucibles, with a cooling rate not higher than 0.5 °C s^{-1}. Specimens for microstructural observations and crystallographic analyses were prepared as the metallurgical procedures. The microstructural observations were performed at room temperature using a JEOL JSM-6500F field emission gun SEM and a Zeiss Supra 40 field emission gun SEM. The EBSD patterns were acquired at the acceleration voltage of 20 kV with two measurement step sizes (0.2 μm and 0.3 μm). The face-centered cubic (FCC) structure (space group $\bar{}$, No. 225) and the diamond cubic structure (space group $\bar{}$, No. 227) were utilized to index the Al and Si phases, respectively. The detailed crystal structure data are given in table 3.1.

Table 3.1 Crystal structure data used for identification of Al and Si phases by SEM/EBSD.

Formula	Structure	Atomic positions	Lattice parameter (Å)	Space group	No.
Al	FCC	4*a*	4.05	$\bar{}$	225
Si	Diamond	8*a*	5.4309	$\bar{}$	227

In the present work, two special efforts were dedicated to separating the eutectic α-Al and Si phases that could not be differentiated by conventional EBSD systems. Firstly, a preliminary separation of the two phases was performed by choosing the "configuring groups

of phases" option incorporated in the Aztec online acquisition software (Oxford Instruments). Under this option, the band width information was automatically used to distinguish the two phases. Secondly, the complete phase differentiation was achieved using the home-made software, "Analysis Tools for Orientation Mapping (ATOM)" [142]. With the fully differentiated EBSD orientations of the two phases, further crystallographic information, including the twin relationship and orientation preference (texture) of Si crystals, as well as the orientation correlation between Si crystals and α-Al matrix, was derived using the Channel 5 data processing software package (Oxford Instruments). Possible orientation relationships (OR) between eutectic Si and α-Al were examined in conjunction with the published ones [25, 30, 38, 39, 86, 100], where an allowable angular deviation of 5° was set to the specified plane and direction parallelisms. For specifying the extension direction and outer surface of Si crystals, the length vectors and surface trace vectors measured in the macroscopic sample coordinate system were transformed into the crystal coordinate system. This was readily done via coordinate transformation between two coordinate systems using the determined EBSD orientation data. Moreover, the representative length direction and surface plane, assessed on a statistical basis, were chosen as the extension direction and outer surface of eutectic Si crystals.

3.3 Results

3.3.1 Differentiation of eutectic α-Al and Si phases

For illustration, the secondary electron (SE) images, EBSD phase-indexed micrographs and EBSD orientation micrographs of the unmodified and Sr-modified Al-12.7Si alloys are presented in Fig. 3.1. It can be seen that the eutectic α-Al and Si phases were fully differentiated without ambiguity. Apparently, the two phases revealed in the EBSD phase-index micrographs (Figs. 3.1a_2 and b_2) correspond well to their counterparts displayed in the SE images (Figs. 3.1a_1 and b_1). This validates the reliability of the above-mentioned phase identification procedure, thus allowing us to provide correct information for both microstructural and crystallographic analyses.

Figs. 3.1a and b show the typical microstructures of the unmodified and the Sr modified Al-Si eutectic alloys, respectively. Both are composed of eutectic colonies, *i.e.*, eutectic Si crystals embedded in the continuous eutectic α-Al matrix. For the unmodified alloy, Si

crystals are in coarse plate-like or needle-like morphologies, see Fig. 3.1a_1. In one eutectic colony, the Si crystals are oriented in roughly the same direction with identical orientation or twin relation, as squared in the black dotted zone A in Fig. 3.1a_3 (Si twin characters will be discussed later). It appears that some Si crystals grow from the interior of the eutectic colony to the exterior. Thus non-smooth colony boundary is observed, on which the Si phase leads over the eutectic α-Al matrix, as marked with A in Fig. 3.1a_3, suggesting that the growth of Si is ahead of α-Al. After 400 ppm Sr was added to the eutectic Al-Si alloys, as shown in Fig. 3.1b, the eutectic silicon crystals are significantly refined from the coarse plates or needles to fine bars or particles. No Si leading over boundaries is found in the Sr modified Al-Si eutectic colonies, indicating that with the addition of Sr modifiers, the rapid anisotropic growth is changed.

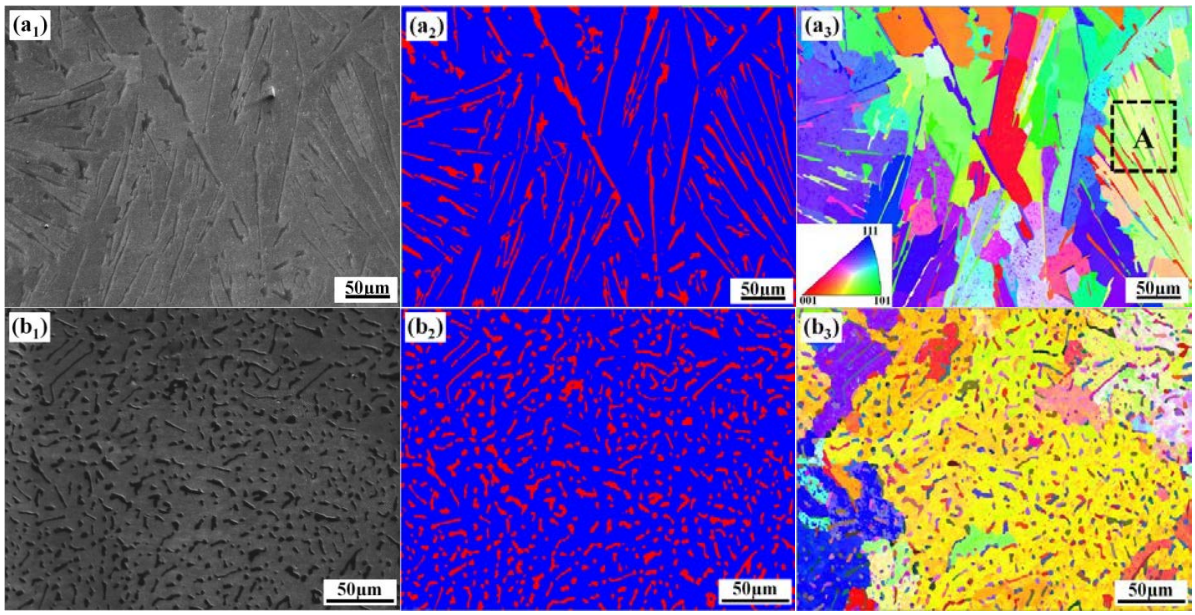

Fig. 3.1 Microstructures of unmodified (upper) and Sr-modified (lower) Al-12.7Si alloys. (a_1) and (b_1) SE images of eutectic phases (Al is in grey and Si in dark grey). (a_2) and (b_2) EBSD phase-index micrographs corresponding to (a_1) and (b_1), respectively (Al is in blue and Si in red). (a_3) and (b_3) EBSD orientation micrographs with color code shown in the lower left corner of (a_3). The step size of EBSD measurements is 0.3 μm.

From the progressive color change (where the colors represent the crystallographic orientations) in the interior of the α-Al matrix in the eutectic colonies in the unmodified and the Sr-modified samples in Figs. 3.1a_3 and b_3, low angle disorientation could be expected in the α-Al matrix. To elucidate this phenomenon, correlated disorientation angle distribution of

α-Al phase in the above two samples is given in Fig. 3.2 (the minimum angle is 2°, bin width is 0.5°). From the figures, it is seen that large amount of low angle disorientation exists in the α-Al matrix in both samples, indicating that the crystal of the α-Al matrix is far from perfect. Large amount of crystal defects could exist. No obvious difference of the disorientation angle distribution between the unmodified and Sr-modified samples can be observed.

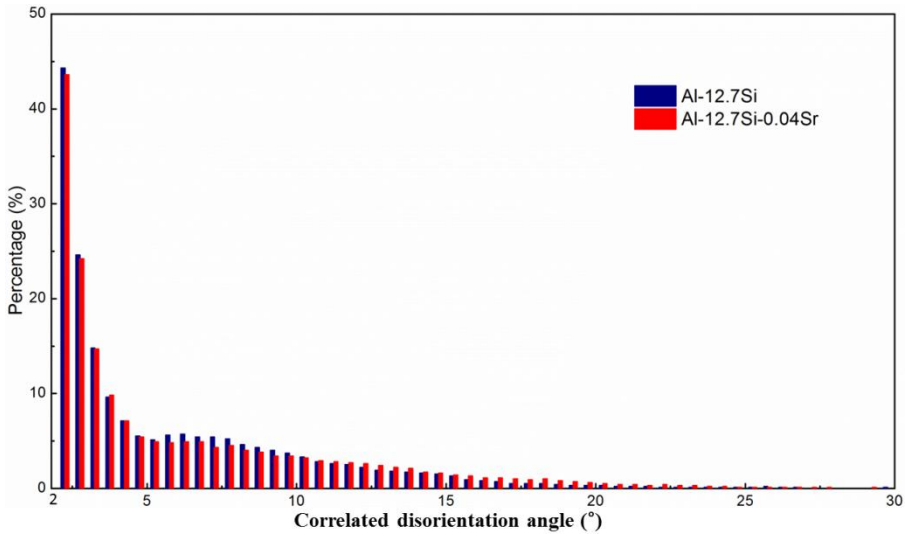

Fig. 3.2 Correlated disorientation angle distribution of α-Al phase in Al-12.7 wt. % Si and Al-12.7 wt. % Si-0.04 wt. % Sr alloys (the minimum angle is 2°, bin width is 0.5°).

3.3.2 Microstructural features of eutectic Si phase

Figs. 3.1a_3 and b_3 demonstrate that the microstructures of the unmodified and Sr-modified Al-12.7Si alloys consist of eutectic colonies, *i.e.* eutectic Si crystals are embedded in the continuous eutectic α-Al matrix. In order to reveal the 3D morphology of unmodified eutectic Si, the secondary electron imaging was performed through capturing simultaneously two perpendicular sample sections (Fig. 3.3a). Generally, eutectic Si crystals have long plate shape (as outlined in yellow in Fig. 3.3a), with irregular changes in width and thickness over the plate length direction. As shown in Fig. 3.1a_3, Si crystals within one eutectic colony appears to be aligned in roughly the same direction with similar crystallographic orientations or twin-related orientations. The distribution of twins contained in one Si plate is schematically illustrated in Fig. 3.3b. Moreover, eutectic Si crystals seem to grow from the colony interior to exterior (as marked with A in Fig. 3.1a_3) and finally lead over the colony

boundary. This elucidates that the growth of eutectic Si into the liquid is ahead of α-Al phase, giving rise to the formation of non-smooth colony boundaries.

With the Sr addition, eutectic Si crystals become significantly refined from plates to fine bars or particles (Fig. 3.1b$_1$). In this case, the eutectic Si growth is largely constrained, no longer leading over the colony boundaries. Clearly, the Sr modification has brought about a remarkable change in the formation of eutectic Si from anisotropic growth to somewhat isotropic growth.

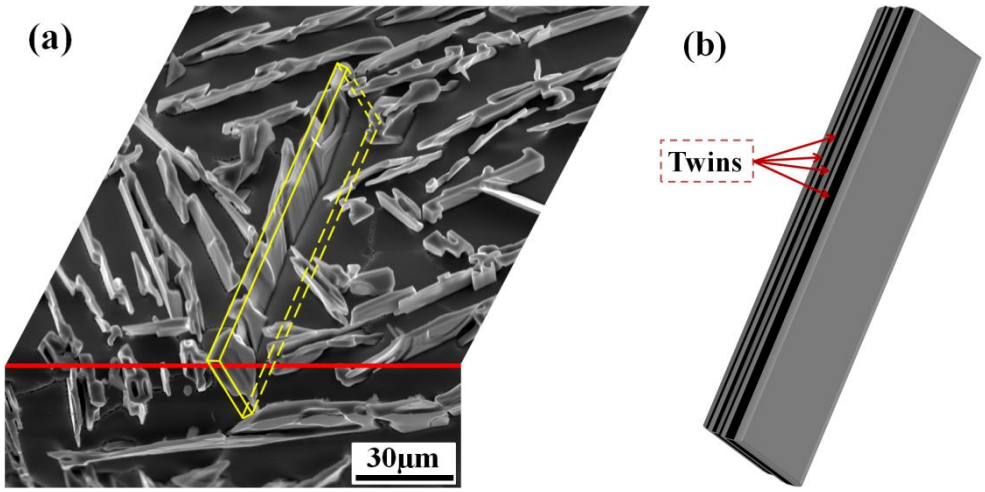

Fig. 3.3 (a) SE image showing the air-view of unmodified eutectic Si crystals exposed in two perpendicular sample sections. The sample was electrolytically polished to partially dissolve the α-Al matrix. The intersection of two perpendicular sample sections is marked with the red line, and one captured eutectic Si plate is outlined with the yellow lines. (b) Illustration of the distribution of multiple twins in one eutectic Si plate.

3.3.3 Extension direction and surface plane of eutectic Si crystals

Detailed calculations show that the length directions and outer surfaces of unmodified eutectic Si crystals correspond to their <1 1 0> directions and {1 1 1} planes, respectively. This suggests that eutectic Si crystals are largely elongated in one <1 1 0> direction and enveloped with the {1 1 1} planes. As an example, Fig. 3.4a presents the EBSD orientation micrograph of one eutectic colony taken from the unmodified Al-12.7Si alloy. Figs. 3.4b-d display the <1 1 0>, {1 1 1} and <1 1 2> pole figures (PFs) of one twinned eutectic Si crystal outlined with the white dashed rectangle in Fig. 3.4a, where the vector $\vec{a}$ represents both the extension directions and outer surface trace direction of the twinned Si crystal. One can see

from Fig. 3.4b that the line OA joining the origin (O) of the <1 1 0> pole figure and the common <1 1 0> pole (A) of the twinned crystal is parallel to vector $\vec{a}$. Thus, the extension direction of the eutectic Si should refer to the <1 1 0> directions. Similarly seen from Fig. 3.4c, the line OB connecting the origin (O) of the {1 1 1} pole figure and the common {1 1 1} pole (B) of the twinned crystal is nearly perpendicular to $\vec{a}$. This indirectly verifies that the outer surface of the eutectic Si refers to the {1 1 1} planes. However, in Fig. 3.4d, there appear no common <1 1 2> poles, indicating that the elongation of the eutectic Si is not along <1 1 2> direction. This is on the contrary to the claim that unmodified eutectic Si elongates in the <1 1 2> directions [12, 43, 85].

Notably, the outer surface planes of the twinned Si crystal (Fig. 3.4b) happen to be parallel to the Si-{1 1 1} twinning planes. Moreover, the extension directions of the two twin-related parts (Fig. 3.4a) are the same and contained in the {1 1 1} twinning planes. This configuration would enable a unidirectional extension of the twinned Si crystal. Close examination has revealed that the {1 1 1} twinning planes are parallel to the plate surfaces and one Si plate is wrapped by several pairs of parallel {1 1 1} planes. As for the Sr-modified Al-12.7Si alloy, no fixed Si extension direction is attainable in one eutectic colony, because eutectic Si crystals are largely refined and differently oriented (Fig. 3.1b$_3$).

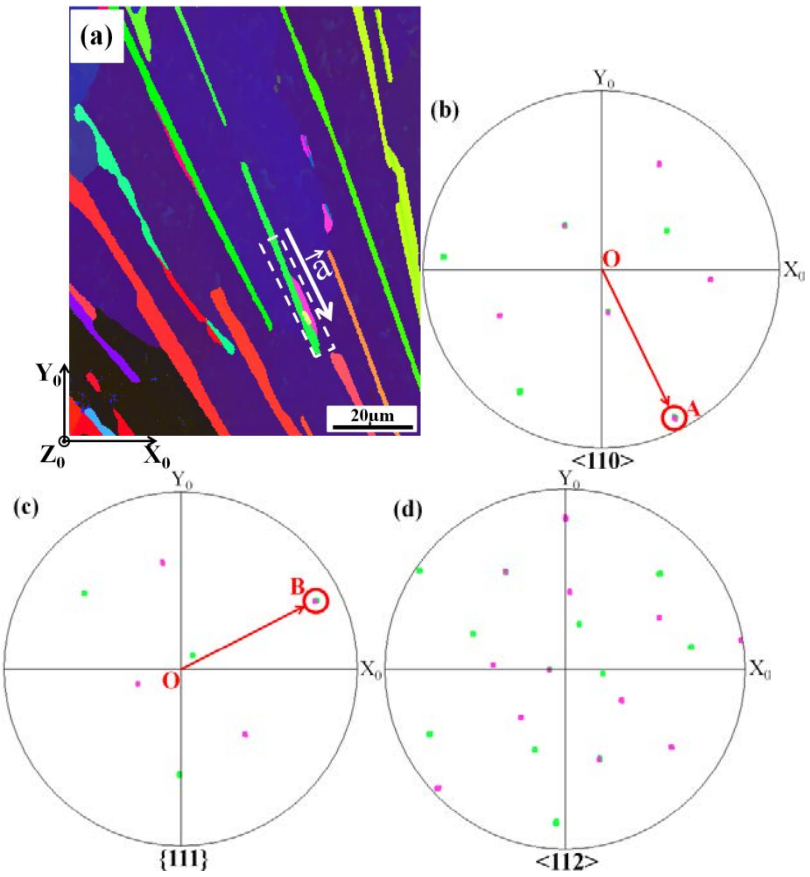

Fig. 3.4 (a) EBSD orientation micrograph of one selected eutectic colony from unmodified Al-12.7Si alloy. (b) <1 1 0>, (c) {1 1 1} and (d) <1 1 2> PFs of one twinned Si crystal outlined with the white dashed rectangle in (a). Note that $\overrightarrow{OA}$ is parallel to $\vec{a}$ and $\overrightarrow{OB}$ is nearly perpendicular to $\vec{a}$ (with an angular deviation of about 4°), where $\vec{a}$ specifies the extension direction of the twinned Si crystal.

3.3.4 Twin characters of eutectic Si crystals

The EBSD orientation micrographs and magnified SEM back-scatter electron (BSE) images of eutectic Si crystals in both unmodified and Sr-modified Al-12.7Si alloys are shown in Fig. 3.5. Notably, almost all eutectic Si crystals contain twins (Figs. 3.5a_1 and b_1). Detailed crystallographic analysis has confirmed that these Si twins are of the {1 1 1} <1 1 $\bar{2}$> reflection type, in consistence with the published results. For the unmodified alloy (Figs. 3.5a_1 and a_2), there appear only one-orientation twin variants with long and straight surface trace running from one tip to the other. Such single-orientation variants are repeatedly distributed over the thickness of eutectic Si plates (Fig. 3.5a_3), exhibiting the multiple twin character required by the TPRE growth mechanism [34, 43]. Clearly, the traces of the {1 1 1} multiple

twinning planes from one twinned Si crystal are parallel to each other and to the outer surface planes of the twinned Si crystal, as illustrated in Fig. 3.3b. In such a way, the multiple twinning would not change the extension direction of eutectic Si crystals.

As for the Sr-modified alloy, the eutectic Si twins (Fig. 3.5b_1) are different in two ways from those observed in the non-modified alloys. One is that twin interface boundaries are often not straight but curved or stepped, as shown in Fig. 3.5b_2. The other is that in many eutectic Si crystals both repeated single-orientation twin variants and multi-orientation twin variants appear, as shown in Figs. 3.5b_1 and b_3. Further crystallographic analysis indicates that the frequently occurred disorientation between multi-orientation twin variants is about 39° around <1 1 0>. Certainly, the formation of multi-orientation Si twins would be responsible for the shape change of modified eutectic Si crystals, provided that the twin-controlled TPRE growth mechanism is effective.

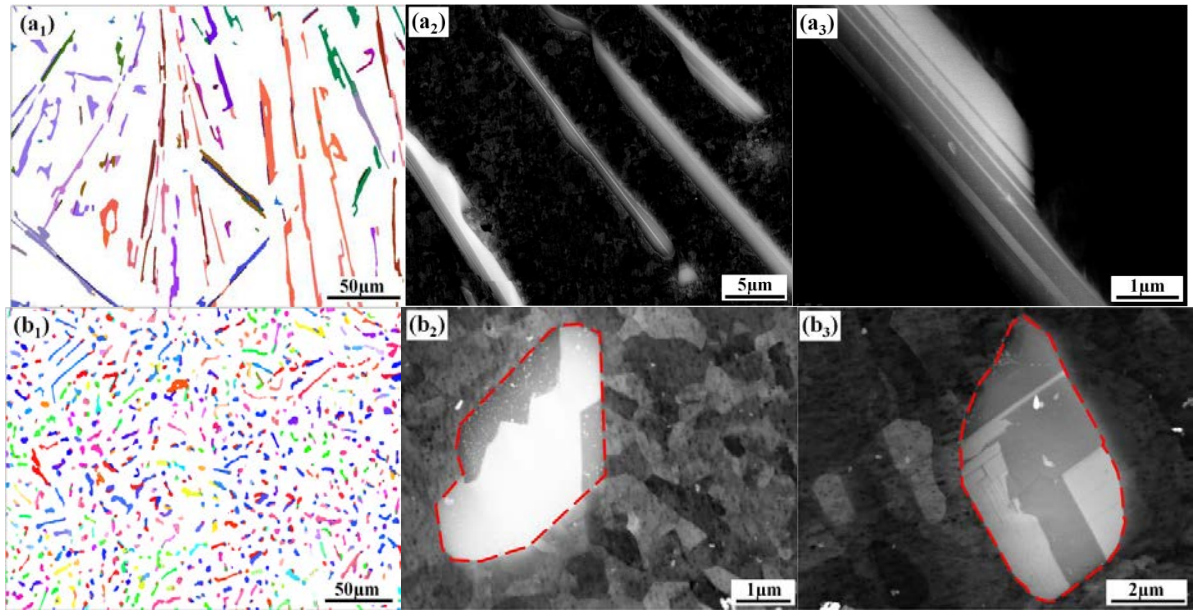

Fig. 3.5 Twin characters of eutectic Si crystals in unmodified (upper) and Sr-modified (lower) Al-12.7Si alloys. (a_1) and (b_1) EBSD orientation micrographs (α-Al matrix is in white). (a_2) BSE image of Si crystals and (b_2) BSE image showing stepped twin interface traces. (a_3) BSE image showing multiple twinning plane traces in one Si crystal. (b_3) BSE image showing repeated single-orientation twin variants and multi-orientation twin variants in one Si crystal. The Sr-modified Si crystals in (b_2) and (b_3) are outlined with the red dashed lines.

3.3.5 Orientation preference of eutectic Si crystals

Fig. 3.6 presents the EBSD orientation micrographs of one eutectic colony taken from the unmodified and Sr-modified Al-12.7Si alloys, as well as the corresponding <1 1 0> PFs of Si crystals. In the unmodified case, local eutectic Si crystals tend to be aligned in the same direction (Fig. 3.6a_1), where two adjacent crystals are correlated with a {1 1 1} <1 1 $\bar{2}$> twin relation. As shown in Fig. 3.6a_2, the twin-related eutectic Si crystals share three <1 1 0> directions (circled in white) that lie in the twinning planes. One of the <1 1 0> directions is the crystal extension direction (marked with A in Fig. 3.6a_2) shared by all Si crystals, which could be the heat flux direction during solidification.

With the Sr addition, although the morphology of eutectic Si crystals changes drastically (Fig. 3.6b_1), a preferred <1 1 0> orientation can still be found over one eutectic colony (Fig. 3.6b_2). In this case, most of the Si crystals share one single <1 1 0> direction (circled with B in Fig. 3.6b_2), showing a tendency to form the <1 1 0>-type fiber texture. This indicates that the growth habit of the unmodified eutectic Si is preserved for the Sr-modified eutectic Si to some extent.

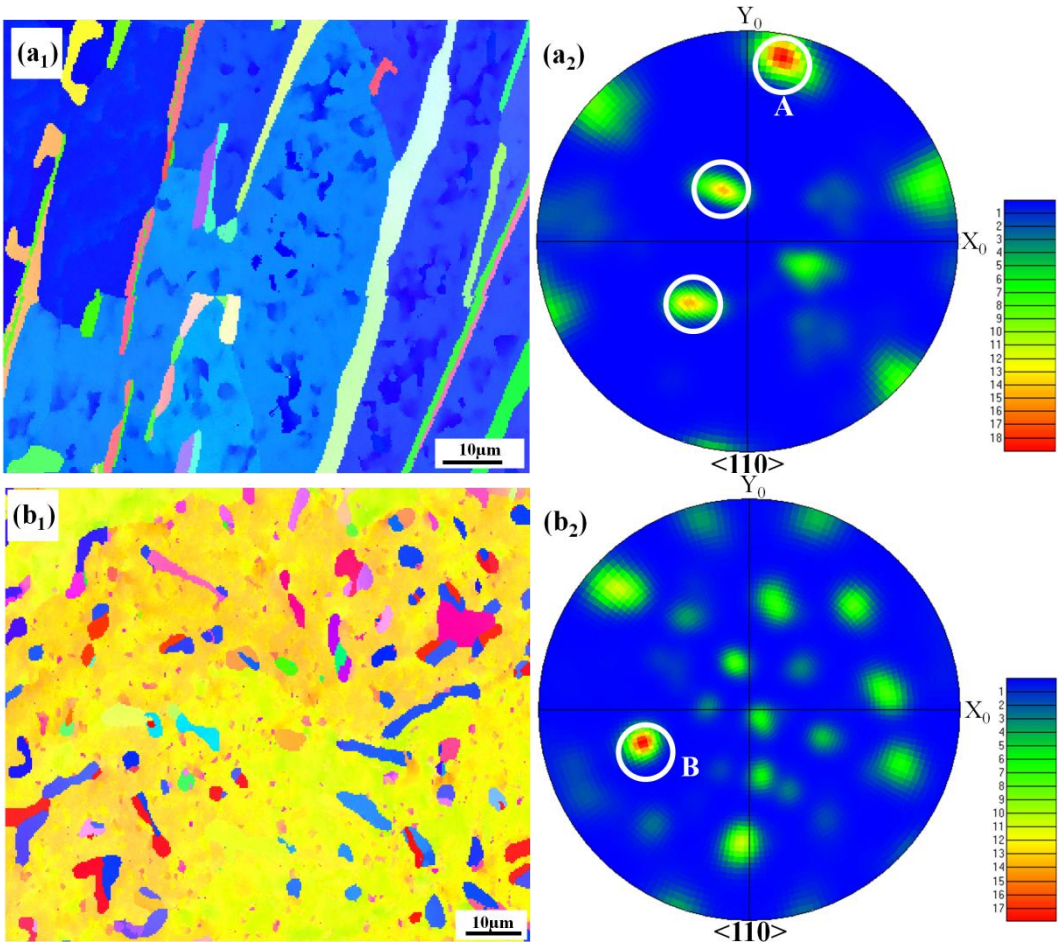

Fig. 3.6 EBSD orientation micrographs of one eutectic colony and corresponding <1 1 0> PFs of eutectic Si crystals in unmodified (upper) and Sr-modified (lower) Al-12.7Si alloys. (a_1) and (b_1) EBSD orientation micrographs. (a_2) and (b_2) <1 1 0> PFs with coincident <1 1 0> poles circled in white.

3.3.6 Orientation relationship between eutectic α-Al and eutectic Si

In literature, four types of direction parallelism between eutectic α-Al and eutectic Si are frequently reported, *i.e.* $<0\ 0\ 1>_{Al}$ // $<1\ 1\ 0>_{Si}$, $<0\ 0\ 1>_{Al}$ // $<0\ 0\ 1>_{Si}$, $<1\ 1\ 2>_{Al}$ // $<1\ 1\ 2>_{Si}$ and $<1\ 1\ 2>_{Al}$ // $<1\ 1\ 0>_{Si}$ [25, 30, 38, 39, 86, 100]. These parallelisms have been examined in the present work. For the unmodified Al-12.7Si alloy, there is no constant OR over the selected eutectic colonies, but very locally the $<1\ 1\ 2>_{Al}$ // $<1\ 1\ 2>_{Si}$ parallelism with some angular deviation (< 5°) may appear, as shown as an example in Fig. 3.7a. For the Sr-modified Al-12.7Si alloy, the orientation correlation between the two phases becomes more random. Even in the same eutectic colony, several direction parallelisms exist, as shown in Fig. 3.7b. Therefore, under the present solidification conditions, no globally representative

ORs can be concluded for both the unmodified and Sr-modified alloys. This indicates that the crystallographic compatibility across the phase interfaces is not the prerequisite for the formation of Al-Si eutectic. In other words, the connecting sites between eutectic Si and α-Al phases are not selective to meet the specific OR (or ORs), but rather random when the local composition of the melt is favorable for the formation of the two phases.

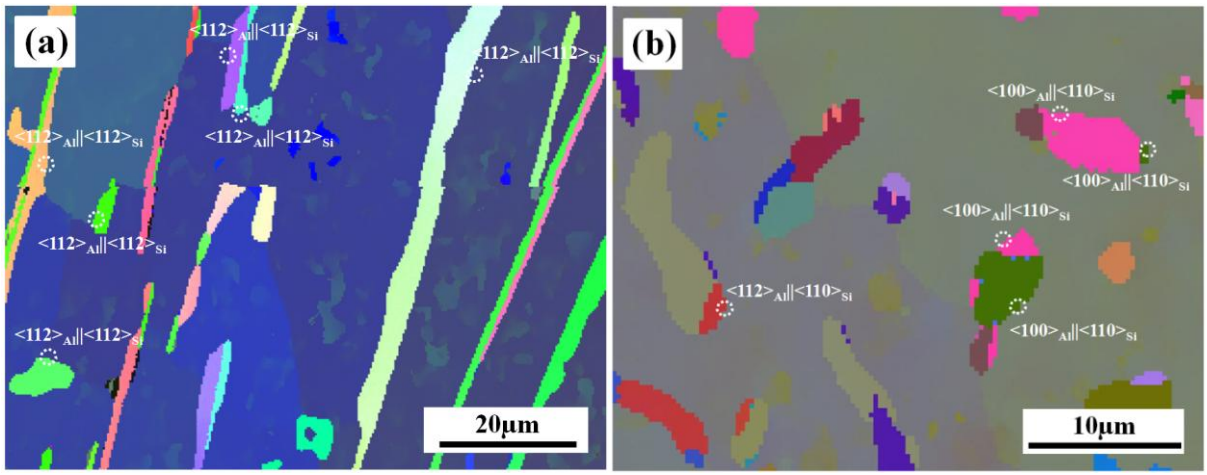

Fig. 3.7 EBSD orientation micrographs of (a) unmodified and (b) Sr modified Al-12.7Si alloys. Possible direction parallelisms between α-Al and adjacent Si are indicated, with a maximum allowable angular deviation of 5°.

3.4 Discussion

3.4.1. Role of stacking fault in Si twinning

From the above observations on both unmodified and Sr-modified Al-12.7Si alloys, twins should be considered as an important microstructural constituent that is always linked with the growth process and the final morphology of eutectic Si crystals. To understand the twin characters of the eutectic Si phase, the atomic correspondence between twinned crystals is constructed with the specified {1 1 1} <1 1 $\bar{2}$> relationship, as illustrated in Fig. 3.8. Clearly, Si twins cannot be easily generated by deformation, as a large amount of shear plus atomic shuffling would be required. Instead, they can be formed by faulted stacking during crystal growth, as Si possesses a relatively small stacking fault energy, about 50 ~ 60 mJ m^{-2} [143].

For a perfect Si crystal, its diamond cubic structure consists of {1 1 1} close packed planes with a stacking sequence of …AABBCCAA…. The formation of a twin would require

faulted {1 1 1} layer, produced by either introducing one C atomic plane in the case of TP 1 or withdrawing one A atomic layer in the case of TP 2 as shown in Fig. 3.8, plus a reversed stacking sequence …AACCBBAA… with respect to the Si matrix. In both cases, only one atomic layer is necessarily faulted. Apparently, the reversed stacking sequence makes the twinned part unstable in the solidification environment. The original stacking sequence could be restored through further introducing a stacking fault. This may be the reason why twinned parts of Si crystals are always thin and twins occur very frequently in one crystal.

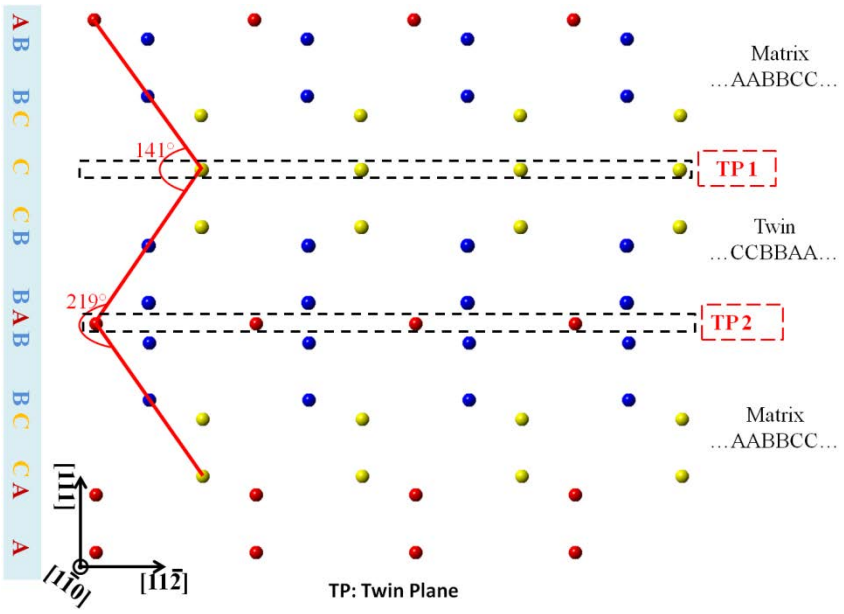

Fig. 3.8 Atomic correspondence between twinned crystals with diamond cubic structure, viewed on (1 $\bar{1}$ 0) plane. Through (1 1 1) twinning planes (TP) marked with TP 1 and TP 2, the atomic stacking sequence …AABBCCAA… of the matrix is changed to be …AABBCCCBBAA… for TP 1 (inserting one C atomic layer) and …CCBBABBCCAA… for TP 2 (withdrawing one A atomic layer), bringing about one 141° re-entrant and one 219° ridge, respectively.

Indeed, the formation of Si twins could be achieved by faulted deposition of atomic layers on the growth front (outer surface) of Si [15]. During the crystallization of a eutectic Si crystal, its lowest-energy {1 1 1} planes are considered to be exposed to the melt. Under the thermo-solutal convection, stacking faults on the {1 1 1} planes can occur when Si atoms from the melt attach to the crystal, thus giving rise to the formation of twins. Molecular dynamic simulations on the growth of Si-Ge nanowires [15] have corroborated the formation of such stacking faults: four-atom Si clusters deposited at faulty locations on the Si-(1 1 1)

facets, leading to the nucleation of twins. As Si crystals grow along the [1 1 1] direction layer-by-layer, this process would be repeated and then multiple parallel twins be formed.

3.4.2 Directional growth of unmodified eutectic Si

For the unmodified Al-12.7Si alloy, it is found that multiple eutectic Si twins are parallel to one another along the length direction of eutectic Si crystals (Fig. 3.5a_3). This is in consistent with the condition required by the TPRE growth mechanism. The repeated single-orientation Si twins provide two or more parallel {1 1 1} planes with 141° re-entrant grooves at the extension front for continuous growth, as illustrated in Fig. 3.8. The presence of 141° re-entrant groove facilitates Si atoms in the melt to preferentially deposit along the <1 1 2> directions of the solidified Si crystals. From Figs. 3.4b and c, it is clear that the growth direction of Si twins is on the {1 1 1} plane and the two twinned parts share the same growth direction. Under such a growth mechanism, eutectic Si crystals would grow efficiently in one or several <1 1 2> directions lying in the {1 1 1} twinning plane. However, the final extension direction of unmodified Si crystals refers to the <1 1 0> directions (Fig. 3.4), rather than <1 1 2> directions. Thus, the Si growth direction in the atomic scale should not be the same as that in the microscopic scale.

To find the reason for the above-mentioned discrepancy in Si growth direction, a three-dimensional model illustrating a Si crystal with one pair of parallel twinning planes (TP 1 and TP 2), is presented in Fig. 3.9. As the eutectic Si is commonly observed to expose its {1 1 1} facets to the melt to lower interfacial energy, the Si crystal depicted in Fig. 3.9 is totally enveloped with {1 1 1} planes. In the growth front (colored in red in Fig. 3.9a), the intersection of one twinning plane with the outer {1 1 1} planes creates one 141° re-entrant groove and one 219° ridge. Taking the case of TP 1 as an example, the 141° re-entrant groove forms between planes 2 and 3, and the 219° ridge between planes 1 and 4 (Fig. 3.9a). Such re-entrant grooves enable the Si crystal to grow along one of the <1 1 2> directions in the respective twinning planes, *i.e.* [1 1 $\bar{2}$] in TP 1 and [$\bar{1}$ 2 $\bar{1}$] in TP 2. With the continuous deposition of Si atoms to the re-entrant grooves, the original {1 1 1} facets 1-6 (colored in red in Fig. 3.9a) evolve into 1*-6* (colored in pink in Fig. 3.9b). During this process, the initial 141° re-entrants are replaced by 219° ridges and vice versa. The growth in the [1 1 $\bar{2}$] direction in TP 1 (the 141° re-entrant between planes 2 and 3) and that in [$\bar{1}$ 2 $\bar{1}$] direction in TP 2 (the 141° re-entrant between planes 4 and 5) would result in the disappearance of these

re-entrants and hence, the termination of further growth in these directions. However, two new 141° re-entrants, one between planes 1* and 4* associated with TP 1 and the other between planes 3* and 6* with TP 2, are created, as shown in Fig. 3.9b.

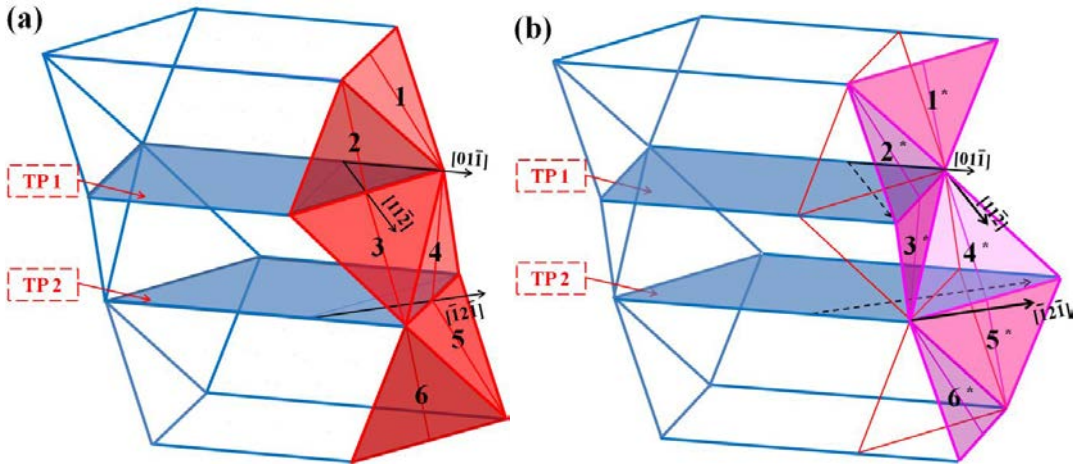

Fig. 3.9 Illustrations of a Si crystal with two parallel twinning planes TP 1 and TP 2. (a) Original configuration of two 141° re-entrants between planes 2 and 3 and between planes 4 and 5, and two 219° ridges between planes 1 and 4 and between planes 3 and 6. (b) Alternative disappearance and creation of 141° re-entrants across TP 1 and TP 2 to realize the <1 1 0> extension.

Although the disappearance of one re-entrant gives rise to the formation of a new re-entrant in the same direction, the Si growth front is shifted in one <1 1 0> direction and the extension pathway becomes zigzag. As illustrated in Fig. 3.10, the $[1\ 1\ \bar{2}]$ growth is interrupted by a shift in the $[\bar{1}\ 0\ 1]$ direction and the $[\bar{1}\ 2\ \bar{1}]$ growth by a shift in the $[1\ \bar{1}\ 0]$ direction, each leading to an extension in the same $[0\ 1\ \bar{1}]$ direction. Under such a scheme, the formed Si crystal (with parallel single-orientation twin variants) does expose only its {1 1 1} planes to the melt. This growth manner is advantageous in terms of interfacial energy, especially for slow solidification with low undercooling, as in the present case. To sustain a continuous growth, at least two parallel twinning planes are required. Such condition is evidenced by the present experimental results, *i.e.* each Si crystal contains more than two twins and their surface traces run from one tip of the crystal to the other. Due to this kind of anisotropic growth, the elongation speed of eutectic Si crystals is higher than the enlargement speed of α-Al matrix characterized by isotropic growth. Thus, the eutectic Si phase could lead over eutectic colony boundaries, as frequently observed in the present experiments.

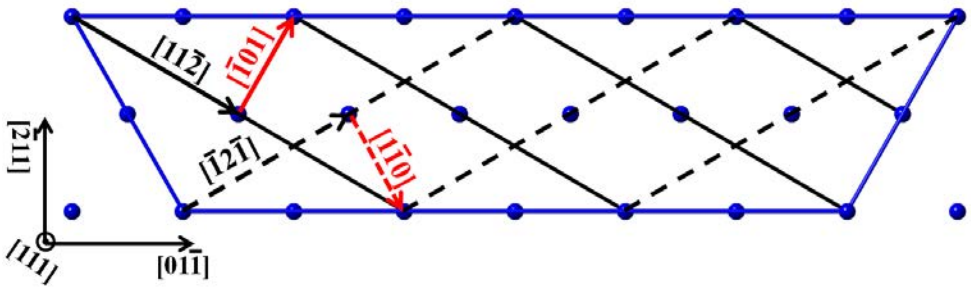

Fig. 3.10 Projection of TP 1 and TP 2 in Fig. 3.9 on one (1 1 1) atomic plane, showing the [0 1 $\bar{1}$] extension of twinned Si crystal through paired <1 1 2> zigzag growth. The growth directions of [1 1 $\bar{2}$] in TP 1 and [$\bar{1}$ 2 $\bar{1}$] in TP 2 are indicated with the black solid and black dashed arrow lines, respectively.

If the whole growth process of eutectic Si follows exactly the above proposed growth manner, Si crystals should be in a form of bar shape. This seems to be in conflict with the present observation that Si crystals are plate shaped. Indeed, the formation of plate-like crystals is also twin-controlled and realized in the TPRE manner. Fig. 3.11 illustrates one twinned Si nucleus with the same twin configuration as in Fig. 3.9. On one {1 1 1} twinning plane (colored in light blue), there are three equivalent <1 1 2> directions, each being associated with one re-entrant groove (highlighted in red). If these re-entrant grooves are all exposed to the melt, they can receive Si atoms to make the nucleus grow. Clearly, such a growth is planar and isotropic, giving rise to the formation of plates on condition that Si is the leading phase during the eutectic solidification.

When eutectic α-Al phase forms simultaneously, the planar isotropic growth of eutectic Si phase should be stopped. Since no specific OR between eutectic Si and α-Al is detected in the present work, one can infer that the formation of eutectic α-Al is controlled by composition preference, other than crystallographic compatibility between the two eutectic phases. The Si growth fronts (*i.e.* the re-entrant grooves) would act as ideal sites for the α-Al nucleation, as around these sites Si atoms are largely consumed and Al atoms are enriched. The formation of eutectic α-Al will cut the connection of certain Si re-entrant grooves to the melt and make them inactive. With a reduced number of re-entrant grooves, the {1 1 1} planar isotropic growth of Si crystals is replaced by the <1 1 0> directional growth, which renders them to develop into long plates. Due to the irregular steric hindrance of α-Al on Si crystals, the morphology of eutectic Si crystals could be very different (equilateral plate-like or bar-like) depending on local solidification conditions. Very often, the morphological variation

occurs in one Si crystal along with the change of local growth conditions (compositional or thermal).

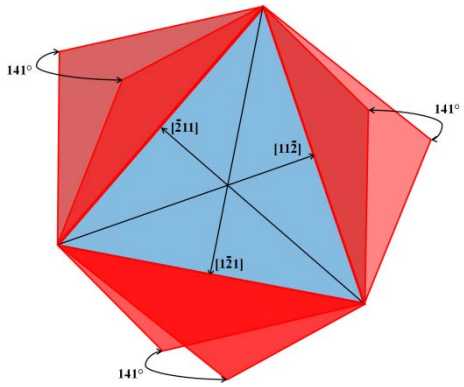

Fig. 3.11 Illustration of twinned Si nucleus with the same twin configuration as shown in Fig. 3.9. One {1 1 1} twinning plane is colored in light blue, and three 141° re-entrant grooves associated with three <1 1 2> directions on the twinning plane are colored in red. For easy visualization, only one twinning plane is shown.

3.4.3 Restricted growth of Sr-modified eutectic Si

With an addition of 400 ppm Sr to the Al-12.7Si alloy, the habit of the eutectic Si growth by forming twins and the <1 1 2> zigzag growth resulting in the <1 1 0> extension remains to some extent. For instance, multiple twin variants are often observed in eutectic Si crystals (Fig. 3.5b_3) and a preferred Si-<1 1 0> orientation is preserved in each eutectic colony (Fig. 3.6b_2). The present result suggests that the morphology modification of eutectic Si crystals occurs at the growth stage, being realized through "poisoning" twin re-entrants as proposed and verified recently by many investigations [5, 79, 109-111]. The Sr modifier should be considered to restrict further growth of eutectic Si crystals associated with the original {1 1 1} twinning planes, which is in accordance with the restricted TPRE growth mechanism [12].

According to our experimental observations, the modification effect by Sr addition on the eutectic Si morphology could be achieved in two different ways. One way is to block the Si growth on one initial {1 1 1} twinning plane and force the formation of new twins with the same twin orientation, which shifts the Si growth to the other {1 1 1} twinning planes that are parallel to the original twinning plane. As a result, the twinning plane trace becomes curved or stepped (Fig. 3.5b_2) and the lateral growth is enhanced. The other way is to block the Si growth along the original direction and force the formation of twins with different

orientations (Fig. 3.5b$_3$). This leads to a change in the growth direction and the appearance of multi-orientation twin variants. Clearly, both the shift and change of the growth direction would retard the preferred <1 1 0> elongation and bring about a refinement of Si crystals. In general, the shift of the growth direction shortens a Si crystal in the initial extension direction and increases its thickness in the lateral direction, whereas the growth direction change results in an isotropic growth and thus the formation of quasi equiaxed crystals. Due to the Sr-induced deceleration of directional extension in Si front, the growth velocities of α-Al matrix and Si crystals in one eutectic colony become comparable. Hence, no eutectic Si crystals would lead over eutectic colony boundary.

3.4.4 Orientation relationships between eutectic Si and eutectic α-Al

The present experiment has evidenced that no representative and statistical ORs exist in both unmodified and Sr-modified Al-12.7Si alloys. As compared with other eutectic alloys, the eutectic Al-Si alloy system is more complex, in which the eutectic Si phase is faceted and the eutectic α-Al is non-faceted. Such a facet/non-facet configuration does not ensure a compatible growth between the two phases. Actually, faceted Si crystals grow up locally with a zigzag pathway, as illustrated in Fig. 3.10. This growth manner cannot offer a smooth environment to establish a specific OR at microscopic level.

Detailed calculations have shown that no low index planes from α-Al could achieve relatively good atomic matches to the outer surfaces of Si crystals (*i.e.* Si-{1 1 1} planes). Moreover, the large thermal incompatibility between the Si and α-Al phases induces local constraints at α-Al/Si interfaces, imposing another difficulty for the establishment of specific ORs. If some certain ORs could be generated at the solidification process, they would have difficulty to be maintained accompanying the deformation of α-Al during the subsequent cooling process. All these arguments suggest that the formation of eutectic Al/Si mixtures during slow solidification does not provide favorable conditions to establish specific OR.

3.5 Summary

The growth characteristics of eutectic Si crystals in slowly solidified Al-12.7Si alloys with and without Sr-modification have been thoroughly investigated by SEM-based EBSD technique. The differentiation of the eutectic Si and α-Al phases was performed with a home-made software ATOM, which represents a prerequisite for the correlated microstructural and

crystallographic analyses of the eutectic microstructures at a large scale with statistical reliability. In both unmodified and Sr-modified cases, the eutectic Si growth was found to be coupled with the formation of {1 1 1} <1 1 $\bar{2}$> twins by faulted stacking of {1 1 1} planes.

For the unmodified eutectic Si crystals, they are in general long plate shaped with appearance of multiple single-orientation twin variants along the length direction. It was demonstrated that the eutectic Si growth in the TPRE manner brings about the Si extension in the <1 1 0> directions, other than the <1 1 2> directions assumed by the model. The microscopic <0 1 $\bar{1}$> extension is realized by a paired <1 1 $\bar{2}$> growth at atomic scale, where the <1 1 $\bar{2}$> growth leads to the disappearance of initial re-entrant grooves and the creation of new re-entrant grooves in the same <1 1 $\bar{2}$> direction, accompanied by a shift in the corresponding <$\bar{1}$ 0 1> direction in the same twinning plane. Such a paired <1 1 $\bar{2}$> zigzag growth ensures Si twins to expose only their lowest-energy {1 1 1} planes to the melt. This is advantageous in term of liquid/solid interfacial energy, especially for slow solidification with low undercooling. Prior to the eutectic α-Al formation, three Si re-entrant grooves associated with one twinning plane are all active, hence the eutectic Si growth is planar isotropic. When the eutectic α-Al forms preferentially at on-growing re-entrant grooves with enriched Al concentration, the number of re-entrants becomes reduced. Thus, the eutectic Si growth changes from planar isotropic to directional (anisotropic) and the equilateral plates evolve to long plates. The reduction of re-entrant grooves during the growth process accounts for the shape irregularity of eutectic Si plates, *i.e.* the occasional changes in width and thickness over the plate length.

As for the Sr-modified eutectic Si crystals, repeated single-orientation twin variants and multi-orientation twin variants, as well as curved or stepped twin boundaries, are frequently observed. The changes in Si morphology were demonstrated to be mainly associated with the growth process, as a result of the restricted TPRE growth and the IIT growth. More specifically, the restricted TPRE growth is realized by deactivating initial twins and forming new twins with the same orientation, which enhances lateral growth. The IIT growth is realized by forming new twins with different orientations, thus changing the initial anisotropic growth to isotropic growth. As a whole, the resultant eutectic Si crystals are significantly refined with the Sr modification.

In both unmodified and Sr-modified alloys, incompatible growth between Si crystals and surrounding α-Al matrix was evidenced by the existence of a large fraction of low angle disorientation in the α-Al matrix. This is due to a large difference in their thermal expansion coefficients. The internal stresses accumulated during solidification and subsequent cooling can be released by the deformation of soft α-Al matrix, which introduces abundant low-angle boundaries in grain interiors. On a statistical basis, no representative OR exists between the eutectic Si and eutectic α-Al phases. This is attributed to the incompatible growth and the incompatible thermal expansion between the two phases.

Chapter 4 Refinement mechanism of Al-Si eutectics by heat treatment

4.1 Introduction

Al-Si alloys are natural metal matrix composite (MMC) materials with hard Si phase embedded in soft α-Al matrix. To achieve an optimum strength-ductility combination of the Al-Si alloy systems, both the eutectic α-Al and Si phases should be refined. For the eutectic Si phase, trace amount of Sr addition has been proved to be an effective method to modify the morphology of eutectic Si crystals as shown in the last chapter. As for the soft eutectic α-Al phase, the refinement can be realized by recovery and recrystallization after being severely defected. It should be noted that there is large thermal incompatibility existing between the eutectic Si and the α-Al phases. Therefore, when the alloy is subjected to temperature change, large thermal stress can be created between the two eutectic phases. And this may result in both plastic deformation of the soft α-Al and fragmentation of the brittle Si crystals. Hence the microstructural refinements of the α-Al/Si eutectics can be expected to be realized during subsequent heat treatments. Thus to investigate the effect of heat treatment on the microstructural refinement, a Sr-modified eutectic Al-Si alloy was crucible slowly cast and heat treated for various times, especially with fast heating rate. Defect multiplication in α-Al phase and the fragmentation of Si phase were examined and the possible formation mechanisms were studied with an aim to provide useful information on heat treatment induced microstructural refinement that could be applicable to other MMC systems.

4.2 Experimental procedure

The materials used in the present work are high-purity crucible slowly solidified Al-12.7 wt. % Si-0.04 wt. % Sr alloys. The ingots of Sr-modified alloys were isothermally heat treated at 520 °C for 1 h, 4 h and 8 h, respectively.

Microstructural observations were performed at room temperature using a JEOL JSM-6500F field emission gun scanning electron microscope (SEM) and a Zeiss Supra 40 field emission gun SEM. The EBSD diffraction patterns were acquired at the acceleration voltage of 20 kV in a beam controlled mode with a step size of 0.1 μm. The crystallographic

orientation examinations were conducted by first differentiating the α-Al phase and the Si phase using the software – Analysis Tools for Orientation Mapping (ATOM) [142]. Then with the fully differentiated EBSD orientation data of the two phases, crystallographic features of α-Al matrix in terms of disorientation angle distribution and GND density tensor were analyzed using the ATOM software. The spheroidization of the eutectic Si (with aspect ratio < 2) was analyzed using the software ATOM. Samples for SEM microstructural observations and crystallographic analyses were prepared using the standard metallurgical techniques. To obtain statistical information, the EBSD orientation data was acquired from sample areas of approximately 0.32 mm^2. To obtain the 3D morphology of the Sr-modified eutectic Si crystals in the as-cast and heat treated Al-12.7Si-0.04Sr alloys, the samples were electrolytically polished in a solution of 20 % perchloric acid in methanol for 10 seconds at 25 V and at a temperature below 10 °C to partially dissolve the α-Al matrix.

The substructural features of the eutectic α-Al and Si in the as-cast and the heat treated Sr-modified alloys, such as dislocation configurations, were further examined with a Philips CM200 TEM. Foil samples for TEM characterizations were prepared in a Carl ZEISS Auriga 40 Focused Ion Beam (FIB) workstation (Oberkochen, Germany). In-situ neutron diffraction measurements were performed during the solidification process at the STRESS-SPEC at Heinz Maier-Leibnitz Zentrum (MLZ) (Garching, Germany).

4.3 Results

4.3.1 Microstructural features of as-cast Sr-modified Al-Si eutectic alloy

The secondary electron (SE) image in Fig. 4.1a shows the 3D morphology of the eutectic Si in the as-cast Al-12.7Si-0.04Sr alloys by partially dissolving the α-Al matrix. It can be seen that, the shapes of Si crystals are very irregular. The crystals are composed of bar or narrow plate shaped segments interconnected into coral-like agglomerates, as outlined in the dashed red rectangle. On the straight parts of the Si crystals, the widths and the thicknesses are not homogeneous but perturbed by steps, ridges and edges. SEM back-scattered electron (BSE) images displayed in Fig. 4.1b demonstrate that the Si crystals contain twin variants with multiple orientations. The specific morphology of the Si crystals in the Sr-modified alloys is realized by restricted TPRE growth and impurity induced twinning (IIT) growth mechanisms through twin variant multiplication as explained in *Chapter 3*.

From the BSE image in Fig. 4.1b, it is seen that the α-Al matrix around the Si crystals contains large amount of fine contrasted domains (around 1 μm in diameter). The appearance of such domains in the BSE image for the present alloys should be of crystallographic orientation origin. This indicates that the large sized α-Al matrix in one eutectic colony contains fine crystallographically misorientated zones, like subgrains.

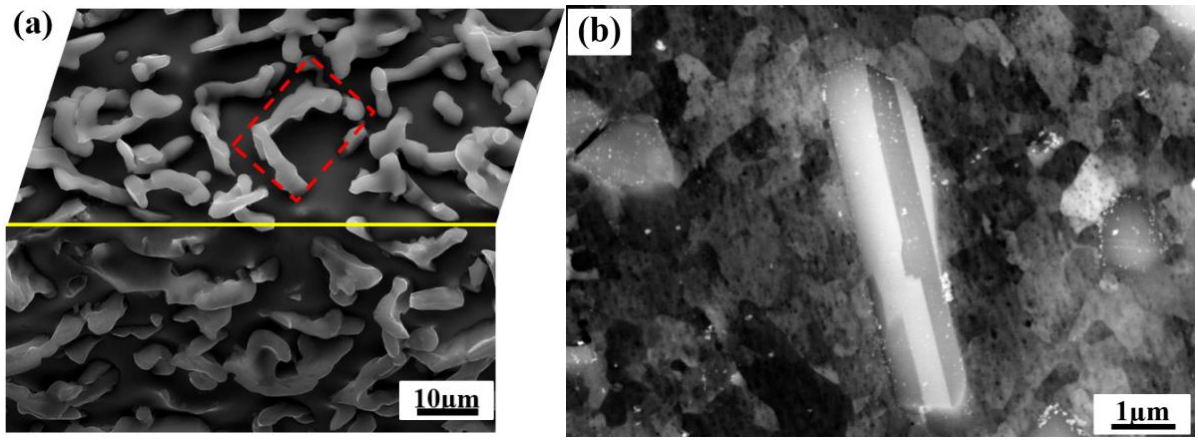

Fig. 4.1 (a) SEM (SE) image displaying a 3D morphology of eutectic Si crystals and (b) SEM BSE image showing Si twin characters and fine contrast domains of α-Al matrix in crucible slowly solidified as-cast Sr-modified Al-12.7Si alloy.

4.3.2 Microstructural evolution with heat treatments

4.3.2.1 α-Al

Figure 4.2 show disorientations superimposed with the EBSD band contrast (BC) micrographs of the as-cast and heat treated Sr-modified Al-12.7Si alloys. In the figures, the eutectic Si crystals are colored in blue and the boundaries of the α-Al matrix with disorientation angles ranging from 2° to 4°, from 4° to 10° and higher than 10° are outlined in green, red and black, respectively. As observed in the as-cast sample in Fig. 4.2a, the coarse α-Al eutectic colony contains unclosed boundaries from low angle to high angle. The distribution of such boundaries is relatively homogeneous within the α-Al matrix. After the specimen was heat treated at 520 °C for one hour (Fig. 4.2b), some high angle boundaries (> 10°) start to close up, marking the formation of new "grains" within the as-cast α-Al colonies. This indicates that "recrystallization" occurred during this heat treatment. The difference of such "recrystallization" from the classic recrystallization lies in two aspects: one is that the alloy does not suffer any macroscopic deformation before the recrystallization; the other is

that the grains are not crystallographically perfect after the recrystallization. As shown in Fig. 4.2b, it can be seen that disorientations up to 4° (the green lines) exist in the newly formed grains. The number of such grains is greatly increased when the sample is heat treated for four hours (Fig. 4.2c), indicating an intensified "recrystallization" of the α-Al matrix. However, after eight hours of heat treatment (Fig. 4.2d), the number of the "recrystallized" grains decreases but their sizes increase, indicating the coarsening of these grains. Some reach 10 μm in diameter. For some large-sized grains, their boundaries are impinged by Si particles, suggesting that Si particles have some pinning effect on the boundaries during the growth of the "recrystallized" grains through boundary migration (Fig. 4.2d).

To quantify the intensification of the "recrystallization" process with the heat treatment, the area fraction of the "recrystallized" grains is analyzed under each heat treatment condition and the results represented in histogram are given in Fig. 4.3. For reference, that from the as-cast alloy is also displayed. The maximum allowed disorientation between the orientation of each constituent pixel of the "grain" and the average orientation of the "grain" is 4°. It is seen from the figures that the amount of the "recrystallized" parts increases with the increase of the isothermal holding time, although the heat treated specimens do not undergo any macroscopic deformation.

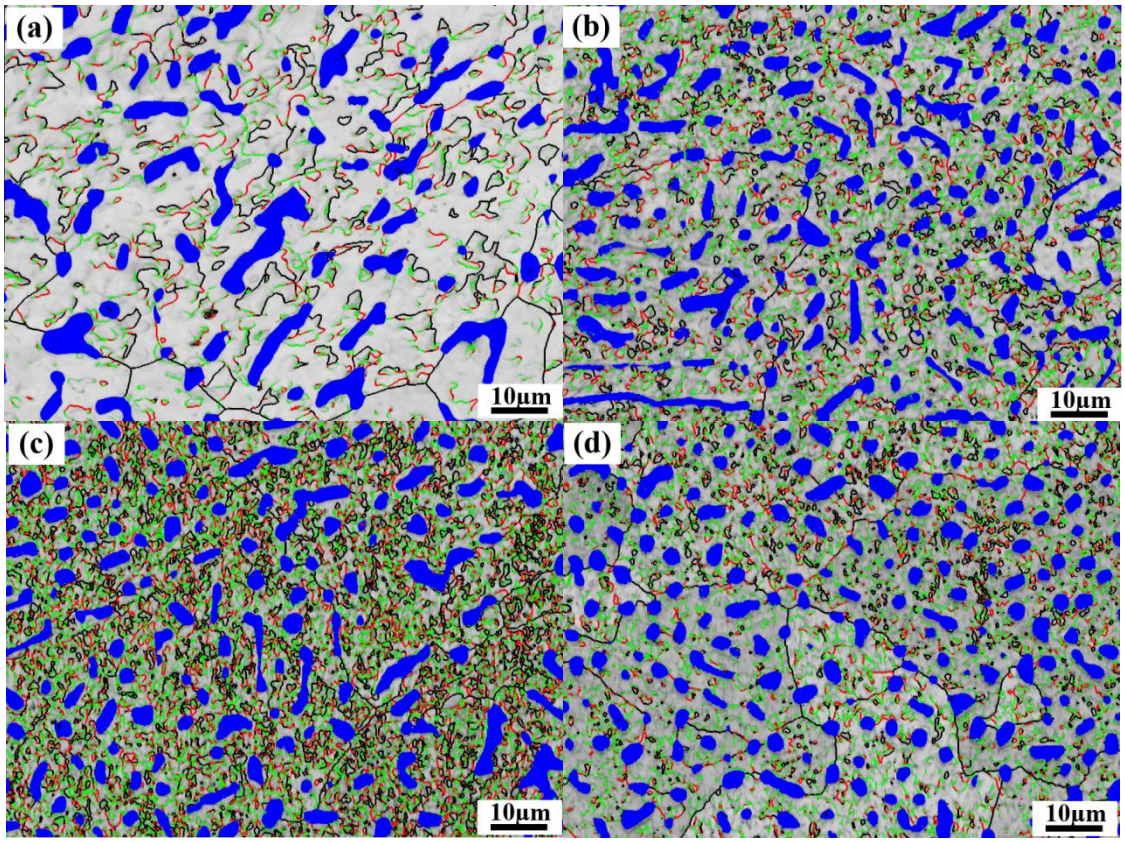

Fig. 4.2 EBSD Band Contrast (BC) micrographs showing microstructural evolution of eutectic α-Al matrix in crucible slowly solidified Al-12.7 wt. % Si-0.04 wt. % Sr alloys with heat treatments: (a) as-cast, slowly solidified, (b) 520 °C-1 h, (c) 520 °C-4 h and (d) 520 °C-8 h. Here Si phase is colored in blue. The boundaries with disorientation angle ranging from 2° to 4°, from 4° to 10° and higher than 10° are colored in green, red and black, respectively.

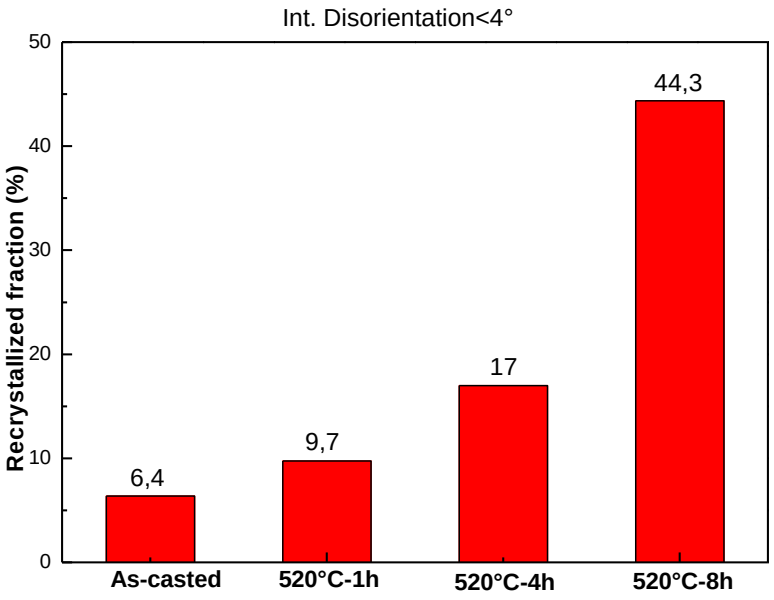

Fig. 4.3 Recrystallized area fraction of the eutectic α-Al phase in the as-cast and the heat treated crucible slowly solidified Al-12.7 wt. % Si-0.04 wt. % Sr alloys (calculated by ATOM software).

However, with the "recrystallization", the newly formed α-Al grains are not purified from crystal defects as the usual process of recrystallization. Instead, it is more defected, as shown by the EBSD local disorientation (< 4°) micrographs in Fig. 4.4, where the Si crystals are represented with their band contrast and the high-angle grain boundaries of the α-Al are represented with black lines. According to the color scale (blue to red: 0 to 4°) shown below the figures, it is seen that the amount of local disorientation of about 2° in the eutectic α-Al matrix increases from the as-cast state (Fig. 4.4a) to the heat treated state (1 h, Fig. 4.4b). The quantity of such misoriented regions reaches the maximum after the 4 h heat treatment (Fig. 4.4c) and then decrease after the 8 h heat treatment (Fig. 4.4d). From Fig. 4.4, it is seen that the misoriented regions are distributed relatively homogeneously within the α-Al matrix without spatial preference with respect to the location of Si crystals. Moreover, they are present even in the domains enclosed by high angle boundaries (the black lines in the figures) formed during the heat treatment. Further TEM analyses show that in the α-Al matrix there exist large amount of dislocation arrays, dislocation networks after the heat treatments, as displayed in the TEM bright field (BF) micrographs in Figs. 4.5a and b. The appearance of

dislocation arrays (Fig. 4.5a) and dislocation networks (Fig. 4.5b) evidences that polygonalization which occurred in α-Al matrix during the heat treatment is the necessary process for recrystallization. During the polygonalization, subgrains with low angle boundaries form, as shown by the grain reference orientation deviation (GROD) [144] micrograph in Fig. 4.5c. These are the classical features of recovery and recrystallization. However, other than the polygonalized dislocations, there also exist large amount of discrete dislocations, as shown in Fig. 4.5d. Together with the intensified appearance of disorientations in α-Al matrix with the heat treatments shown by the local disorientation micrograph in Figs. 4.4b and c, one can consider that new dislocations are generated even when the heat treatment is applied. These results further confirmed that two opposite processes occur in the heat treated samples. One is the recovery and recrystallization that consume crystal defects. The other is the generation of crystal defects that multiplies the amount of dislocations. The two processes were in competition. With the heat treatment until 4 h, the latter prevails the former, whereas, with longer timed heat treatment, the former prevails. However, for the Si crystals, very few dislocations were observed.

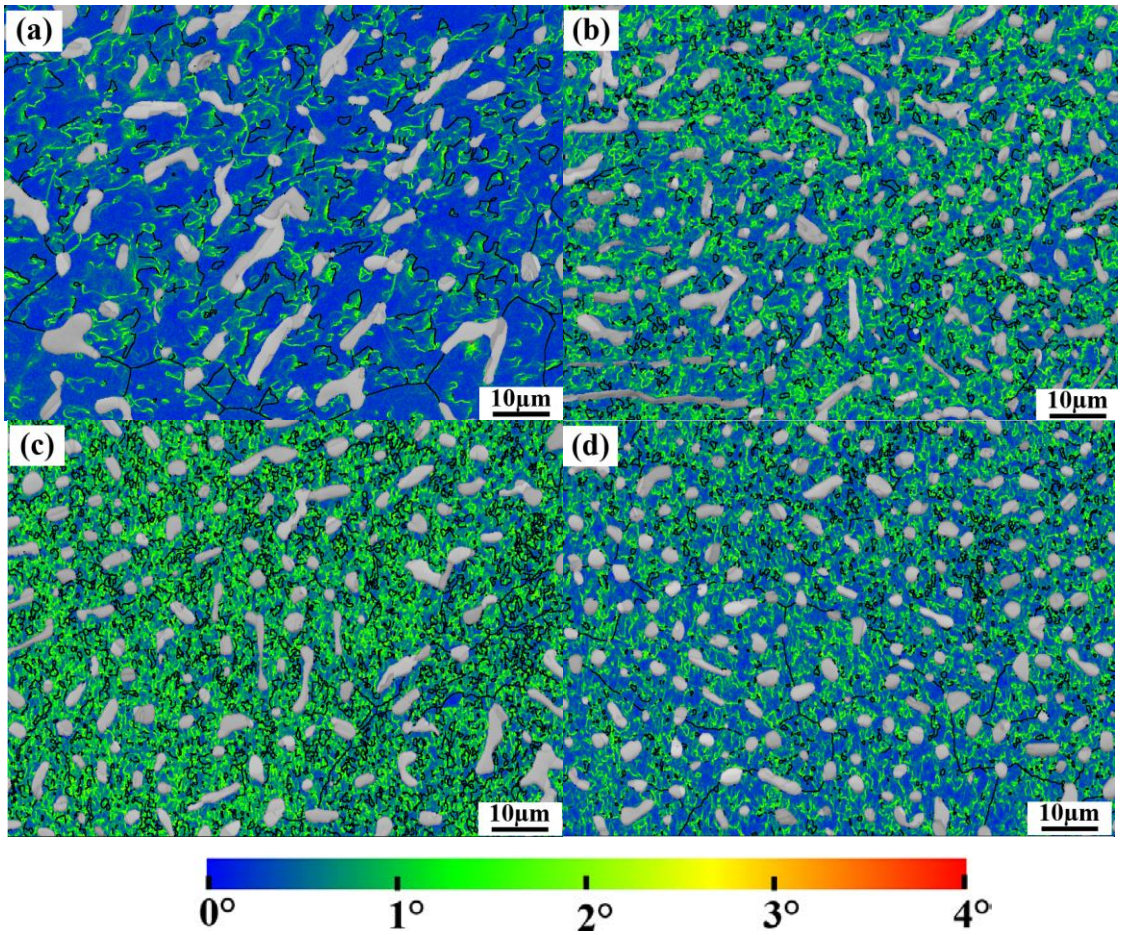

Fig. 4.4 Local disorientation micrographs of eutectic α-Al matrix of Al-12.7 wt. % Si-0.04 wt. % Sr alloy: (a) as-cast, (b) 520 °C-1 h, (c) 520 °C-4 h and (d) 520 °C-8 h. Here Si phase is represented with their band contrast. Filter binning is 3×3; sub-grain boundary angle = 4°. The black lines mark high angle boundaries (> 10°).

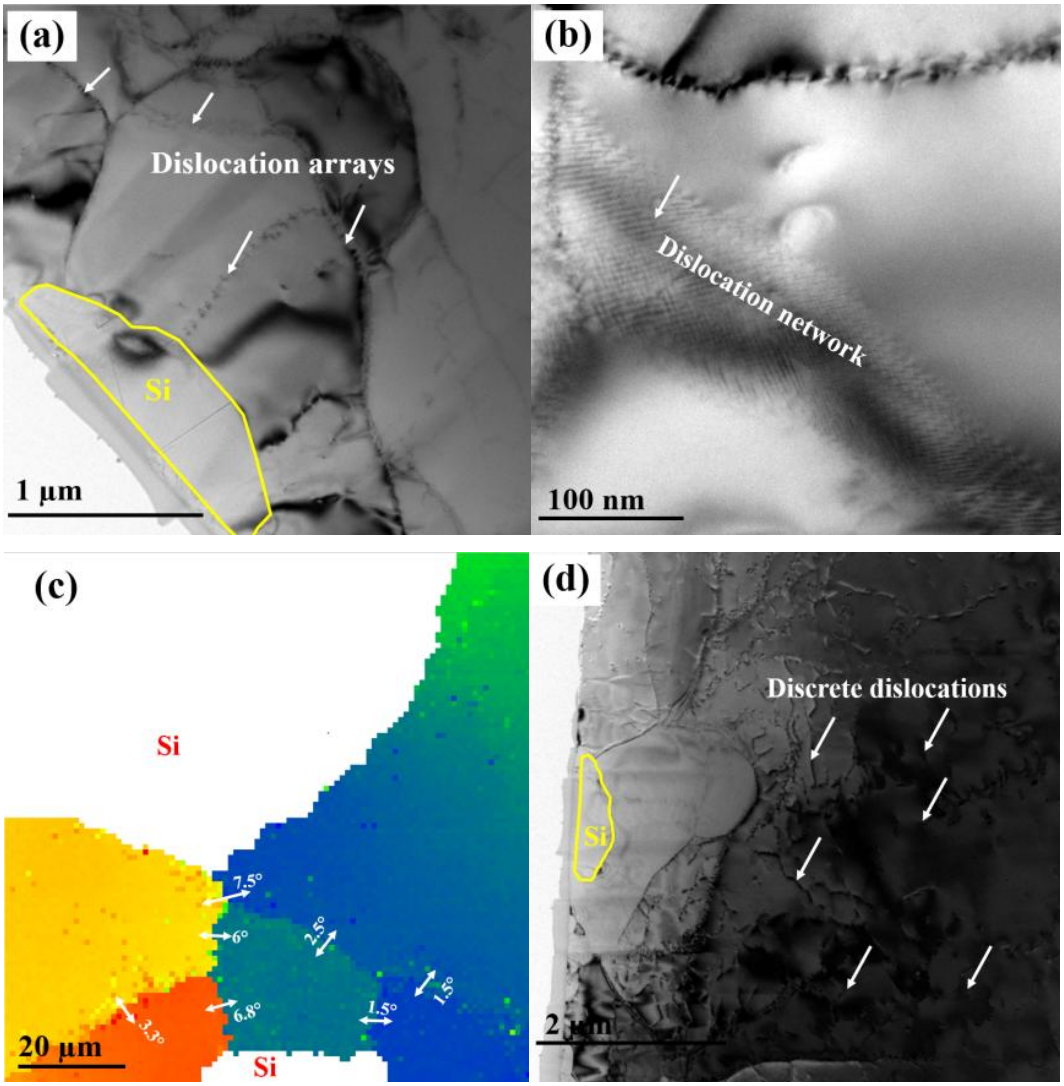

Fig. 4.5 (a, b) TEM Bright Field (BF) micrographs characterizing 'cells/subgrain' boundaries formed by (a) dislocation arrays and (b) dislocation network in 520 °C - 4 h sample. (c) Grain reference orientation deviation (GROD) micrograph (from automated TEM orientation mapping) illustrating the subgrains formed through polygonalization. (d) BF micrographs showing the discrete dislocations.

To further evaluate microscopic lattice distortion of the α-Al matrix induced by defect multiplication, GND density of the as-cast and the heat treated specimens was investigated,

using the measured EBSD orientation data of the α-Al. In the analyses, only disorientations within 1°-4° are taken into account, considering that the disorientations below 1° may be caused by angular imprecision of the SEM/EBSD measurement system and the disorientations higher than 4° may correspond to sub-grain boundaries. The results are presented in histograms, as displayed in Fig. 4.6. It is seen from Fig. 4.6 that the density of GND increases from the as-cast state to the heat treated states, reaching the maximum at 4 h heat treatment.

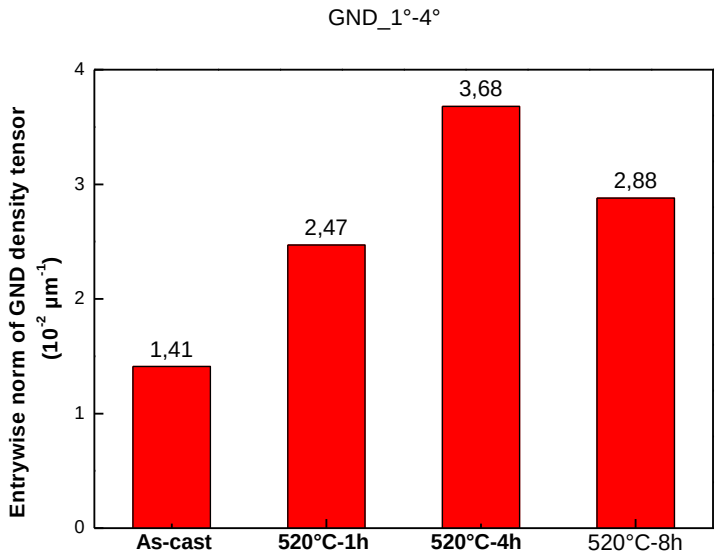

Fig. 4.6 Entry-wise norm of GND density tensor in the as-cast and in the heat treated samples calculated by ATOM software. Disorientation value is between 1°-4°.

4.3.2.2 Si phase

Accompanying the polygonalization and defect multiplication of the eutectic α-Al matrix during the heat treatments, the morphology of the eutectic Si crystals also changes. As seen in Fig. 4.2, the interconnected and branched as-cast Si crystals (Fig. 4.2a) fragmentize and spheroidize with post heat treatments (Figs. 4.2b, c and d). In consequence, the number of Si particles increases with the increase of the isothermal holding time. Due to the fragmentation and spheroidization, the morphology of most Si crystals changes from the curved bar shape (Fig. 4.2a) in the as-cast state to the short straight bar shape after the heat treatments (Figs. 4.2b (520 °C-1h) and c (520 °C-4h) and finally to nearly spherical shape (Fig. 4.2d (520 °C-8h)). To quantify the morphological evolution of the eutectic Si crystals, the occurrence of

their aspect ratios were analyzed and the results are presented in Fig. 4.7. It is seen from the figures that the amount of small valued aspect ratios (< 2, representing nearly equiaxed shape) increases from the as-cast to the heat treated states and with the isothermal holding time, whereas the amount of large valued ratios (> 4) decreases, indicating the fragmentation of the large sized Si crystals.

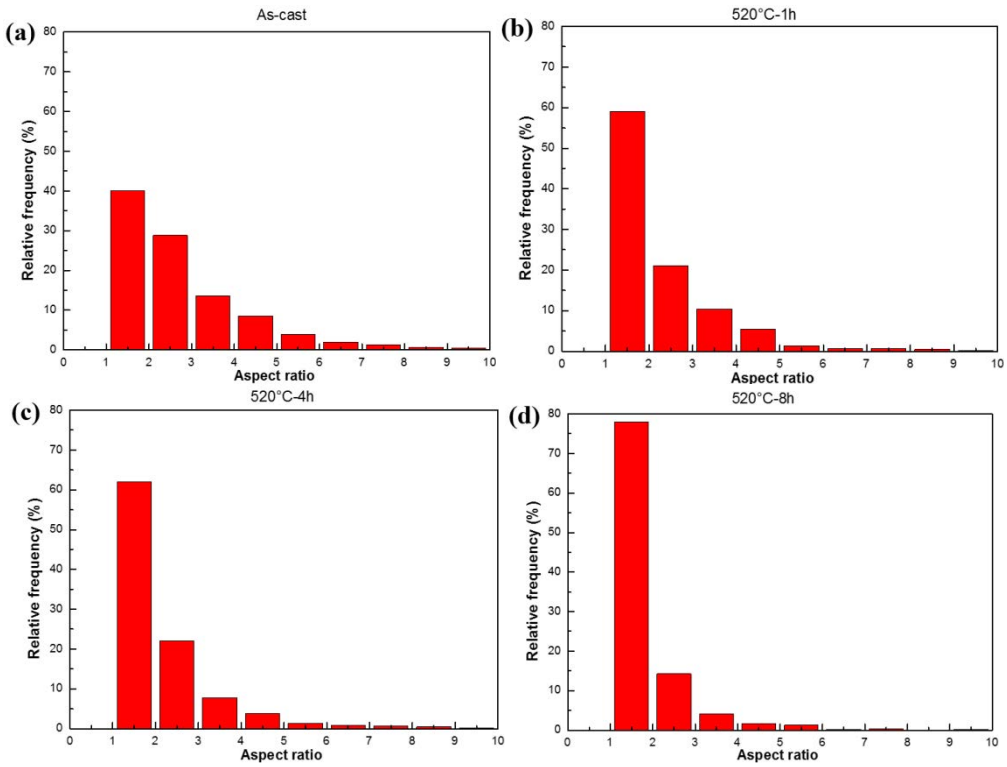

Fig. 4.7 Occurrence of the aspect ratios of eutectic Si crystals in the as-cast and heat treated Al-12.7Si-0.04Sr samples.

A close 3D examination of the morphological evolution of the Si crystals with the heat treatments using the samples with partially dissolved α-Al matrix reveals the characteristics of Si fragmentations, as shown in Fig. 4.8. The morphological evolution of the Si particles is realized by three steps: first disconnection at the joints of the interconnected bars, as seen in Fig. 4.8a (520 °C-1 h), then at the "necks" of the straight bars where the thickness or the width of the bars changes, as shown in Figs. 4.8b (520 °C-4 h), c, and d (520 °C-8 h), and finally spheroidization of the fragmented Si crystals, as displayed in Fig. 4.8e (520 °C-8 h). The Si crystal is finally spheroidized into round shape enveloped with planar facets as shown in Fig. 4.8e. The facets are mostly composed of {1 1 1} planes that are the closest packed planes providing the lowest surface energy for a diamond structured crystal [34, 145]. The

characteristic features of the factures of the fragmented Si crystals demonstrate that there are two kinds of rupture occurring during the fragmentation. One is ductile with obvious necking (Fig. 4.8b) and the other is brittle with flat rupture surface (Figs. 4.8c and d). By nature Si belongs to brittle materials. The ductile fracture should be due to diffusion effect occurring during heat treatment and should be slow. The brittle fracture should be related to local mechanical constraints and could be rapid. Considering that each Si crystal is monocrystalline or composed of twins, the brittle fracture can only be realized by cleavage. Further examination showed that the cleavage plane is $\{1\ 1\ 1\}_{Si}$ and in most cases the cleavage were initiated from the $\{1\ 1\ 1\}_{Si}$ twinning planes, as shown as an example in Fig. 4.9a.

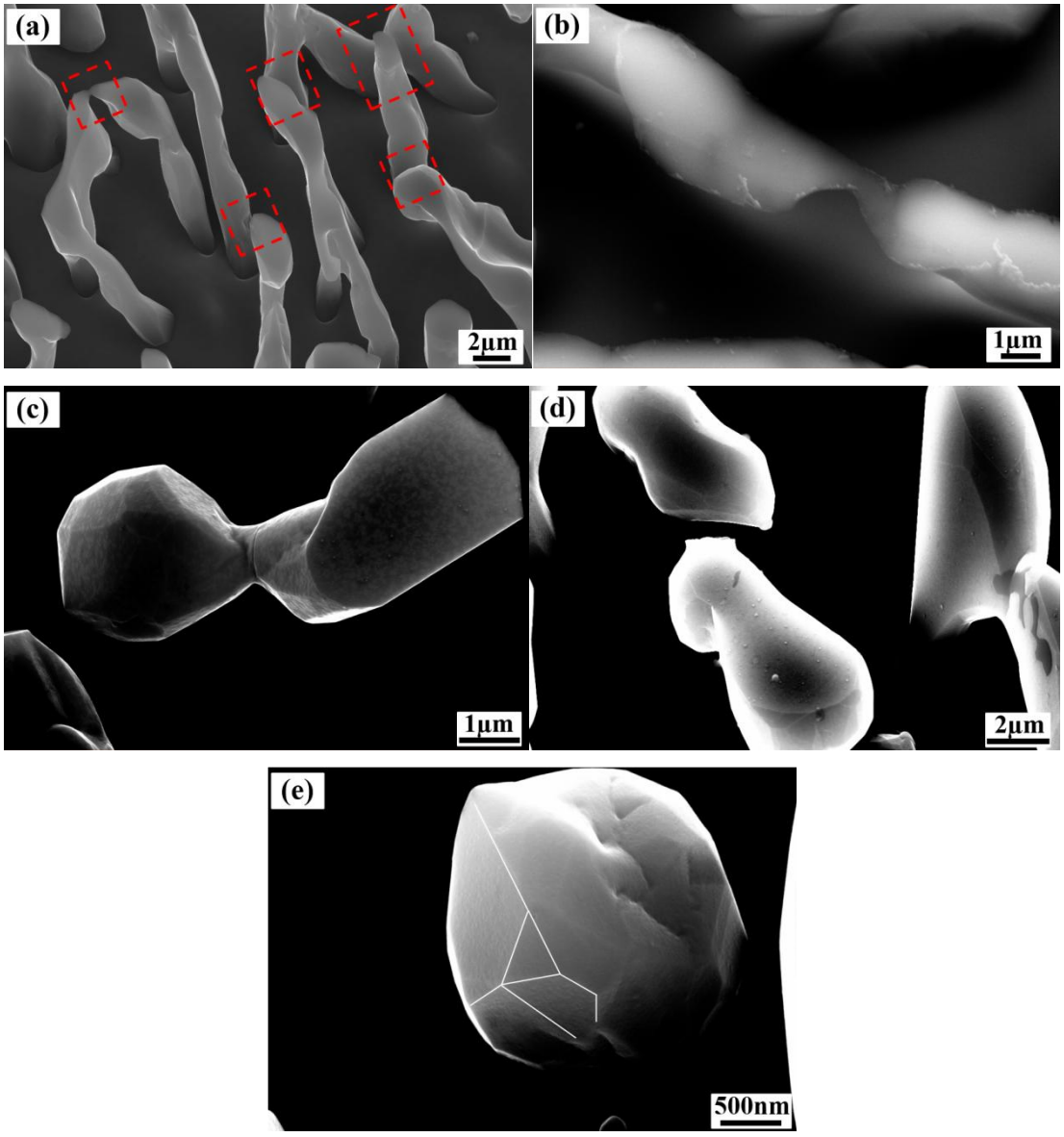

Fig. 4.8 SEM SE micrographs demonstrating the morphological evolution of eutectic Si crystals in Al-12.7Si-0.04Sr alloy with heat treatments by disconnection, fragmentation and spheroidization. (a) 520 °C-1 h, where the red dashed rectangles outline the disconnected joints between Si bars. (b) 520 °C-4 h, showing the necking of Si crystal. (c), (d) and (e) 520 °C-8 h, showing cracks of Si crystals, the separation along the crack, and the final spheroidization.

With the fragmentation of the Si crystals, two phenomena occur concomitantly. One is that the fragmented crystals are spatially separated as shown in Fig. 4.9b. The separation is accompanied by a relative rotation between the separated crystals and disorientations of 4 to 20° can be generated. The other is that the separation does not create voids or cracks between the separated parts of the initial Si crystal. The gaps are all filled with α-Al, as shown in Fig. 4.9b.

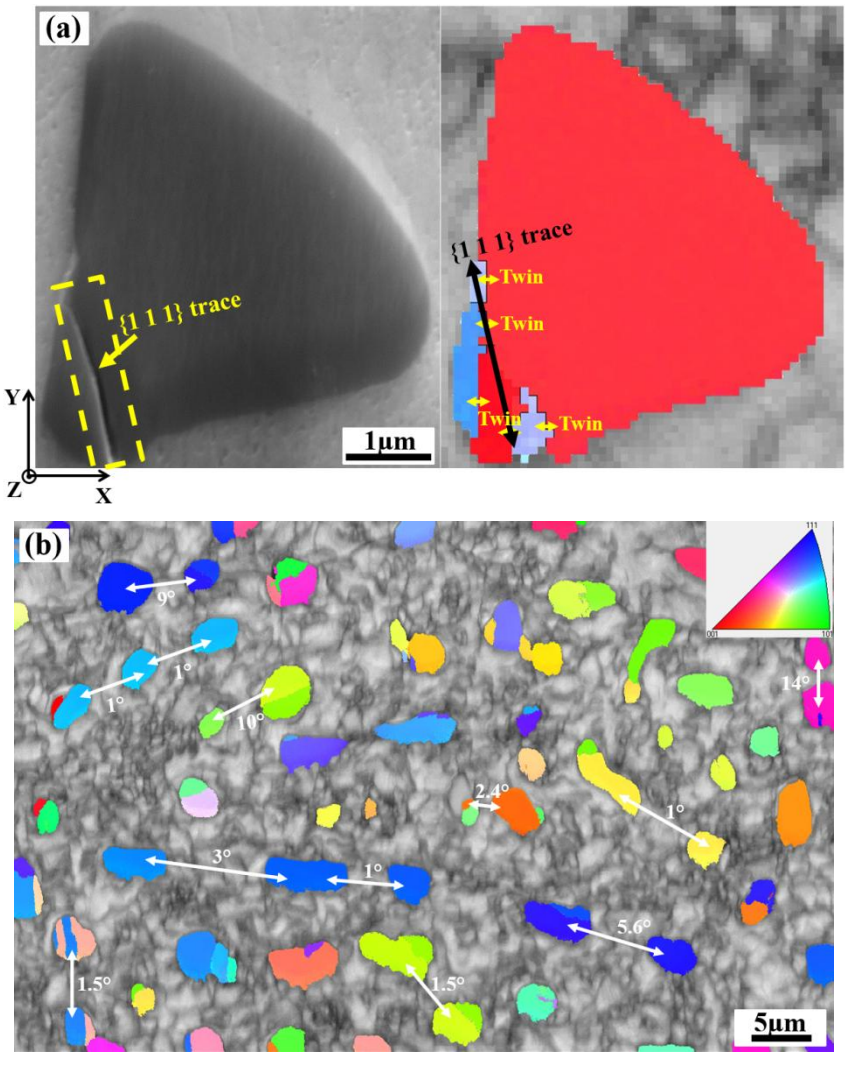

Fig. 4.9 (a) SEM SE micrograph and EBSD Y-axis inverse pole figure (IPF) micrograph showing cleavage initiated from $\{1\ 1\ 1\}_{Si}$ twinning plane of eutectic Si phase in Al-12.7Si-0.04Sr alloy (heat treated at 520 °C for 4 h). The crack is outlined with the yellow rectangle in the SEM SE image and the trace of the {1 1 1} plane is marked with the white line. There is a 6°-7° relative rotation between the fragmented parts. (b) EBSD micrograph (Si: IPF, α-Al: BC) showing fragmented and separated Si crystals.

4.3.3 Thermal expansion of Si crystal and α-Al matrix

Fig. 4.10 shows the neutron diffraction patterns of the Al-12.7Si-0.04Sr alloy acquired during cooling down from 468 °C to 46 °C with a rate of 30 °C/min. It is seen that the peaks of α-Al shift drastically toward the higher 2θ range with the decrease of the temperature, whereas those of Si shift very slightly. This indicates that the lattice parameter of α-Al decrease rapidly during cooling down. The lattice strain of both the Si crystal and the α-Al phase calculated from the peak shifts are 13×10^{-3} and 3×10^{-3}, respectively. The difference is in the order of 10. With such unequal thermal expansions, large mechanical constraints can be expected between the two phases when they are exposed to heat, especially when they experience temperature gradient.

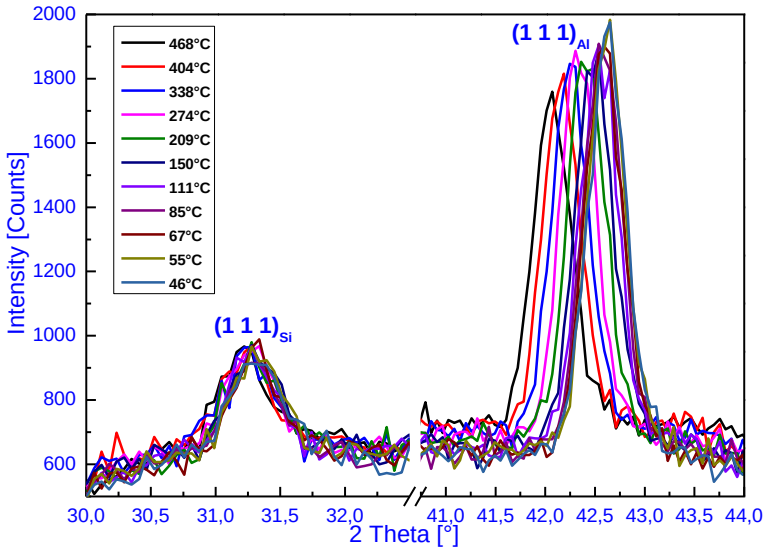

Fig. 4.10 In-situ neutron diffraction patterns of the eutectic Si crystals and the α-Al phase during cooling from 468 °C to 46 °C at a cooling rate of 30 °C/min.

4.4 Discussion

The large thermal expansion difference between the two phases evidenced in the present work suggests that large mechanical constraints can be produced in the places where temperature gradient exists. For the present work, after solidification, the samples were subjected to heat treatments that consist of heating, isothermal holding and cooling in their solid state. Under the mechanical constraints, the responses of the Si and the α-Al should be very different, as Si is hard and brittle with almost zero plasticity before rupture, whereas α-Al is soft and ductile with pronounced plastic capacity.

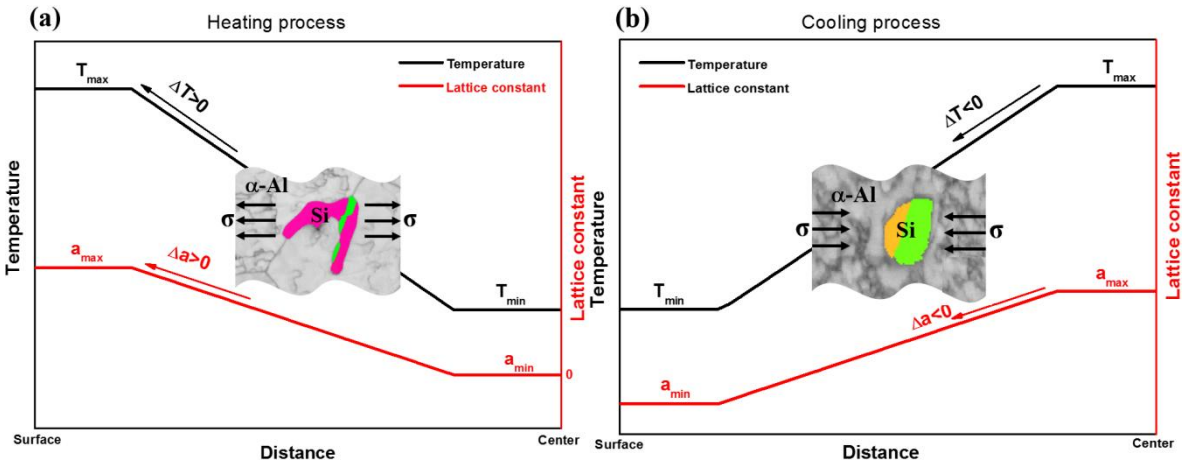

Fig. 4.11 Illustration of variations of temperature and lattice constant from sample surface to sample interior during heating and cooling process. For simplicity, linear variations are assumed.

When heating is applied to the sample, heat is transferred from the sample surface to the sample interior. A long range positive temperature gradient ($\Delta T > 0$) can be created between the hot end (exterior) and the cold end (interior) of the sample before a homogeneous temperature field is established through the sample, resulting in a positive expansion gradient in the direction from the sample interior to the sample surface, as illustrated in Fig. 4.11a. The magnitude of the temperature gradient and its spatial spread is heating or cooling rate dependent. The faster the heating or cooling rate is, the higher the magnitude and the shorter spread are. Under the temperature gradient, an expansion gradient is created, resulting in a kind of tension along the gradient, as illustrated in Fig. 4.11a. As in the present alloy, α-Al is in majority as matrix and Si is in smaller size distributed dispersedly within α-Al, the extension amount is mainly defined by the α-Al that is more than 10 times of that of Si. Thus

for Si crystals, only about 10 % of the tension exerted by the thermal expansion of the α-Al can be accommodated through their own thermal expansion. The rest can only be accommodated by forming voids or through the deformation of the surrounding α-Al matrix. Considering that the shape of the as-cast Si crystals are irregular and interconnected, like corals with sharp turns at the joints and surface ridges and edges, they must be very fragile to the mechanical constraints, especially under a tensile environment. Ruptures (mainly by cleavage) can be expected to occur. Once the Si crystals crack, the fractured parts will be further dragged away, forming voids to accommodate the exerted thermal expansion by the surrounding α-Al. Since the shape of the Si crystals is irregular, the mechanical constraints can be locally deviated in direction and in magnitude. Thus relative rotations between the fractured parts, as evidenced by the above experiments, could occur. As the temperature gradient sweeps the whole sample volume from the surface to the center during the heating process before the set temperature is reached, all Si crystals have chance to undergo certain forms of mechanical constraints (mainly tension) and thus have chance to crack (partially or totally).

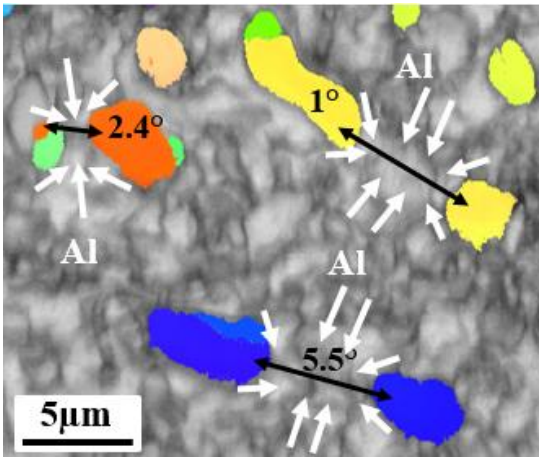

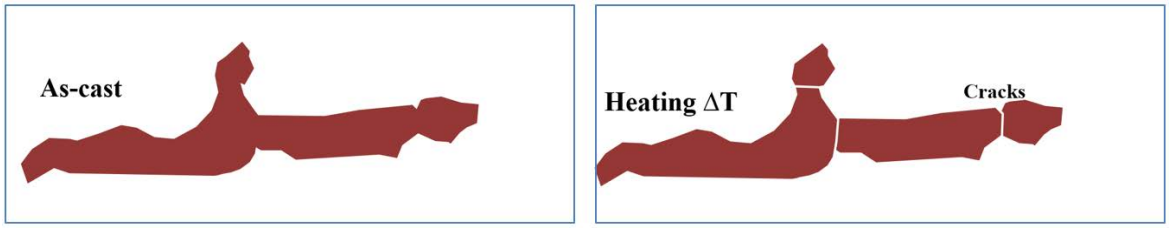

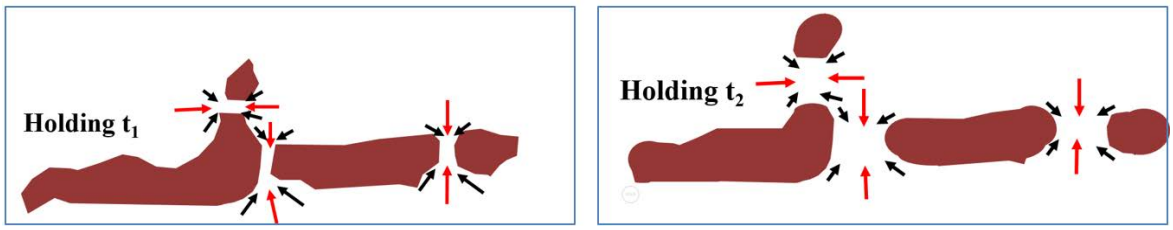

Fig. 4.12 Illustration of fragmentation and spheroidization of Si and the related diffusion in the adjacent α-Al. Diffusion induced by Si cracks is in red and that induced by spheroidization in black.

When the isothermal holding of the heat treatment comes, a homogeneous temperature field is established in the sample. The microscopic mechanical constraints induced by the thermal expansion incompatibility between the two phases disappear. However, nano scaled and even atomic scaled mechanical constraints, such as capillary force induced by Si cracks and surface tension induced by curvature variations due to shape irregularity of Si, exist. These mechanical constraints will provoke atomic diffusion in both Si crystals and in α-Al matrix, as the material is exposed to relatively high temperature (520 °C that is 57 °C below the melting point). For the Si crystals, the diffusion happens mainly at the places with curvature change (surface grooves resulting from internal twin boundaries, surface steps or ridges due to shape irregularities and corners at the fractures). The curvature variations thus induce the so-called "shape instability" [120, 122] that drives the fusing of the Si bars through the so-called "boundary induced ovulation" at the twin boundary-surface intersections and the "perturbation induced ovulation" at the surface ridges or edges until a homogeneous curvature is reached (spherical shape). This process change the cylindrical shaped Si to short bar shape and finally to spherical shape. The diffusion in the α-Al is mainly to accommodate the shape change of the hard Si crystals. Under the capillary force created by the fracture of the Si crystals, Al atoms diffuse toward the gaps generated by the Si cracks. As the diffusion of Al atoms is substitutional, the migration of the atoms in the direction toward the cracks creates a flow of vacancies in the opposite direction, through which the gaps between the fractured Si crystals are filled with Al atoms and the voids are transferred to the interiors of the α-Al matrix. For each block of α-Al delimited by Si crystals, Si tunnels exist in various directions, as illustrated in Fig. 4.12, and the α-Al suffers mass transfer in various directions. Thus vacancy concentration gradient will be created between different main diffusion directions (in red in Fig. 4.12), making the α-Al crystal defected. Further affected by local Al diffusion that

accommodates Si diffusion (in black in Fig. 4.12) induced by shape instability, such vacancy gradients will be further modified and become spatially spread and irregular. Linear and planar defects can form with the agglomeration of the vacancies. Due to the formation of the crystal defects in the α-Al, the stored energy increases. Thus recovery and then recrystallization happen as the material is exposed to high temperature. Domains with low-angle or high-angle boundaries form. Two processes, *i.e.*, defect formation and defect annihilation progress dynamically and in competition during the isothermal holding. At the early stage of the isothermal holding, canalization of α-Al between fractured Si crystals and shape instability diffusion of Si are prevalent. Thus defect multiplication is dominant as has been evidenced by the disorientation micrographs in Figs. 4.4b and c. With the prolongation of the holding time, Si tunnels are mostly filled and the number of spherical particles increase. Microscopic diffusion becomes less intense. Recovery and recrystallization prevail over defect multiplication. Domains with less lattice distortion form and enlarge, as evidenced by the disorientation micrographs in Fig. 4.4d. Due to the continuous and irregular lattice movements of α-Al induced by defect formation and by recovery and recrystallization, the fractured Si particles move and rotate with the surrounding α-Al. Thus the spatial distance between them enlarges and the disorientation between them also increases, making the distribution of the Si particles more disperse and more crystallographically random.

When cooling starts, heat is transferred from the sample interior to the sample surface. An inverse temperature gradient ($\Delta T < 0$) is established from the sample surface to the sample interior with respect to that of the heating process, creating a contraction gradient ($\Delta a < 0$), as illustrated in Fig. 4.11b. Similar to the heating process, the contraction amount is dominated by the α-Al that is one order higher than that of the Si crystals. In such circumstance, the Si crystals are subjected to a compression by the surrounding α-Al. As Si is much harder than α-Al and almost non-deformable, and moreover, the number of irregular shaped Si crystals is greatly reduced, large amount of requested thermal contraction of α-Al cannot be absorbed by the volume occupied by Si crystals and has to be accommodated by α-Al through its plastic deformation, giving rise to the formation of crystal defects. However, for the present heat treatments, the heating rate is much higher (cold samples are dipped very rapidly in the salt bath of 520 °C) than the cooling rate (air cooling). The temperature gradient on heating should be much higher and much narrower in distance than those on cooling, thus the mechanical constraints during heating is much more intensive and rapid. The destructing

effect on Si crystals and on α-Al is much more pronounced. Moreover, the irregular shape and the interconnecting feature of the Si crystals further aggravate this effect. Thus the formation of crystal defects should be dominant during heating and during the subsequent isothermal holding.

4.5 Summary

An eutectic Al-12.7 wt. % Si alloy with 400 ppm Sr addition was slowly cast and heat treated at 520 °C for various time (1 h, 4 h and 8 h) in the present study. Intense formation of crystal defects in α-Al without any macroscopic deformation during the heat treatments was experimentally revealed. This process was found to occur in connection with the fragmentation and spheroidization of eutectic Si crystals that are in coral shape composed of sharp corners and surface ridges or edges. Subjected to rapid heating during the heat treatment by which large temperature gradient can be created and sweep through the whole sample volume from the surface to the center, Si crystals crack at the fragile places, like sharp corners for example, due to the limited accommodating capacity of the Si crystals to the giant thermal expansion of the surrounding α-Al matrix, resulting in the refinement of eutectic Si phase. The fractures generate a kind of "capillarity" force that attracts the Al atoms to fill the gap produced by the fracture. As the diffusion of Al atoms is substitutional, the migration of Al atoms toward the gap generates a flow of vacancies in the opposite direction. In this way, the voids produced by Si fracture are transferred to the interior of the α-Al matrix. As the Si crystals are distributed dispersedly in the α-Al matrix, each block of α-Al bounded by Si crystals could undergo such diffusion in any places where fractured Si crystals are present. Thus the diffusion of the vacancies towards the interior of α-Al could happen in different places and in different directions with different quantities. Moreover, such defect transfer is constantly perturbed by local diffusion of Al atoms to accommodate the spheroidization of Si due to its shape instability. In this way, the crystal of the α-Al phase are severely perturbed and then defected, giving rise to the formation of crystal defects. As the defects are formed at high temperature during the heat treatment, recovery and even recrystallization of the α-Al crystals are activated, resulting in the formation of new and refined grains of the eutectic α-Al phase.

The heat treatment induced microstructural refinement revealed in the present work is applicable to any materials composed of two phases with large thermal expansion difference

and large Young's modulus difference, even composite materials. The results of the present work provide useful information for the design of heat treatment procedure to realize an integrated refinement and spheroidization of the hard phase and the refinement of the ductile matrix phase to achieve optimally combined strength and ductility.

Chapter 5 Neutron diffraction study of texture evolution of DS Al-12.7Si-0.04Sr alloy

5.1 Introduction

It is known that the post heat treatment can bring about recrystallization of the eutectic α-Al grains and spheroidization of the eutectic Si phase in the Sr-modified Al-12.7Si alloys. Thus it is meaningful to investigate the effect of post heat treatment on the global texture evolution of both eutectic phases. Considering the coarse grain size of eutectic α-Al phase in Sr-modified Al-Si eutectic alloys [88, 92, 95], the conventional laboratory X-ray diffraction technique is limited for texture characterization. The highly penetrating character of the neutron radiation is a pertinent alternative for such an analysis. Therefore, in this part of work, neutron diffraction technique is utilized for quantitative texture investigation. Besides, directional solidified Al-12.7Si-0.04Sr alloys that have characteristic heat flow directions were used to prepare the required specimens.

5.2 Experimental procedure

The materials used in the present work are slowly directionally solidified (DS) high-purity Al-12.7 wt. % Si-0.04 wt. % Sr alloys. The ingots were then isothermally treated for four hours at 520 °C in a salt bath furnace and cooled down to room temperature in air. The cylindrical sample was sectioned longitudinally and transversely with respect to the solidification direction for microstructural observations. Sample sections are illustrated in Fig. 5.1 and the microstructural analyses were performed in the center and the edge areas (close to the outer circle of the specimens), as indicated in the figures.

The low magnification microstructural characterization was performed at the center and edge positions of the transverse section at room temperature, using a JEOL JSM-6490 tunsgen (W) filament scanning electron microscope (SEM). The EBSD diffraction patterns were acquired at the acceleration voltage of 20 kV at a magnification of 80× with a step size of 3 μm. Moreover, the microstructural characterization of the finer eutectic Si phase was performed at high magnification (3000×) at the center and the edge positions of the cross section, utilizing a JEOL JSM-6500F field emission gun SEM equipped with an EBSD

camera and the Aztec acquisition software package (Oxford Instruments). The EBSD maps were acquired at the acceleration voltage of 20 kV, with a step size of 0.07 μm. To increase the measurement resolution for a better distinguish of α-Al from Si, the 2 × 2 binning was used. All samples for SEM observations were prepared using the standard metallographic techniques, as described in *Chapter 2*.

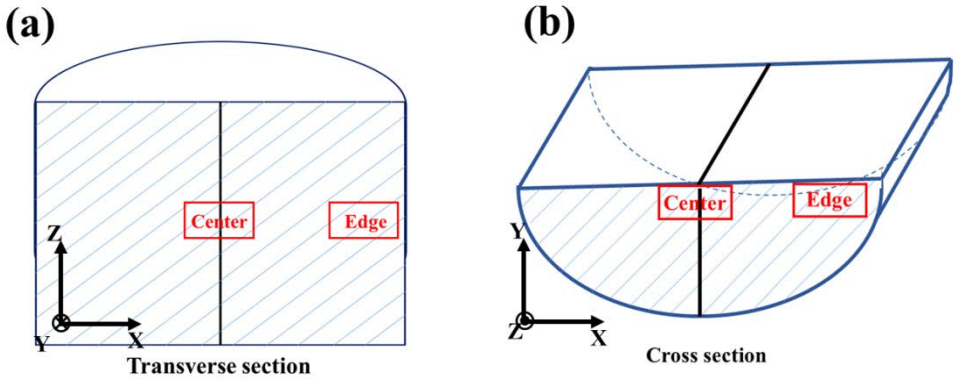

Fig. 5.1 Microstructural observation positions of the cylindrical samples on the (a) longitudinal and (b) cross sections. Z axis is parallel to the directional solidification (DS) direction.

The through-volume texture measurements were performed at the STRESS-SPEC at Heinz Maier-Leibnitz Zentrum (MLZ), Garching, Germany, using a neutron diffractometer located at a thermal beam port and comprising a highly flexible monochromator arrangement.

5.3 Results

5.3.1 Microstructural features

5.3.1.1 As-cast alloy

Figure 5.2 show the EBSD orientation micrographs of the directionally solidified (DS) Al-12.7Si-0.04Sr alloys, observed at the center (Fig. 5.2a) and at the edge sites (Fig. 5.2b) on the longitudinal section. The DS direction is parallel to the Z axis, as shown in Fig. 5.2a. In the figures, the eutectic Si phase cannot be fully revealed, as the step size is too large (3 μm). As shown in Fig. 5.2, the α-Al grains in both the center and edge positions are elongated along the DS direction. Besides, the α-Al phase displays a larger grain size in the edge position than those in the center position. The grain size of α-Al phase in the edge position

can be as large as more than 1 mm in diameter (Fig. 5.2b). The micro-texture features of α-Al phase will be detailed later.

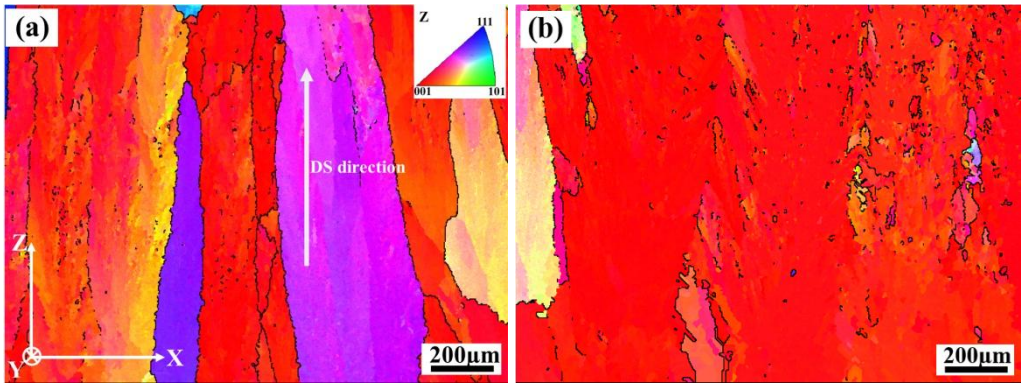

Fig. 5.2 EBSD orientation micrographs of the longitudinal section of as-cast Al-12.7Si-0.04Sr alloy at low magnification of 80×. (a) The center and (b) the edge position of the longitudinal section of the cylindrical specimen. Step size is 3 μm. Here Z axis is parallel to the directional solidification (DS) direction. The color code is shown in the upper right corner of (a).

For the eutectic Si crystals in the as-cast Al-12.7Si-0.04Sr alloy, they were observed from the cross section at high magnification of 3000×. The secondary electron (SE) images of the center and edge positions are displayed in Fig. 5.3. It is seen that the eutectic Si crystals are uniformly distributed within the eutectic α-Al matrix in both center and edge positions. However, there is a slight difference in Si density at the center and edge positions, indicating the inhomogeneous casting conditions. The sizes of eutectic Si crystals at the center position (Fig. 5.3a) are finer than those at the edge position (Fig. 5.3b). Moreover, it can be seen that the directionally solidified eutectic Si crystals display curved bar shape in the 2D SE images similar to that found in slowly crucible solidified Al-12.7Si-0.04Sr alloy (Fig. 4.1). Thus, it can be assumed that the bar-shaped Si crystals may possess a preferred extension along the heat flux direction during the solidification, either along the axial direction (Z axis) or the radial directions of the cylindrical specimens.

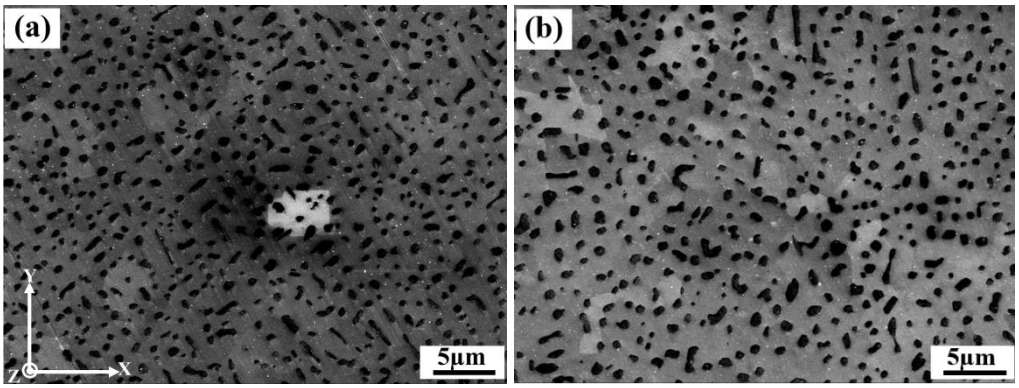

Fig. 5.3 SEM SE images of (a) center and (b) edge positions on the cross section of the as-cast Al-12.7Si-0.04Sr alloy. α-Al phase is in grey and Si in black.

5.3.1.2 Si morphology variation with heat treatment

As shown in Fig. 5.4, the EBSD orientation micrographs of eutectic Si on the cross sections in the as-cast (Fig. 5.4a) and heat treated (Fig. 5.4b) Al-12.7Si-0.04Sr alloys are presented. Eutectic Si twins are frequently observed in the crystallographic orientation maps. After heat treatment, the coarsening and spheroidization of the Si crystals are observed, as shown in Fig. 5.4b. The example Si crystals are outlined with the dashed red rectangles and magnified in the insert at the upper right corner of the corresponding EBSD maps. As seen in the as-cast alloy (Fig. 5.4a), the volumes of the twinned parts in one Si crystal is not identical. One part is much larger (denoted matrix) than the other part (denoted twin), as shown in the insert in Fig. 5.4a. However, after the heat treatment, the volumes of the twinned parts become comparable, as seen in the insert in Fig. 5.4b. Clearly, there is a growth of the twinned part with minor volume fraction together with the global coarsening of the Si crystals during the post heat treatment.

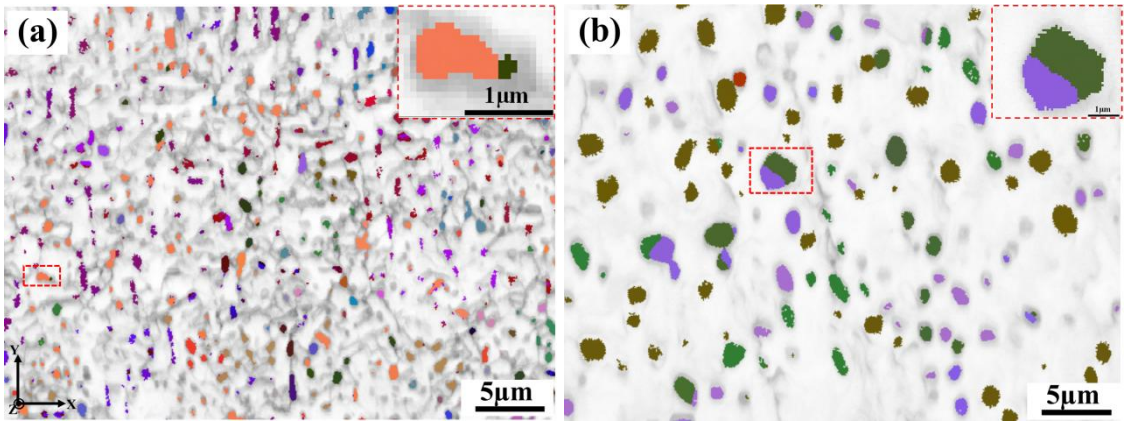

Fig. 5.4 EBSD orientation micrographs (Si: All Euler, α-Al: band contrast) on the cross section of (a) as-cast and (b) 520 ℃-4 h heat treated Al-12.7Si-0.04Sr alloy. The step size of EBSD measurements is 0.07 μm. DS direction is parallel to Z axis. The example twinned Si crystals are outlined with the red dashed rectangles in the two figures and further magnified in the inserts in the upper right corners.

5.3.2 Texture features

5.3.2.1 α-Al phase

Figure 5.5 illustrate the macroscopic texture represented by the recalculated pole figures ({1 0 0}, {1 1 0}, {1 1 1}) and the ODF $\varphi_2 = 45°$ section of α-Al phase in the as-cast Al-12.7Si-0.04Sr specimen, which is measured by neutron diffraction technique. The incident beam is in the radius direction of the cylindrical specimen. It is clearly seen that in general the α-Al phase has an apparent fiber texture with <1 0 0> // Z axis (the DS direction). However, the fiber is not continuous but rather interrupted, as shown in both the pole figures and the ODF $\varphi_2 = 45°$ section in Fig. 5.5. The orientation intensities are mainly concentrated in several locations, as displayed in the ODF $\varphi_2 = 45°$ section in Fig. 5.5b. There are three high intensity locations on the <1 0 0> // DS orientation line (marked by the Euler angles). Among them, the one at (44°, 0°, 45°) has the highest intensity (20). In fact, the non-continuous feature of the <1 0 0> // DS fiber of the α-Al is due to grain size effect. As mentioned above, α-Al matrix is in columnar shape with length and diameter in millimeter range, especially in the outer circle region the cylindrical specimen. As the sizes of the α-Al are giant, the number of α-Al columns is limited; hence not enough orientations are available to form a continuous fiber.

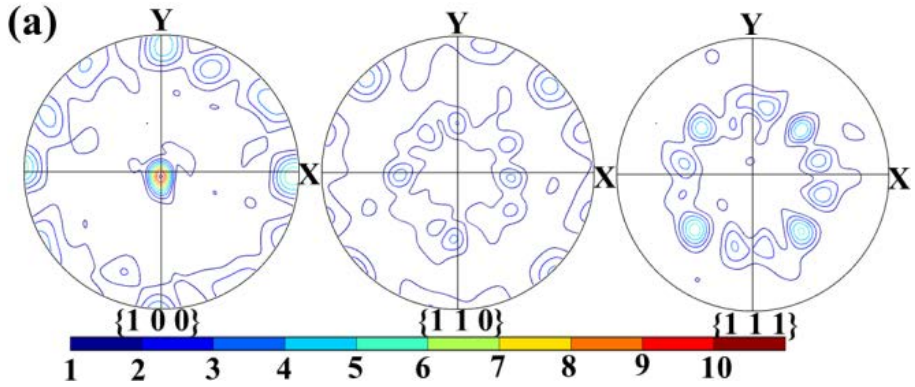

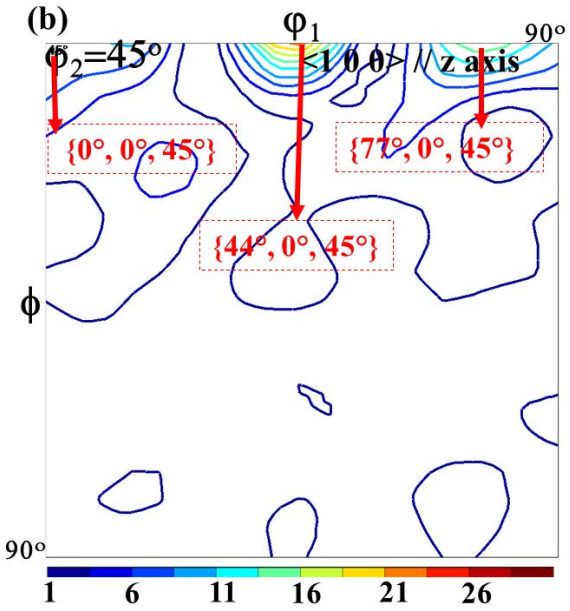

Fig. 5.5 Global texture: (a) Recalculated pole figures of {1 0 0}, {1 1 0}, {1 1 1} and (b) ODF $\varphi_2 = 45°$ section of α-Al phase in as-cast Al-12.7Si-0.04Sr alloy.

Figure 5.6 presents the micro-texture of α-Al phase in the as-cast Al-12.7Si-0.04Sr specimen obtained from the orientation data contained in the EBSD maps in Fig. 5.2. Figs. 5.6a and b display the {1 0 0} pole figures of the α-Al phase in the center position of the cylindrical specimen plotted with the scatter orientation data and the corresponding pole density plot, and Figs. 5.6c and d display those from the edge position of the cylindrical specimen. As seen from the figures, the {1 0 0} pole densities in the central area of the specimen are somewhat dispersed from the <1 0 0> fiber, whereas those in the edge area are concentrated in this fiber. Correlating the pole figures in Fig. 5.6 with the microstructures in Fig. 5.2, one can find that the dispersion of the <1 0 0> orientation from the DS direction in the central area is due to the fact that α-Al colonies with different orientations formed (Fig. 5.2a). Moreover, the sizes of α-Al columns are also relatively smaller with respect to those in the edge areas. The texture type in microscopic scale is in consistency with the macroscopic feature, but local variations can be further revealed by SEM/EBSD.

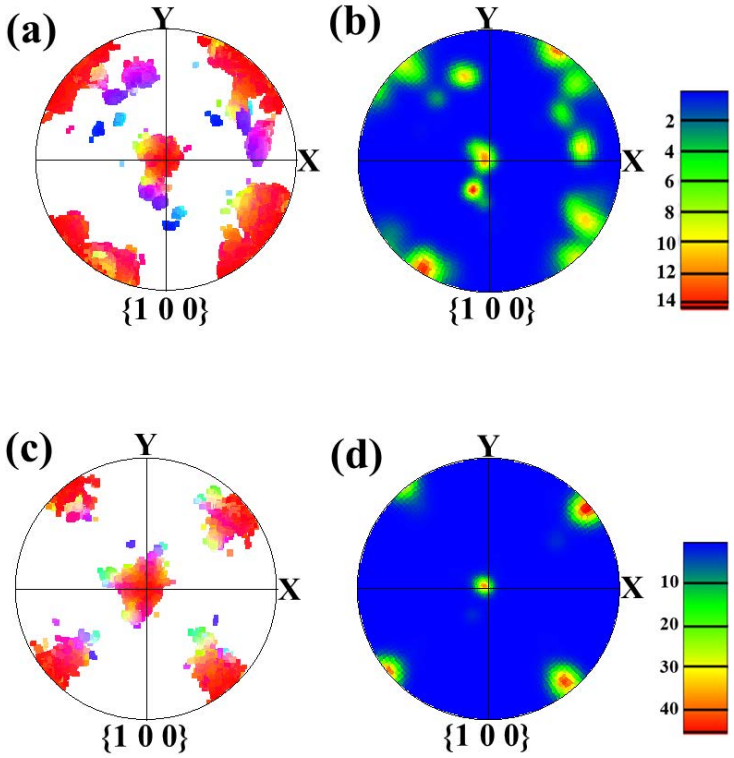

Fig. 5.6 Micro-texture: {1 0 0} pole figures of α-Al phase displayed in Fig. 5.2 in the as-cast Al-12.7Si-0.04Sr alloy from scatter EBSD data and corresponding pole density figure: (a, b) center, and (c, d) edge position. Here Z axis is parallel to DS direction.

Fig. 5.7 represents the recalculated pole figures ({1 0 0}, {1 1 0}, {1 1 1}) and ODF φ_2 = 45° section of α-Al phase after 520 ℃-4 h heat treatment. It is seen from the figures, that the fiber texture with <1 0 0> // Z axis, containing three high intensity partials, still exists, similar to that observed in the as-cast alloy (Fig. 5.5), but the intensities are lowered. The one at (57°, 0°, 45°) has highest intensity about 14 (Fig. 5.7b), weaker than the counterpart one (20) of the as-cast specimen. These results indicate that the heat treatment weakens the texture but does not change the type of the texture of the α-Al phase.

To obtain quantitative information of texture intensity evolution, the texture index [146] value of the major component was calculated by JTEX software and the results together with the texture component and the local intensity are listed in table 5.1. It is seen that after the heat treatment, the texture index value of the major component of the α-Al phase decreases from 5.72 to 3.22.

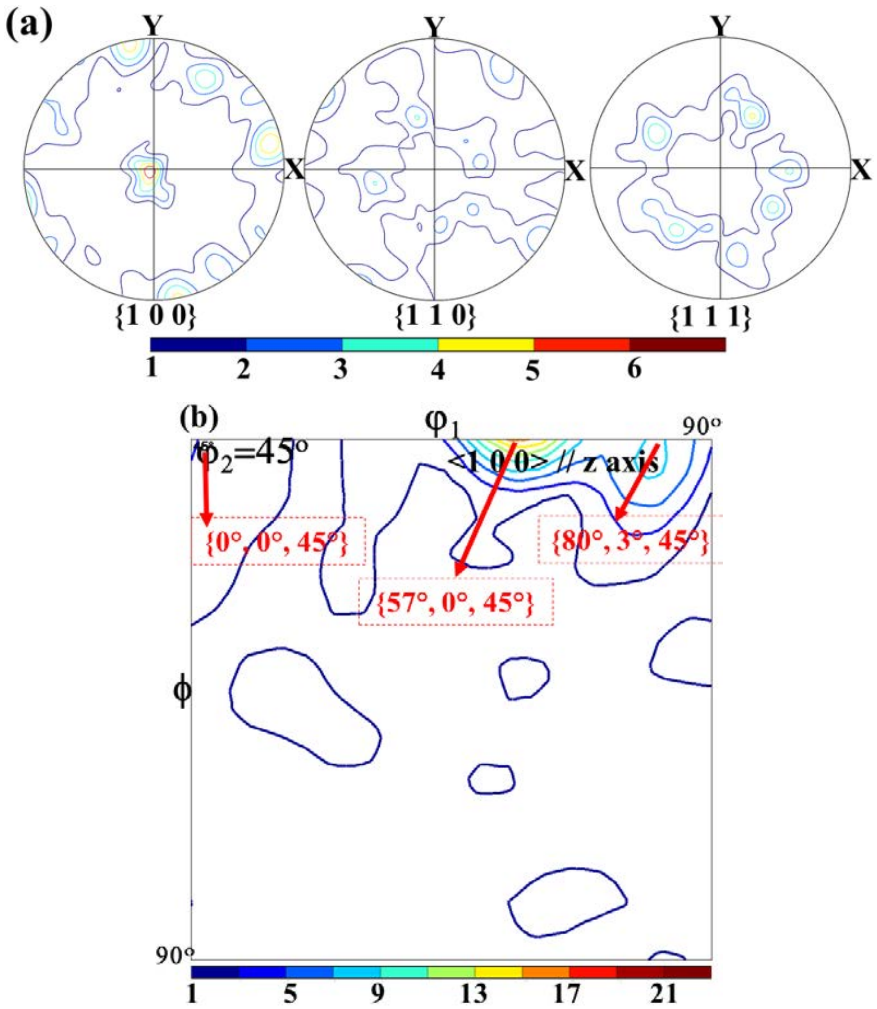

Fig. 5.7 Global texture: (a) Recalculated pole figures of {1 0 0}, {1 1 0}, {1 1 1} and (b) ODF $\varphi_2 = 45°$ section of α-Al phase after 520 ℃-4 h heat treatment.

Table 5.1 Texture intensity of α-Al phase in as-cast and heat treated Al-12.7Si-0.04Sr alloys.

Sample	Phase	Texture component	Texture local intensity (ODF)	Texture index
As-cast	Al	(44°, 0°, 45°) <1 0 0> // z axis	20	5.72
Heat treated	Al	(57°, 0°, 45°) <1 0 0> // z axis	14	3.22

5.3.2.2 Si phase

Figure 5.8 show the recalculated {100}, {110} and {111} pole figures and the ODF $\varphi_2 = 0°$ and $\varphi_2 = 45°$ sections of the eutectic Si phase in the as-cast DS Al-12.7Si-0.04Sr alloy. It is seen that globally the orientation distribution of Si crystals is nearly random without strong preference. However above the mean distribution (intensity level = 1), there are some high intensities situated at some characteristic locations, as shown in Fig. 5.8b. The components are: <0 1 4>, <0 6 7>, <0 7 6>, <0 5 1>, <1 1 8>, <1 1 3>, <2 2 1> and <1 1 0> // Z axis, the DS direction. Among them, <0 1 4>, <0 5 1> and <1 1 8> are close to <1 0 0> fiber texture; <0 6 7> and <0 7 6> are close to <1 1 0> fiber texture. In summary, the eutectic Si phase show four characteristic texture components: <1 0 0>, <1 1 0>, weak <2 2 1> and weak <1 1 3> // Z.

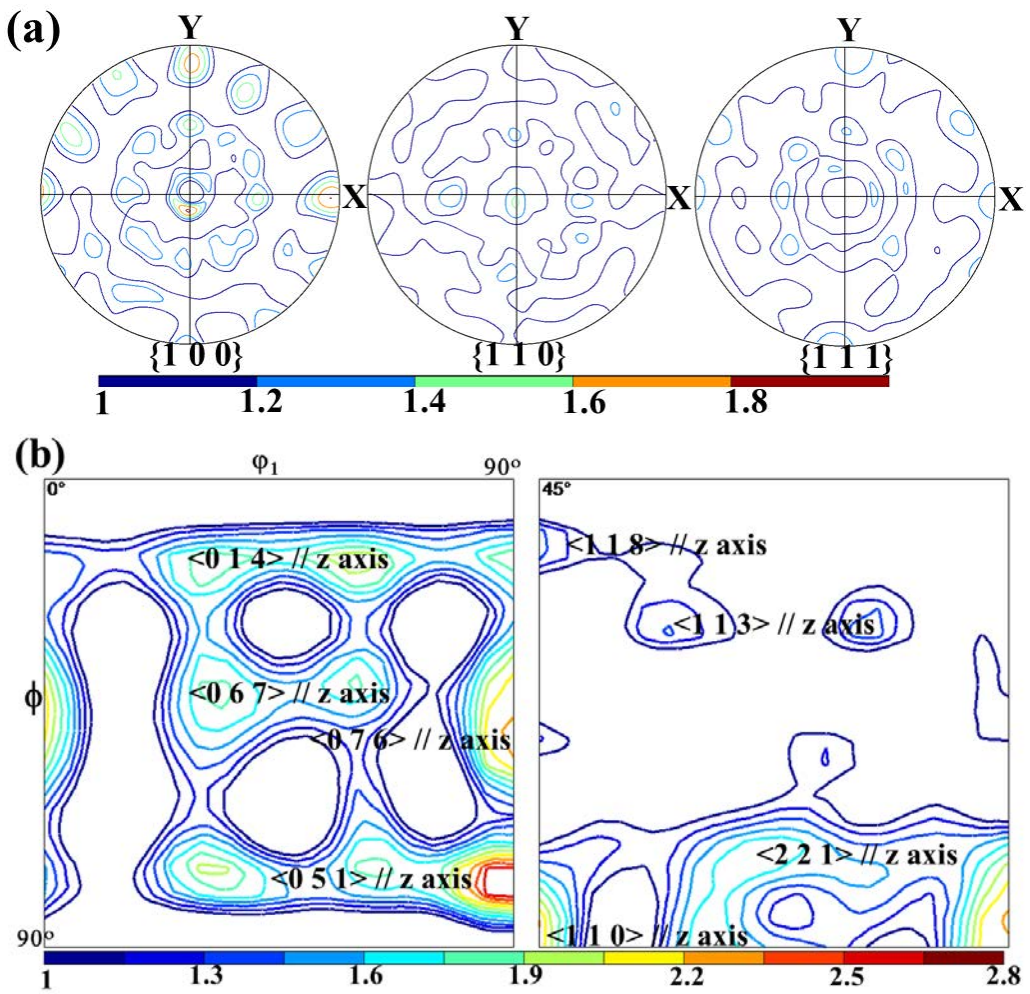

Fig. 5.8 Global texture: (a) Recalculated pole figures of {1 0 0}, {1 1 0}, {1 1 1} and (b) ODF $\varphi_2 = 0°$ and $\varphi_2 = 45°$ sections of eutectic Si phase in as-cast Al-12.7Si-0.04Sr alloy.

Figure 5.9 illustrates the micro-texture of Si phase represented by {1 0 0} and {1 1 0} pole figures in two different eutectic colonies in the as-cast Al-12.7Si-0.04Sr specimen obtained from the EBSD orientation data. As shown in Fig. 5.9a, the eutectic Si crystals in one colony display a <1 0 0> preferred orientation along the DS direction. Under such an orientation, two of the <1 1 0> directions are in the radius directions of the cylindrical specimen. This colony is located in the outer circle of the specimen. However, for the colony located at the center area of the specimen, <1 1 0> fiber is present in the Z axis, as shown in Fig. 5.9b.

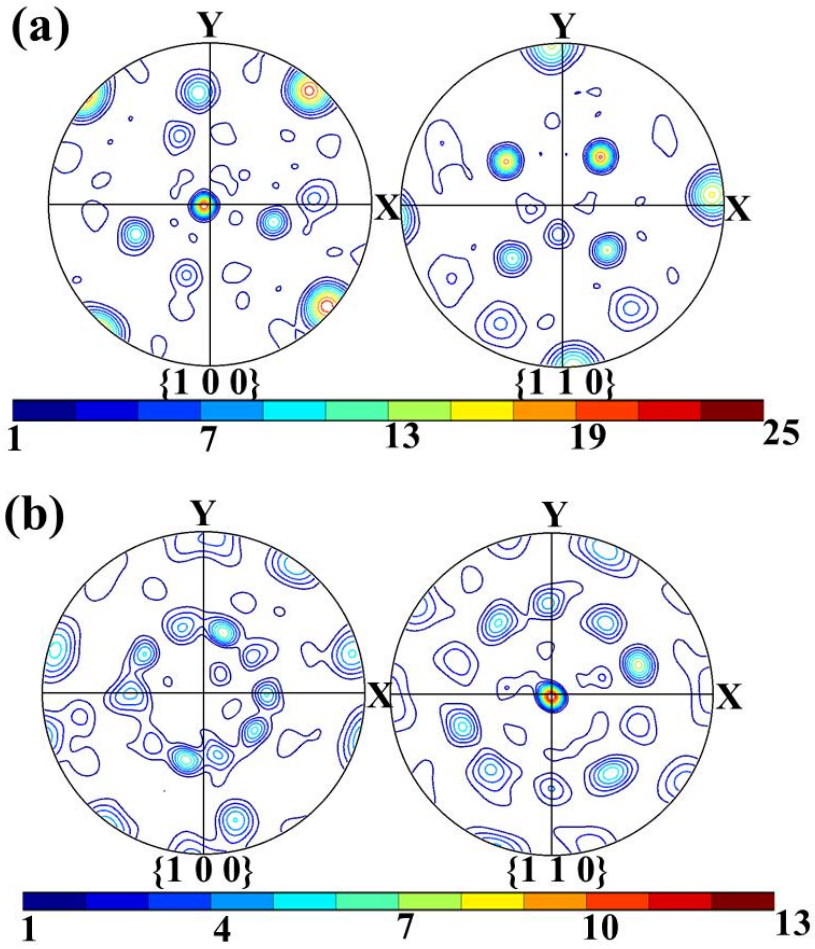

Fig. 5.9 Micro-texture of eutectic Si phase in two selected eutectic colonies in as-cast Al-12.7Si-0.04Sr alloy showing two different preferred orientations: (a) $<1\ 0\ 0>_{Si}$ // Z and (b) $<1\ 1\ 0>_{Si}$ // Z axis. Here Z axis is parallel to DS direction.

Statistical investigation of local orientation characteristics by SEM/EBSD indicates that the appearance of the multi- texture components of Si phase is attributed to the multiple twin characters; and the <1 0 0>, <1 1 0>, <2 2 1> and <1 1 3> components are twin related orientations. As an example, Fig. 5.10a shows an EBSD orientation micrograph (Si: All Euler, Al: Band Contrast) and the corresponding {1 0 0}, {1 1 0}, {1 1 1} and {2 2 1} pole figures of a multi-twinned Si crystal in as-cast DS Al-12.7Si-0.04Sr alloy. It is seen that the Si crystal contain three parts interrelated by the {1 1 1} <1 1 $\bar{2}$> twin relationship. From the pole figures, one can see that the purple Si matrix has one <1 1 0> // Z, and the red Si twin has one <1 0 0> // Z and the green Si twin has one <2 2 1> // Z. This indicates the appearance of <1 0 0>, <1 1 0> and <2 2 1> directions in the Z direction are due to the multiple twins formed in Si crystals. Fig. 5.10b shows another example of twinned Si crystal, represented with an EBSD orientation micrograph (Si: IPF, Al: Band Contrast) and the corresponding <2 2 1>, <1 1 3> and <1 1 0> pole figures. It is seen that <2 2 1> and <1 1 3> components are twin related orientations.

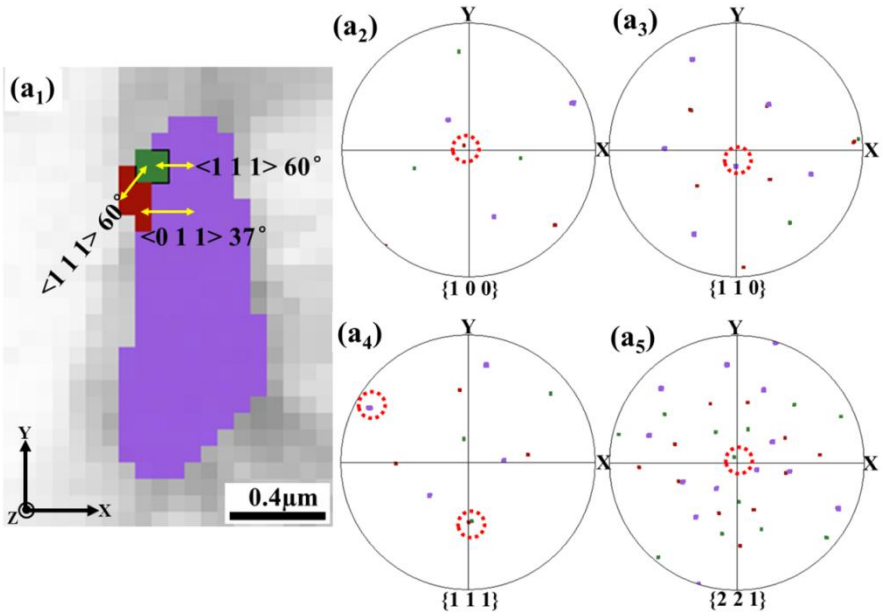

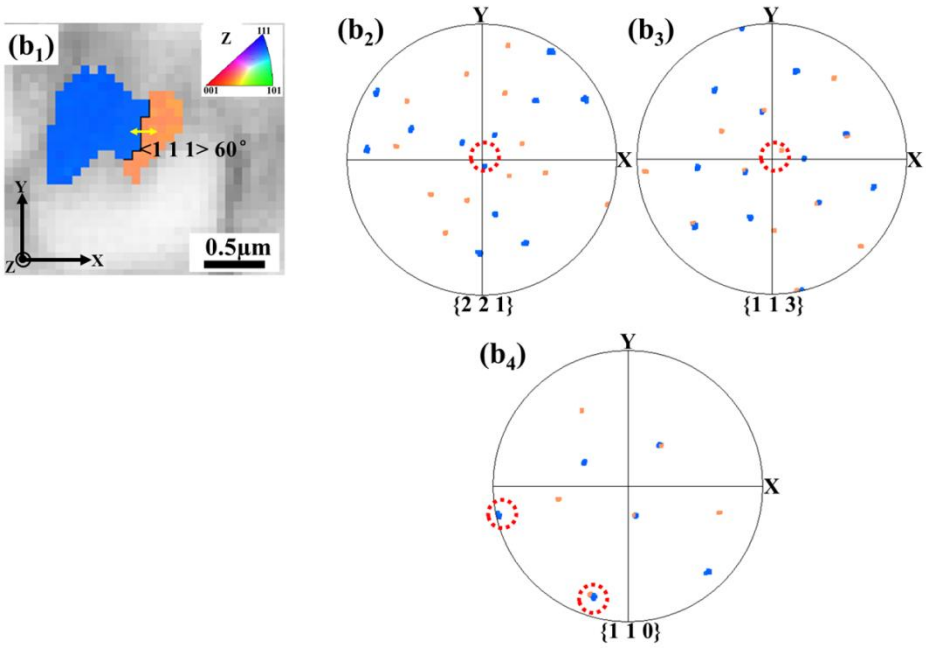

Fig. 5.10 Examples of orientation feature of twinned Si crystals. (a_1) EBSD orientation micrograph (Si: All Euler, Al: Band contrast) and the corresponding (a_2) {1 0 0}, (a_3) {1 1 0}, (a_4) {1 1 1} and (a_5) {2 2 1} pole figures (PFs) of one multiply twinned Si crystal in as-cast DS Al-12.7Si-0.04Sr alloy. Here Z axis is parallel to DS direction. The red poles of {1 1 1} PF in (a_4) indicate the twin relationship; other poles marked by red circles indicate the specific direction along Z axis (DS direction). (b_1) EBSD orientation micrograph (Si: IPF, Al: Band Contrast) and the corresponding (b_2) {2 2 1}, (b_3) {1 1 3} and (b_4) {1 1 0} pole figures (PFs) of one twinned Si crystal. The color code is shown in (b_1).

Figure 5.11 show the {1 0 0}, {1 1 0} and {1 1 1} pole figures and ODF $\varphi_2 = 0°$ and $\varphi_2 = 45°$ sections of the eutectic Si phase after the heat treatment. In general, the texture is still weak but above the mean level, four components in the previous DS direction can be observed.

The results of the eutectic Si from the as-cast Al-12.7Si-0.04Sr alloy (as shown in Fig. 5.8) and the heat treated alloy investigated by neutron diffraction (as shown in Fig. 5.11) indicate that the eutectic Si phase has a preferred <1 0 0> and <1 1 0> fibers in the DS direction, as well as two other weak components, <2 2 1> and <1 1 5> in the DS direction. Once heat treated, the Si particles are coarsened, as shown in Fig. 5.4. Simultaneously, there are changes occurring to some components. The <1 1 0> is weakened and the <2 2 1> is

strengthened. The <1 1 3> disappears and the <1 1 5> appears with relatively high intensity. It should be noted that <1 1 3> is very close to <1 1 5>, hence the <1 1 5> component may be a component originated from the <1 1 3> through crystal rotations during the heat treatment. For the quantitative information of the intensity evolution of these components, their texture indices are evaluated and the results are displayed in table 5.2.

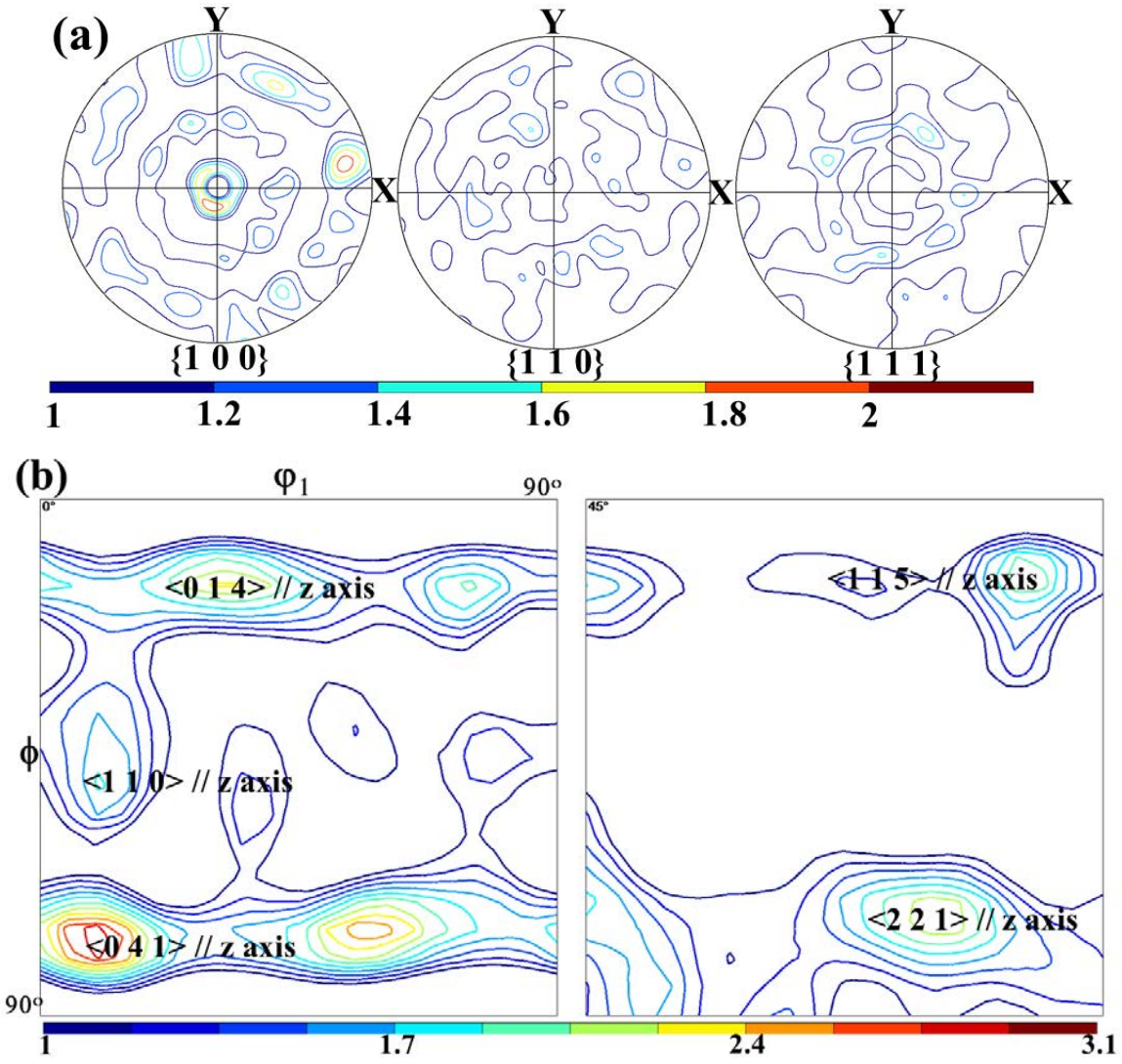

Fig. 5.11 Global texture: (a) Recalculated pole figures of {1 0 0}, {1 1 0}, {1 1 1} and (b) ODF $\varphi_2 = 0°$ and $\varphi_2 = 45°$ sections of Si phase in heat treated Al-12.7Si-0.04Sr alloy.

Table 5.2 Texture evolution of eutectic Si phase in as-cast and heat treated Al-12.7Si-0.04Sr alloys.

Sample	Phase	Texture component	Texture local intensity (ODF)	Texture index

As-cast	Si	<1 0 0> // z axis	2.5	1.2
		<1 1 0> // z axis	2.3	
		Weak <2 2 1> // z axis	1.6	
		Weak <1 1 3> // z axis	1.2	
Heat treated	Si	<1 0 0> //z axis	2.7	1.26
		<2 2 1> // z axis	2.1	
		<1 1 5> // z axis	1.9	
		Weak <1 1 0> // z axis	1.6	

5.4 Discussion

During the present directional solidification, the heat transfer is in two characteristic directions depending on the regions in the cylindrical specimen. In the central region, the heat transfer is mainly in the axial direction, *i.e.*, the DS direction, whereas in the area close to the outer circle of the cylindrical specimen (edge position), the heat transfer happens also in the radius direction that is perpendicular to the DS direction. As for the two phases, the preferred growth direction is not the same. In addition, the sizes of the microstructures of the two phases are not the same. α-Al is in millimeter and sub millimeter range and Si is in micrometer and sub micrometer range. Thus, specific texture characters are developed in the two phases during the solidification process.

5.4.1 α-Al phase

The as-cast α-Al demonstrates a characteristic texture of cast FCC metals, *i.e.,* <1 0 0> close to the heat transfer direction [147]. During solidification, the α-Al crystals grow rapidly in one of their <1 0 0> directions that is along the heat flow direction. The directional solidification ensures a constant macroscopic heat flow direction, hence the formed α-Al crystals can grow continuously and finally columnar shaped α-Al with large sizes is formed (Fig. 5.2). During the casting, if one <1 0 0> direction of the α-Al crystals is in the DS direction, their two other <1 0 0> directions are in the radius directions of the cylindrical specimen that are also heat evacuation directions, especially in the areas close to the outer circle of the specimen. Thus α-Al crystals formed in the outer cycle orient their fast growth directions to the favorable heat evacuation directions hence they can grow into giant single

crystals. In this way, a strong and discontinued <1 0 0> fiber typed texture is formed. The intensity of the fiber becomes further strengthened and concentrated for the α-Al in the areas approaching the outer circle of the cylindrical specimen. When the specimen was heat treated, the influence is mainly on the intensity of the texture components. The intensity decrease by heat treatment should be related to the recovery and recrystallization of the α-Al matrix. As revealed in *Chapter 4*, large thermal incompatibility is created during the cooling of casting and the fast heating of the heat treatment between α-Al and Si that results in the fragmentation of Si crystals and the formation of large amount of crystal defects in α-Al matrix. Recovery and recrystallization of α-Al matrix happen during the isothermal holding stage. Recrystallized domains with deviated orientation from that of the parent crystal form, resulting in the weakening of the intensity of the initial orientation. As the orientation diversification is not abrupt but progressive, the general type of initial texture is conserved.

5.4.2 Si phase

During directional solidification, the eutectic Si phase displays two main fiber texture components: <1 0 0> // Z axis and <1 1 0> // Z axis, as well as two other weak components: <2 2 1> and <1 1 3> fiber textures. During directional solidification, the appearance of the <1 0 0> and <1 1 0> fiber textures are attributed to the different heat evacuation conditions. As shown in Fig. 5.9, the Si phase in different eutectic colonies displays different fiber textures. If the crystal is oriented with its one <1 0 0> direction in the axial direction, there will be two other <1 0 0> directions in the radius directions (see Fig. 5.9a). Such Si crystals would preferentially form in the outer cycle of the cylindrical specimen, which enable the simultaneously heat transfer along the axial and radial directions. The Si-<1 1 0> preferred elongation of eutectic Si crystals in the same eutectic colony has been elucidated in *Chapter 3*. Thus it can be concluded that the <1 1 0> preferred growth direction is along the heat transfer direction. However, when the Si crystals tend to grow rapidly along the <1 1 0> directions, there is only one main heat flow direction which is along the axial direction (DS direction). Therefore, the <1 1 0> // Z orientated Si crystals are mainly formed in the central regions of the cylindrical specimen.

The other <1 1 3> // Z and <2 2 1> // Z fiber texture components are produced by the twinned parts of the <1 0 0> oriented and the <1 1 0> oriented Si crystals. As these directions are not the favorable extension directions of Si crystals, the twinned part cannot grow to large size, thus the intensities of these two components are relatively weak.

When the specimen was heat treated, as revealed by the microstructure observation, the twinned parts with minor volume fraction obviously grow. Due to such microstructural change, the volume of the twinned parts increase at the expense of the matrix part, thus the intensities of <2 2 1> and <1 1 5> increase, whereas that of the <1 1 0> component decreases. As revealed in *Chapter 4*, during the heat treatment, the Si crystals fragmentize and spheroidize. The fragmentation is accompanied by the rotation of the broken parts. This may contribute to the appearance of <1 1 5> and the disappearance of <1 1 3> component and the local intensification of the <1 1 5> component.

5.5 Summary

An eutectic Al-12.7Si alloy with 400 ppm Sr addition was slowly directionally solidified and heat treated at 520 ℃ for four hours in this part of work. The microstructural features and micro-textures were analyzed by SEM/EBSD and the macro-textures were analyzed by neutron diffraction.

In the as-cast Al-12.7Si-0.04Sr alloy, the α-Al phase displays a strong <1 0 0> fiber texture in the favorable heat evacuation direction (DS). Due to the large columnar shape of the α-Al phase, the fiber texture is not continuous. Giant <1 0 0> // Z α-Al grains are mainly formed in the outer circle region of the cylindrical specimen due to the favorable heat evacuation directions available for the three <1 0 0> directions (one in DS direction and two other in radius directions). After heat treatment, the texture intensity of the α-Al phase decreases due to the recovery and recrystallization, but the texture type does not change.

For the eutectic Si phase in the as-cast alloy, the orientations are characterized by a weak texture with the intensities of several specific components above the mean level. Two main fiber texture components, <1 0 0> // Z axis and <1 1 0> // Z axis, are accompanied by two weak components, <2 2 1> // Z and <1 1 3> // Z. The <1 1 0> // Z component is from the Si crystals located in the center region of the cylindrical specimen, as the available heat transfer direction (DS) is in the <1 1 0> favorable direction for Si growth and <1 0 0> // Z component is from the crystals located mainly in the outer circle of the cylindrical specimen where two of the <1 1 0> directions can be oriented to the favorable heat transfer directions (radius directions). The <2 2 1> // Z and <1 1 3> // Z components are from multiple twins of the <1 1 0> // Z and <1 0 0> // Z crystals. The weak intensities of these two components are related to their minor volume fraction. Once heat treated, the twinned parts with minor volume fractions

enlarge at the expense of their twin related matrix, thus the <1 1 0> // Z is weakened accompanied by the intensification of the components from the twins. The disappearance of the <1 1 3> component and the appearance of the <1 1 5> component is due to crystallographic rotation of Si crystals during their fragmentation.

Chapter 6 Conclusion and perspective

6.1 Conclusion

From the above studies, following conclusions can be drawn.

(1) Twin controlled growth of eutectic Si crystals in unmodified and Sr-modified eutectic Al-Si alloys

For the unmodified eutectic Si crystals, they are in general in long plate shape with multiple single-orientation twin variants along the length direction. The preferred extension direction is <1 1 0>, other than the <1 1 2> directions assumed by the TPRE model. The <1 1 0> extension is realized by paired <1 1 2> zigzag growth on parallel twinning planes, leading to alternative disappearance and creation of 141° re-entrants. This growth manner ensures Si crystals to expose only their low-energy {1 1 1} planes to the melt. This is advantageous in terms of liquid/solid interfacial energy, especially for slow solidification with low undercooling. Prior to the eutectic α-Al formation, three Si re-entrant grooves associated with one twinning plane are all active, hence the eutectic Si growth is planar isotropic. When the eutectic α-Al forms preferentially at on-growing re-entrant grooves with enriched Al concentration, the number of re-entrants becomes reduced. Thus, the eutectic Si growth changes from planar isotropic to anisotropic and the equilateral plates evolve to long plates. The reduction of re-entrant grooves during the growth process accounts for the shape irregularity of eutectic Si plates, *i.e.* the occasional changes in width and thickness over the plate length.

As for the Sr-modified eutectic Si crystals, multi-orientation twin variants, as well as curved or stepped twin boundaries, are formed. The changes in eutectic Si morphology were demonstrated to be mainly associated with the growth process, as a result of the restricted TPRE growth and the IIT growth. More specifically, the restricted TPRE growth is realized by deactivating initial twins and forming new twins with the same orientation, which enhances lateral growth. The IIT growth is realized by forming new twins with different orientations, thus changing the initial anisotropic growth to isotropic growth. As a whole, the resultant eutectic Si crystals are significantly refined with Sr addition.

(2) The further refinement of eutectics by heat treatment

After post heat treatment, large amount of crystal defects in α-Al without any macroscopic deformation during the heat treatments was experimentally revealed. This process was found to occur in connection with the fragmentation and spheroidization of eutectic Si crystals that are in coral shape composed of sharp corners and surface ridges or edges. On the experimental basis, the refinement mechanisms of the α-Al phase and the Si crystals were worked out.

Subjected to rapid heating during the heat treatment by which large temperature gradient can be created and sweep through the whole sample volume from the surface to the center, Si crystals crack at the fragile places, like sharp corners for example, due to the limited accommodating capacity of the Si crystals to the giant thermal expansion of the surrounding α-Al matrix. The fractures generate a kind of "capillarity" force that attracts the Al atoms to fill the gap produced by the fracture. Due to the substitutional feature of Al diffusion, the migration of vacancies toward the interior of the α-Al is induced when Al moves to the gaps, thus the voids of the Si fracture are transferred to the α-Al. Such defect transfer is constantly perturbed by local diffusion of Al atoms to accommodate the spheroidization of Si due to its shape instability. In this way, the α-Al phase is severely perturbed and then defected, giving rise to the formation of crystal defects. As the defects are formed at high temperature during the heat treatment, recovery and even recrystallization of the α-Al crystals are activated, resulting in the refinement of the α-Al phase.

(3) The global texture investigation

Neutron diffraction was utilized to investigate the global texture of both α-Al phase and Si phase in the directionally solidified and the heat treated (520 ℃-4 h) Al-12.7Si-0.04Sr alloys.

In the as-cast Al-12.7Si-0.04Sr alloy, the α-Al phase displays a strong <1 0 0> fiber texture in the directional solidification (DS) direction, as the preferential growth direction of FCC metal is <1 0 0>. Due to the large columnar shape of the α-Al phase, the fiber texture is not continuous. The α-Al phase displays a larger colony size in the outer circle than that in the central region of the cylindrical specimen. This is due to the favorable heat evaluation in this region. The α-Al phase with one <1 0 0> direction parallel to the DS direction can have two other <1 0 0> directions in the radial directions of the cylindrical specimen that are also the heat evacuation directions. After the heat treatment, the texture intensity of α-Al phase

decreases resulting from the recovery and recrystallization occurring inside the α-Al matrix, but the <1 0 0> fiber type keeps unchanged.

During DS, the eutectic Si phase displays two main fiber texture components above the mean orientation distribution: <1 0 0> and <1 1 0>, as well as other two weak components, <2 2 1> and <1 1 3>, in the DS direction. This is due to the fact that Si crystals tend to orient their <1 1 0> direction to the heat transfer direction. Most of the <1 0 0> oriented Si crystals are in the outer circle region of the cylindrical specimen where the two of their <1 1 0> directions are in the radius directions, the heat evacuation directions and the <1 1 0> orientated Si crystals are in the central region with their one <1 1 0> direction in the DS direction. The two weak <2 2 1> and <1 1 3> fiber components are from the twinned part of the <1 0 0> and the <1 1 0> oriented Si. The weak intensities of the <2 2 1> and the <1 1 3> components are related to their minor volume fraction.

Once heat treated, the twinned parts with minor volume fractions enlarge at the expense of their twin related matrix, thus the <1 1 0> // Z is weakened accompanied by the intensification of the components from the twins. The disappearance of the <1 1 3> component and the appearance of the <1 1 5> component is due to crystallographic rotation of Si crystals during their fragmentations at elevated temperature.

6.2 Perspective

With the results obtained in the present work, we have clarified the growth mechanisms of Si crystals and the influence of post heat treatment on microstructure refinement, which opens some new perspectives for practical application oriented studies. In this PhD work, it is reported that post heat treatment can refine both the eutectic α-Al matrix through recrystallization by introducing crystal defects and the eutectic Si crystals by fragmentations. Thus, further investigation on optimization of heat treatment parameters to achieve recrystallization of the eutectic α-Al phase and further refinement of the Sr-modified eutectic Si particles, especially for the cast components, is meaningful for providing guidance for practical industrial applications.

To further improve the mechanical properties, *i.e.* wear resistance and strength, the addition of alloying elements is quite necessary to achieve precipitation strengthening of α-Al matrix. Besides, post hot deformation can be applied to the Sr-modified eutectic Al-Si alloys.

This can be expected to further refine eutectic Si crystals and provide larger driving force for the recrystallization of eutectic α-Al phase.

Publication list

1. **X. Liu**, B. Beausir, Y. Zhang, W. Gan, H. Yuan, F. Yu, C. Esling, X. Zhao, L. Zuo. Heat treatment induced defect formation in α-Al matrix in Sr-modified eutectic Al-Si alloy, 2016. (To be submitted to the **Acta Materiallia** magazine)

2. **X. Liu**, Y. Zhang, B. Beausir, W. Gan, F. Liu, F. Yu, C. Esling, X. Zhao, L. Zuo. Neutron diffraction study of texture evolution of DS Al-12.7Si-0.04Sr alloys, 2016. (Under revision)

3. **X. Liu**, Y. Zhang, B. Beausir, F. Liu, C. Esling, F. Yu, X. Zhao, L. Zuo. Twin-controlled growth of eutectic Si in unmodified and Sr-modified Al-12.7%Si alloys investigated by SEM/EBSD, **Acta Mater.** 97 (2015) 338-347.

4. **X. Liu,** Y. Zhang, B. Beausir, F. Liu, C. Esling, F. Yu, X. Zhao, L. Zuo. Growth characteristics of eutectic silicon in unmodified and Sr-modified Al-12.7%Si alloys investigated by SEM/EBSD, **Texture and Anisotropy European days in Metz**, 2015.03, Metz, France. (**Oral presentation**)

References

[1] H. Ye. An overview of the development of Al-Si-alloy based material for engine applications, J. Mater. Eng. Perfom. 12 (2003) 288-297.

[2] S. Lampman, T. Zorc, S. Henry, J. Daquila, A. Ronke. Properties and selection: nonferrous alloys and special-purpose materials, ASM Handbook 2 (1990) 592-633.

[3] M. Ebisawa, T. Hara, T. Hayashi, H. Ushio. Production process of metal matrix composite (MMC) engine block. SAE Tech. Paper 910835 (1991).

[4] J.R. Davis. Metals handbook desk edition, second Ed., ASM international, 1998.

[5] M. Timpel, N. Wanderka, R. Schlesiger, T. Yamamoto, N. Lazarev, D. Isheim, G. Schmitz, S. Matsumura, J. Banhart. The role of strontium in modifying aluminium-silicon alloys, Acta Mater. 60 (2012) 3920-3928.

[6] L. Zuo, F. Yu. Recent development on wrought Al-Si alloys based on direct chill casting, Rare Met. 28 (2009) 78-83.

[7] L. Zuo, F. Yu. DC casting, deformation and strengthening of Al-Si alloys, Mater. Sci. Forum 706-709 (2012) 186-193.

[8] S. Hegde, K.N. Prabhu. Modification of eutectic silicon in Al-Si alloys, J. Mater. Sci. 43 (2008) 3009-3027.

[9] S. Prasad, R. Asthana. Aluminum metal-matrix composites for automotive applications: tribological considerations, Tribol. Lett. 17 (2004) 445-453.

[10] F.J. Kneisler, D.A. Martens, R.W. Midgley. The Vega 2300 Engine. SAE Tech. Paper 710147 (1971).

[11] J.L. Murray, A.J. McAlister. The Al-Si (Aluminum-Silicon) system, Bull. Alloy Phase Diagr. 5 (1984) 74-84.

[12] K.F. Kobayashi, L.M. Hogan. The crystal growth of silicon in Al-Si alloys, J. Mater. Sci. 20 (1985) 1961-1975.

[13] S.-Z. Lu, A. Hellawell. The mechanism of silicon modification in aluminum-silicon alloys: Impurity induced twinning, Metall. Trans. A 18 (1987) 1721-1733.

[14] M. Shamsuzzoha, L.M. Hogan, D.J. Smith, P.A. Deymier. A transimission and high-resolution electron microscope study of cozonally twinned growth of eutectic silicon in unmodified Al-Si alloys, J. Cryst. Growth 112 (1991) 635-643.

[15] S.A. Dayeh, J. Wang, N. Li, J.Y. Huang, A.V. Gin, S.T. Picraux. Growth, defect formation, and morphology control of germanium-silicon semiconductor nanowire heterostructures, Nano Lett. 11 (2011) 4200-4206.

[16] M. Shamsuzzoha, L.M. Hogan. The role of non-cozonal twinning in the growth of fibrous silicon in strontium-modified Al-Si eutectic, J. Mater. Sci. 24 (1989) 2849-2859.

[17] X. Liu, Y. Zhang, B. Beausir, F. Liu, C. Esling, F. Yu, X. Zhao, L. Zuo. Twin-controlled growth of eutectic Si in unmodified and Sr-modified Al–12.7%Si alloys investigated by SEM/EBSD, Acta Mater. 97 (2015) 338-347.

[18] A.K. Dahle, K. Nogita, S. McDonald, J. Zindel, L. Hogan. Eutectic nucleation and growth in hypoeutectic Al-Si alloys at different strontium levels, Metall. Mater. Trans. A 32 (2001) 949-960.

[19] A.K. Dahle, K. Nogita, S.D. McDonald, C. Dinnis, L. Lu. Eutectic modification and microstructure development in Al–Si Alloys, Mater. Sci. Eng. A 413–414 (2005) 243-248.

[20] J. Eiken, M. Apel, S.-M. Liang, R. Schmid-Fetzer. Impact of P and Sr on solidification sequence and morphology of hypoeutectic Al–Si alloys: Combined thermodynamic computation and phase-field simulation, Acta Mater. 98 (2015) 152-163.

[21] Y. Cho, A.K. Dahle. Authors' Reply to Discussion of "The Structure of Al-Si Alloys", Metall. Mater. Trans. A 40 (2009) 1011-1012.

[22] M. Zarif, B. Mckay, P. Schumacher. Study of heterogeneous nucleation of eutectic Si in high-purity Al-Si alloys with Sr addition, Metall. Mater. Trans. A 42 (2011) 1684-1691.

[23] S.-M. Liang, R. Schmid-Fetzer. Phosphorus in Al-Si cast alloys: Thermodynamic prediction of the AlP and eutectic (Si) solidification sequence validated by microstructure and nucleation undercooling data, Acta Mater. 72 (2014) 41-56.

[24] T. Ludwig, P. Schaffer, L. Arnberg. Influence of Phosphorus on the Nucleation of Eutectic Silicon in Al-Si Alloys, Metall. Mater. Trans. A 44 (2013) 5796-5805.

[25] C.R. Ho, B. Cantor. Heterogeneous nucleation of solidification of Si in Al-Si and Al-Si-P alloys, Acta Metall. Mater. 43 (1995) 3231-3246.

[26] Y. Cho, H.-C. Lee, K. Oh, A. Dahle. Effect of Strontium and Phosphorus on Eutectic Al-Si Nucleation and Formation of β-Al_5FeSi in Hypoeutectic Al-Si Foundry Alloys, Metall. Mater. Trans. A 39 (2008) 2435-2448.

[27] P.B. Crosley, L. Mondolfo. The modification of aluminum-silicon alloys, AFS Trans. 74 (1966) 53-64.

[28] B. Yang, D. Stefanescu, J. Leon-Torres. Modeling of microstructural evolution with tracking of equiaxed grain movement for multicomponent Al-Si alloy, Metall. Mater. Trans. A 32 (2001) 3065-3076.

[29] W. Khalifa, F. Samuel, J. Gruzleski. Iron intermetallic phases in the Al corner of the Al-Si-Fe system, Metall. Mater. Trans. A 34 (2003) 807-825.

[30] S. Shankar, Y.W. Riddle, M.M. Makhlouf. Nucleation mechanism of the eutectic phases in aluminum-silicon hypoeutectic alloys, Acta Mater. 52 (2004) 4447-4460.

[31] Y. Zhang, H. Zheng, Y. Liu, L. Shi, R. Xu, X. Tian. Cluster-assisted nucleation of silicon phase in hypoeutectic Al–Si alloy with further inoculation, Acta Mater. 70 (2014) 162-173.

[32] K. Nogita, S.D. McDonald, K. Tsujimoto, K. Yasuda, A.K. Dahle. Aluminium phosphide as a eutectic grain nucleus in hypoeutectic Al-Si alloys, J. Electron Microsc. 53 (2004) 361-369.

[33] W.B. Pearson. A Handbook of Lattice Spacings and Structures of Metals and Alloys, Pergamon Press, London, 1958.

[34] D. Hamilton, R. Seidensticker. Propagation mechanism of germanium dendrites, J. Appl. Phys. 31 (1960) 1165-1168.

[35] S.-Z. Lu, A. Hellawell. Growth mechanisms of silicon in Al-Si alloys, J. Cryst. Growth 73 (1985) 316-328.

[36] N. Cabrera, D. Vermilyea, R. Doremus, B. Roberts, D. Turnbull. Growth and perfection of crystals, Wiley, New York (1958) 393.

[37] A. Hellawell. The growth and structure of eutectics with silicon and germanium, Prog. Mater. Sci. 15 (1970) 3-78.

[38] K. Kobayashi, P. Shingu, R. Ozaki. Crystallographic study of the eutectic microstructure in Al-Si system. Proc. of Sheffield Inter. Conf. on Solidification Casting, Metal Society, London (1979) 101-105.

[39] M. Shamsuzzoha, L. Hogan. The crystal morphology of fibrous silicon in strontium-modified Al-Si eutectic, Philos. Mag. A 54 (1986) 459-477.

[40] J.H. Li, M. Albu, F. Hofer, P. Schumacher. Solute adsorption and entrapment during eutectic Si growth in A-Si-based alloys, Acta Mater. 83 (2015) 187-202.

[41] H.A.H. Steent, A. Hellawell. Structure and properties of aluminium-silicon eutectic alloys, Acta Metall. 20 (1972) 363-370.

[42] M. Day, A. Hellawell. The microstructure and crystallography of aluminium-silicon eutectic alloys, Proc. R. Soc. London A 305 (1968) 473-491.

[43] M. Shamsuzzoha, L.M. Hogan. Crystal morphology of unmodified aluminium-silicon eutectic microstructures, J. Cryst. Growth 76 (1986) 429-439.

[44] A.K. Dahle, K. Nogita S.D. McDonald, and L.M. Hogan. Eutectic nucleation and growth in hypoeutectic Al-Si alloys at different strontium levels, Metall. Mater. Trans. A 32A (2001) 949-960.

[45] J. Corrochano, J.C. Walker, M. Lieblich, J. Ibáñez, W.M. Rainforth. Dry sliding wear behaviour of powder metallurgy Al–Mg–Si alloy-$MoSi_2$ composites and the relationship with the microstructure, Wear 270 (2011) 658-665.

[46] D. Casellas, A. Beltran, J.M. Prado, A. Larson, A. Romero. Microstructural effects on the dry wear resistance of powder metallurgy Al–Si alloys, Wear 257 (2004) 730-739.

[47] J. Shen, Z. Xie, Y. Gao, B. Zhou, Q. Li, Z. Su, H. Le. Microstructure characteristics of a hypereutectic Al-Si alloy manufactured by rapid solidification/powder metallurgy process, J. Mater. Sci. Lett. 20 (2001) 1513-1515.

[48] S.C. Lim, M. Gupta, Y.F. Leng, E.J. Lavernia. Wear of a spray-deposited hypereutectic aluminium-silicon alloy, J. Mater. Process Tech. 63 (1997) 865-870.

[49] V.C. Srivastava, R.K. Mandal, S.N. Ojha. Microstructure and mechanical properties of Al–Si alloys produced by spray forming process, Mater. Sci. Eng. A 304–306 (2001) 555-558.

[50] F. Yu, D.S. Dwarakadasa, S. Ranganathan. Microstructure and mechanical properties of spray-formed Al–Si–Pb alloys, J. Mater. Process Tech. 137 (2003) 164-167.

[51] F. Wang, H. Liu, Y. Ma, Y. Jin. Effect of Si content on the dry sliding wear properties of spray-deposited Al–Si alloy, Mater. Design 25 (2004) 163-166.

[52] F. Wang, Y. Ma, Z. Zhang, X. Cui, Y. Jin. A comparison of the sliding wear behavior of a hypereutectic Al–Si alloy prepared by spray-deposition and conventional casting methods, Wear 256 (2004) 342-345.

[53] F. Wang, Z. Zhang, Y. Ma, Y. Jin. Effect of Fe and Mn additions on microstructure and wear properties of spray-deposited Al–20Si alloy, Mater. Lett. 58 (2004) 2442-2446.

[54] A.K. Srivastava, V.C. Srivastava, A. Gloter, S.N. Ojha. Microstructural features induced by spray processing and hot extrusion of an Al–18% Si–5% Fe–1.5% Cu alloy, Acta Mater. 54 (2006) 1741-1748.

[55] C. Cui, A. Schulz, J. Epp, H.W. Zoch. Deformation behavior of spray-formed hypereutectic Al–Si alloys, J. Mater. Sci. 45 (2010) 2798-2807.

[56] S.C. Yoon, S.-J. Hong, S.I. Hong, H.S. Kim. Mechanical properties of equal channel angular pressed powder extrudates of a rapidly solidified hypereutectic Al-20 wt% Si alloy, Mater. Sci. Eng. A 449-451 (2007) 966-970.

[57] K. He, F. Yu, D. Zhao, L. Zuo. Characterization of precipitates in a hot-deformed hypereutectic Al–Si alloy, J. Alloys Compd. 539 (2012) 74-81.

[58] K. He, F. Yu, D. Zhao, L. Zuo. Microstructural evolution of direct chill cast Al-15.5Si-4Cu-1Mg-1Ni-0.5 Cr alloy during solution treatment, Res. Dev. 8 (2011) 264-268.

[59] K. He, F. Yu, D. Zhao, L. Zuo. Effect of phosphorus modification on the microstructure and mechanical properties of DC cast Al-17.5Si-4.5Cu-1Zn-0.7Mg-0.5Ni alloy, T. Indian I. Metals 62 (2009) 367-371.

[60] F. Yu, J. Pei, K. He, D. Zhao, L. Zuo. Solidification microstructure and temperature field during direct chill casting of Al-16Si alloy, T. Indian I. Metals 62 (2009) 347-351.

[61] F. Yu, Y. Li, J. Cui. Banded structure in the semi-continuously DC cast Al-15Si alloy, T. Indian I. Metals 58 (2005) 591-696.

[62] G. Sigworth. The Modification of Al-Si Casting Alloys: Important Practical and Theoretical Aspects, Int. J. Metalcast. 2 (2008) 19-41.

[63] L. Mondolfo. Nucleation in eutectic alloys, J. Aust. I. Met. 10 (1965) 169-177.

[64] M. Marzouk, M. Jain, S. Shankar. Effect of Sr-modification on the bendability of cast aluminum alloy A356 using digital image correlation method, Mater. Sci. Eng. A 598 (2014) 277-287.

[65] A. Pacz. Alloy 1 (1921) 387,900.

[66] Z. Jeffries. Aluminum-Silicon Alloys, J. Chem. Met. Eng 26 (1922) 750-754.

[67] J. Edwards, R. Archer. The New Aluminum-Silicon Alloys, Chem. Metall. Eng. 31 (1924) 504-508.

[68] R.S. Archer, L.W. Kempf. Modification and properties of sand-cast aluminum-silicon alloys, Trans. Am. Inst. Min. Metall. Eng. 73 (1926) 581-621.

[69] A. Gwyer, H. Phillips. The Constitution and Structure of the Commercial Aluminium-Silicon Alloys, J. Inst. Metals 36 (1926) 283-324.

[70] H.V.G. M.M. Makhlouf. The aluminum–silicon eutectic reaction: mechanisms and crystallography, J. Light Met. 1 (2001) 199-218.

[71] D.C. Jenkinson, L.M. Hogan. The modification of aluminium-silicon alloys with strontium, J. Cryst. Growth 28 (1975) 171-187.

[72] A. Knuutinen, K. Nogita, S.D. McDonald, A.K. Dahle. Modification of Al-Si alloys with Ba, Ca, Y and Yb, J. Light Met. 1 (2001) 229-240.

[73] J.H. Li, P. Schumacher. Effect of Y addition and cooling rate on refinement of eutectic Si in Al-5 wt%Si alloys, Int. J. Cast. Metals Res. 25 (2012) 347-357.

[74] J.H. Li, S. Suetsugu, Y. Tsunekawa, P. Schumacher. Refinement of Eutectic Si Phase in Al-5Si Alloys with Yb Additions, Metall. Mater. Trans. A 44A (2013) 669-681.

[75] K. Nogita, A.K. Dahle. Effects of boron on eutectic modification of hypoeutectic Al–Si alloys, Scr. Mater. 48 (2003) 307-313.

[76] Q. Liu. Effect of Antimony on the Growth Kinetics of High Purity Al-Si Alloys, Scr. Mater. 38 (1998) 1083-1089.

[77] K. Nogita, Stuart D. McDonald, A.K. Dahle. Eutectic modification of Al-Si alloys with rare earth metals, Mater. Trans. 45 (2004) 323-326.

[78] J. Li, X. Wang, T. Ludwig, Y. Tsunekawa, L. Arnberg, J. Jiang, P. Schumacher. Modification of eutectic Si in Al–Si alloys with Eu addition, Acta Mater. 84 (2015) 153-163.

[79] K. Nogita, H. Yasuda, M. Yoshiya, S.D. McDonald, K. Uesugi, A. Takeuchi, Y. Suzuki. The role of trace element segregation in the eutectic modification of hypoeutectic Al-Si alloys, J. Alloys Compd. 489 (2010) 415-420.

[80] L. Lu, K. Nogita, A.K. Dahle. Combining Sr and Na additions in hypoeutectic Al-Si foundry alloys, Mater. Sci. Eng. A 399 (2005) 244-253.

[81] P. Hess, E. Blackmun. Strontium as a modifying agent for hypoeutectic aluminum-silicon alloys, AFS Trans. 83 (1975).

[82] C. Kim, R. Heine. Fundamentals of Modification in the Aluminum-Silicon System, J. Inst. Metals 92 (1963) 367-376.

[83] M.F.X. Gigliotti, G.A. Colligan. The effects of sodium on the growth velocity and growth morphology of silicon in Al-Si alloys, Metall. Trans. 3 (1972) 933-940.

[84] J. Bell, W. Winegard. Interconnexion of Silicon in Modified Aluminium-Silicon Eutectic, Nature 208 (1965) 177.

[85] K. Nogita, J. Drennan, A.K. Dahle. Evaluation of silicon twinning in hypo-eutectic Al-Si alloys, Mater. Trans. 44 (2003) 625-628.

[86] G. Heiberg, L. Arnberg. Investigation of the microstructure of the Al-Si eutectic in binary aluminium-7 wt% silicon alloys by electron backscatter diffraction (EBSD), J. Light Met. 1 (2001) 43-49.

[87] S.D. McDonald, K. Nogita, A.K. Dahle. Eutectic nucleation in Al–Si alloys, Acta Mater. 52 (2004) 4273-4280.

[88] S. McDonald, A. Dahle, J. Taylor, D. StJohn. Eutectic grains in unmodified and strontium-modified hypoeutectic aluminum-silicon alloys, Metall. Mater. Trans. A 35 (2004) 1829-1837.

[89] G. Laslaz. Dual macrostructure in hypoeutectic Al-Si alloys: dendrites and eutectic grains. Its effects on shrinkage behaviour, Processing of 4th International Conference on Molten Aluminium Processing (1995) 459-480.

[90] R. Meussner. The Structure of Aluminum-Silicon Alloys. Naval Res. Lab. 5341 (1959).

[91] S.D. McDonald. Eutectic solidification and porosity formation in unmodified and modified hypoeutectic aluminium-silicon alloys, Ph. D. thesis, The University of Queensland, 2002.

[92] G. Powell, G. Colligan. Silicon morphology in sodium modified Al-Si eutectic alloys, Mater. Res. Bull. 5 (1970) 431-436.

[93] R. Plumb, J. Lewis. The modification of aluminium-silicon alloys by sodium, J. Inst. Metals 86 (1958).

[94] B.M. Thall, B. Chalmers. Modification in aluminium silicon alloys, J. Inst. Metals 77 (1950) 79-79.

[95] J. Denton, J. Spittle. Solidification and susceptibility to hydrogen absorption of Al–Si alloys containing strontium, Mater. Sci. Technol. 1 (1985) 305-311.

[96] H.V. Guthy, S. Shankar, M.M. Makhlouf. Variation In Hydrogen Content Of Al-Si Hypoeutectic Melts With Strontium Addition. Processing of 6th International Conference on Molten Aluminium Processing (2001) 177-186.

[97] S.C. Flood, J.D. Hunt. Modification of Al-Si eutectic alloys with Na, Met. Sci. 15 (1981) 287-294.

[98] Y. Tsumara. On the Theory of Modification of Aluminium–Silicon Alloys, Nippon Kinzoku Gakkaisi 21 (1957) 69-83.

[99] M. Day. Modification of aluminium-silicon eutectic alloys by metallic sodium, J. Inst. Metals 98 (1970) 57-59.

[100] M. Shamsuzzoha, L.M. Hogan. The twinned growth of silicon in chill-modified Al-Si eutectic, J. Cryst. Growth 82 (1987) 598-610.

[101] M. Shamsuzzoha, L.M. Hogan. Twinning in fibrous eutectic silicon in modified Al-Si Alloys, J. Cryst. Growth 72 (1985) 735-737.

[102] L. Clapham, R. Smith. Segregation behaviour of strontium in modified and unmodified Al-Si alloys, J. Cryst. Growth 92 (1988) 263-270.

[103] M. Kim, Y. Hong, H. Cho. The effects of Sc on the microstructure and mechanical properties of hypo-eutectic Al-Si alloys, Met. Mater. Int. 10 (2004) 513-520.

[104] K. Nogita, H. Yasuda, K. Yoshida, K. Uesugi, A. Takeuchi, Y. Suzuki, A.K. Dahle. Determination of strontium segregation in modified hypoeutectic Al-Si alloy by micro X-ray fluorescence analysis, Scr. Mater. 55 (2006) 787-790.

[105] C.J. Simensen, O. Nielsen, F. Hillion, J. Voje. NanoSIMS analysis of trace element segregation during the Al-Si eutectic reaction, Metall. Mater. Trans. A 38A (2007) 1448-1451.

[106] M. Faraji, L. Katgerman. Distribution of trace elements in a modified and grain refined aluminium–silicon hypoeutectic alloy, Micron 41 (2010) 554-559.

[107] J. Barrirero, M. Engstler, F. Mücklich. Atom Probe analysis of Sr distribution in AlSi foundry alloys, Light Met. TMS (2013) 291-296.

[108] M. Timpel, N. Wanderka, R. Schlesiger, T. Yamamoto, D. Isheim, G. Schmitz, S. Matsumura, J. Banhart. Sr–Al–Si co-segregated regions in eutectic Si phase of Sr-modified Al–10Si alloy, Ultramicroscopy 132 (2013) 216-221.

[109] J. Barrirero, M. Engstler, N. Ghafoor, N. de Jonge, M. Odén, F. Mücklich. Comparison of segregations formed in unmodified and Sr-modified Al-Si alloys studied by atom probe tomography and transmission electron microscopy, J. Alloys Compd. 611 (2014) 410-421.

[110] J. Manickaraj, A. Gorny, Z.H. Cai, S. Shankar. X-ray nano-diffraction study of Sr intermetallic phase during solidification of Al-Si hypoeutectic alloy, Appl. Phys. Lett. 104 (2014) 073102**.**

[111] P. Srirangam, S. Chattopadhyay, A. Bhattacharya, S. Nag, J. Kaduk, S. Shankar, R. Banerjee, T. Shibata. Probing the local atomic structure of Sr-modified Al-Si alloys, Acta Mater. 65 (2014) 185-193.

[112] J.F. Su, X. Nie, V. Stoilov. Characterization of fracture and debonding of Si particles in AlSi alloys, Mater. Sci. Eng. A 527 (2010) 7168-7175.

[113] R. Jamaati, S. Amirkhanlou, M.R. Toroghinejad, B. Niroumand. Significant improvement of semi-solid microstructure and mechanical properties of A356 alloy by ARB process, Mater. Sci. Eng. A 528 (2011) 2495-2501.

[114] I. Gutierrez-Urrutia, M.A. Muñoz-Morris, D.G. Morris. Contribution of microstructural parameters to strengthening in an ultrafine-grained Al–7% Si alloy processed by severe deformation, Acta Mater. 55 (2007) 1319-1330.

[115] F. Lasagni, A. Lasagni, E. Marks, C. Holzapfel, F. Mücklich, H.P. Degischer. Three-dimensional characterization of 'as-cast' and solution-treated AlSi12(Sr) alloys by high-resolution FIB tomography, Acta Mater. 55 (2007) 3875-3882.

[116] G. Requena, G. Garcés, M. Rodríguez, T. Pirling, P. Cloetens. 3D Architecture and Load Partition in Eutectic Al-Si Alloys, Adv. Eng. Mater. 11 (2009) 1007-1014.

[117] E. Ogris, A. Wahlen, H. Lüchinger, P.J. Uggowitzer. On the silicon spheroidization in Al–Si alloys, J. Light Met. 2 (2002) 263-269.

[118] R. Wang, W. Lu. Spheroidization of Eutectic Silicon in Direct-Electrolytic Al-Si Alloy, Metall. Mater. Trans. A 44 (2013) 2799-2809.

[119] G. Sharma, R.V. Ramanujan, G.P. Tiwari. Instability mechanisms in lamellar microstructures, Acta Mater. 48 (2000) 875-889.

[120] T.H. Courtney, J.C.M. Kampe. Shape instabilities of plate-like structures—II. Analysis, Acta Metall. 37 (1989) 1747-1758.

[121] E. Werner. Thermal shape instabilities of lamellar structures, Zeitschrift für Metallkunde 81 (1990) 790-798.

[122] J.C.M. Kampe, T.H. Courtney, Y. Leng. Shape instabilities of plate-like structures—I. Experimental observations in heavily cold worked in situ composites, Acta Metall. 37 (1989) 1735-1745.

[123] A. Karma, A. Sarkissian. Morphological instabilities of lamellar eutectics, Metall. Mater. Trans. A 27 (1996) 635-656.

[124] E. Werner. The spheroidization of thin plates, Acta Metall. 37 (1989) 2047-2053.

[125] H.P. Stüwe, O. Kolednik. Shape instability of thin cylinders, Acta Metall. 36 (1988) 1705-1708.

[126] S. Zherebtsov, M. Murzinova, G. Salishchev, S.L. Semiatin. Spheroidization of the lamellar microstructure in Ti–6Al–4V alloy during warm deformation and annealing, Acta Mater. 59 (2011) 4138-4150.

[127] E. Ogris. Development of Al-Si-Mg alloys for semi-solid processing and silicon spheroidization treatment (SST) for Al-Si cast alloys. Ph D Thesis. Insititute of metallurgy, ETH Zürich, 2002.

[128] P. Zhu, Q. Liu, T. Hou. Spheroidization of eutectic silicon in Al-Si alloys, AFS Trans. 93 (1985) 609-614.

[129] M.E. Keeffe, C.C. Umbach, J.M. Blakely. Surface self-diffusion on Si from the evolution of periodic atomic step arrays, J. Phys. Chem. Solids 55 (1994) 965-973.

[130] S.-i. Fujikawa, K.-i. Hirano, Y. Fukushima. Diffusion of silicon in aluminum, Metall. Trans. A 9 (1978) 1811-1815.

[131] R. Pérez, P. Gumbsch. An ab initio study of the cleavage anisotropy in silicon, Acta Mater. 48 (2000) 4517-4530.

[132] R. Pérez, P. Gumbsch. Directional Anisotropy in the Cleavage Fracture of Silicon, Phys. Rev. Lett. 84 (2000) 5347-5350.

[133] D. Sherman, M. Markovitz, O. Barkai. Dynamic instabilities in {1 1 1} silicon, J. Mech. Phys. Solids 56 (2008) 376-387.

[134] S.K. Chaudhury, V. Warke, S. Shankar, D. Apelian. Localized Recrystallization in Cast Al-Si-Mg Alloy during Solution Heat Treatment: Dilatometric and Calorimetric Studies, Metall. Mater. Trans. A 42 (2011) 3160-3169.

[135] N. Haghdadi, A. Zarei-Hanzaki, H.R. Abedi, D. Abou-Ras, M. Kawasaki, A.P. Zhilyaev. Evolution of microstructure and mechanical properties in a hypoeutectic Al–Si–Mg alloy processed by accumulative back extrusion, Mater. Sci. Eng. A 651 (2016) 269-279.

[136] J.J. Fundenberger, A. Morawiec, E. Bouzy, J.S. Lecomte. Polycrystal orientation maps from TEM, Ultramicroscopy 96 (2003) 127-137.

[137] A. Morawiec, J.-J. Fundenberger, E. Bouzy, J.-S. Lecomte. EP–a program for determination of crystallite orientations from TEM Kikuchi and CBED diffraction patterns, J. Appl. Crystallogr. 35 (2002) 287-287.

[138] L.A. Giannuzzi, F.A. Stevie. A review of focused ion beam milling techniques for TEM specimen preparation, Micron 30 (1999) 197-204.

[139] H.-G. Brokmeier, W. Gan, C. Randau, M. Völler, J. Rebelo-Kornmeier, M. Hofmann. Texture analysis at neutron diffractometer STRESS-SPEC, Nucl. Instrum. Meth. A 642 (2011) 87-92.

[140] C. Randau, U. Garbe, H.-G. Brokmeier. StressTextureCalculator: a software tool to extract texture, strain and microstructure information from area-detector measurements, J. Appl. Crystallogr. 44 (2011) 641-646.

[141] J.-J. Fundenberger. B. Beausir. JTEX - Software for Texture Analysis, Université de Lorraine – Metz, 2015.

[142] B. Beausir, J.J. Fundenberger. ATOM − Analysis Tools for Orientation Mapping, Lorraine University - Metz, 2014.

[143] E. Aerts, P. Delavignette, R. Siems, S. Amelinckx. Stacking fault energy in silicon, J. Appl. Phys. 33 (1962) 3078-3080.

[144] S. Dziaszyk, E.J. Payton, F. Friedel, V. Marx, G. Eggeler. On the characterization of recrystallized fraction using electron backscatter diffraction: A direct comparison to local hardness in an IF steel using nanoindentation, Mater. Sci. Eng. A 527 (2010) 7854-7864.

[145] X. Yang, K. Fujiwara, K. Maeda, J. Nozawa, H. Koizumi, S. Uda. Crystal growth and equilibrium crystal shapes of silicon in the melt, Prog. Photovolt: Res. Appl. 22 (2014) 574-580.

[146] J. Ricote, D. Chateigner. Quantitative texture analysis applied to the study of preferential orientations in ferroelectric thin films, Bol. Soc. Esp. Cerám. Vidrio 38 (1999) 587-591.

[147] J. Hirsch, E. Nes, K. Lücke. Rolling and recrystallization textures in directionally solidified aluminium, Acta Metall. 35 (1987) 427-438.